UNIVERSITA' DEGLI STUDI DI ROMA
"TOR VERGATA"

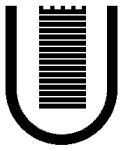

FACOLTA' DI INGEGNERIA MECCANICA

DOTTORATO DI RICERCA IN
INGEGNERIA DELL'ENERGIA-AMBIENTE

XX CICLO

"LEAN-BURN OPERATION FOR NATURAL GAS/AIR MIXTURES: THE DUAL-FUEL ENGINES"

DOCENTE GUIDA:
PROF. STEFANO CORDINER

COORDINATORE:
PROF. FABIO GORI

CANDIDATO:
ING. RICCARDO SCARCELLI

Abstract

The research activity on internal combustion engines (ICE) is increasingly cast to find an alternative solution to reduce the wide utilization of petroleum fuels like diesel oil and gasoline, for environmental, political and economic concerns.

Natural gas is an ideal fuel to be operated in internal combustion engines, since its characteristics allow for much lower environmental impact (less NO_X, PM and PAH emissions) and reduced fuel consumption and CO_2 emissions with respect the conventional fuels. It also is particularly suitable to be operated under high volumetric compression ratio engines, thus providing higher efficiency, and moreover it is characterized by a wide flammability range. This latter aspect promotes the employment of a lean burn strategy, thus further increasing the engine efficiency and reducing the exhaust emissions.

The dual-fuel natural gas/diesel concept allows extending the lean flammability limit of NG with respect to SI-NG operations and simultaneously reducing the NO_X-PM trade-off affecting diesel combustion. Such a technology consists in introducing NG as main fuel in a conventional diesel engine. A certain amount of diesel pilot injection is preserved to act as the ignition source for the air/NG mixture.

The easiness of dual-fuel conversion, just introducing a feeding system for the NG and optimizing the diesel pilot quantity, makes such technology rather inviting especially as a retrofit for the existing diesel vehicles, which could not meet the more and more stringent emission regulations in the future, thus accelerating the effectiveness of a pollutants reduction strategy, especially in urban areas.

In the present study, the dual-fuel combustion process with its inherent complexity, deriving from the different combustion mechanism of the two fuels (diesel oil and NG), is investigated both from an experimental and a numerical point of view.

The experimental activity has the main target to analyze the problems connected with the conversion of a heavy-duty diesel engine to dual-fuel operation, and to put into evidence the influence of the main engine parameters on performance and pollutants

formation. Further devices like throttling, catalyst and EGR have been subsequently analyzed to further reduce the exhaust emissions.

The numerical activity, characterized by a mixed 1-D/3-D approach, has been carried out with the initial target of a correct understanding of the complex dual-fuel combustion mechanism. A diagnostic approach has been thus followed, to the aim of getting useful information on the combustion progress by means of the analysis of the experimental in-cylinder pressure data. A detailed multi-dimensional simulation of the whole working cycle of the engine has been subsequently performed, to provide for the correct representation of the fluid-dynamic effect involved in dual-fuel operations. Such an approach allows for the complete description of the engine overall behavior and the dual-fuel combustion in detail.

As far as 3-D simulation tools are concerned, the open-source KIVA-3V code has been utilized, and a fair number of mathematical models have been introduced, with respect the KIVA original version, to correctly represent diesel spray processes and overall combustion. In particular, the WAVE model has been utilized to describe both the diesel jet atomization and the droplet breakup process. The Shell model has been introduced to represent the low-temperature chemistry of the diesel fuel, thus allowing for the correct description of the auto-ignition process. Overall combustion has been simulated by means of a flamelet (CFM model) and a characteristic-time (CTC model) approach. A comparison between these strategies has been performed and main assumptions, advantages, limits and results of each of the two models have been put into evidence. The numerical model has been finally validated by the comparison with the experimental data.

A further section has been here reported to suggest another strategy to improve the lean burn operation of NG/air mixtures. Introducing a certain amount of H_2 (up to 15÷20% in volume) no modification to the engine has to be introduced, and a higher combustion speed can be obtained, due to the much higher laminar flame speed of H_2. Such an advantage could be exploited to extend the lean flammability limit for NG engines without suffering from instability and low efficiency.

Table of Contents

Chapter 1
INTRODUCTION

1.1 Overview and Objectives

Natural gas is used as a fuel for transport applications in many countries around the world, and its use in vehicle applications is growing. Besides displacing imported petroleum fuels, one of the primary benefits of using natural gas as a vehicle fuel is the potential to substantially reduce exhaust emissions of harmful pollutants such as particulate matter (PM) and nitrogen oxides (NO_X). To maximize the benefits of any natural gas vehicle program, several factors must be considered, including natural gas fuel quality, vehicle engine technology, retrofits versus new vehicles/engines, and safety.

Since the early 1990s, Natural Gas for Vehicles (NGV), generally used in compressed form, has attracted renewed interest throughout the world. A number of countries have carried out large-scale development programs. At the national scale, tax incentives have been implemented to promote the use of this motor fuel. For the time being, the world market of natural gas vehicles remains small and heavily concentrated: over half of the world fleet is located in the Americas, mainly in Argentina and Brazil (Table 1.1). According to the Natural Gas Vehicle Coalition, at the beginning of 2006 there were about 130,000 Natural Gas Vehicles (NGV) on the road in the United States, and more than 4 million worldwide. In Europe to date, the market has only developed to a very small extent. At the instigation of European authorities, this situation seems about to change. The European Commission has set an indicative target: NGV is to represent 10% of transport energy consumption by 2020. The first country to use NGV to a significant

extent, Italy is currently Europe's largest market and represents more than 380,000 vehicles. Possessing natural gas resources, Italy began building up its fleet long ago.

Country	Vehicle fleet (thousands)	Consumption (Mtoe)	Number of stations
Italy	382	0.36	509
United States	130	0.43	1340
Germany	27.2	not available	558
Japan	24.7	n.a.	288
Canada	20.5	0.04	222
Ireland	9.8	n.a.	10
France	7.4	0.04	105
South Korea	6.5	0.13	170
Sweden	5.3	0.02	65
Argentina	1439.5	1.89	1402
Brazil	948.3	0.91	1080
Pakistan	800	n.a.	740
India	204	n.a.	198
China	97.2	0.07	355
Ukraine	67	n.a.	147
Colombia	60	0.09	90
Egypt	59.4	0.16	90
Iran	48	0.00	72
Venezuela	44.1	0.12	149
Russia	41.8	0.03	213
Armenia	38.1	n.a.	60
Bangladesh	35	n.a.	95
Bolivia	28.8	n.a.	59
Malaysia	14.9	0.03	39
Tadjikistan	10.6	n.a.	53
Indonesia	6.6	0.03	17
Byelorussia	5.5	0.02	24
Chile	5.5	0.03	12
Thailand	5.5	0.01	34
World	**4603**	**4.22**	**8722**

Table 1. 1 NGV worldwide in 2006

In recent years, technology has improved allowing a proliferation of natural gas vehicles, in particular for vehicle fleets, such as taxicabs and public buses. Nowadays, virtually all types of natural gas fuelled vehicles may be found either in production for sale to the public or under development, from passenger cars, trucks, buses, vans, and even heavy-duty utility vehicles. Today, most of the heavy gas-powered vehicles are buses and refuse collection vehicles. These applications are especially appropriate for use in urban areas, for a number of reasons. They generate low levels of noise and polluting emissions. In a city, it is not a problem if a vehicle has a limited range or onboard fuel

storage capacity. Finally, with respect to logistics, there is a concentration (compressors) at the depot.

In light vehicles, natural gas can be used in bi-fuel vehicles (gasoline/NGV) or in vehicles running exclusively on natural gas. The intrinsic properties of natural gas are best exploited in dedicated vehicles. Nevertheless, the problem is that the motorist needs access to a widespread NGV distribution network. There are few NGV service stations in existence today, which is why carmakers have generally included bi-fuel (gasoline/NGV) rather than dedicated models in their vehicle range.

A country or region's current pattern of fuel usage is also important when evaluating the potential benefits of a natural gas vehicle program. For example, Brazil currently produces significant amounts of ethanol from domestically grown sugar cane for use as a vehicle fuel, primarily in light-duty cars. Anyway, it is highly dependent on imported petroleum to supply diesel fuel for heavy-duty vehicles. At the same time, Brazil's natural gas production ranks fifth in Latin America and recent discoveries suggest that the potential exists to increase production substantially. Brazil is also a highly urbanized country, with significant transportation related air quality problems in its major cities. As such, Brazil could potentially reap significant environmental, public health, and economic benefits from increasing its use of domestic natural gas reserves for transportation. A significant portion of Brazil's light-duty fleet already runs on domestically produced ethanol. The criteria pollutant emission reductions that can be achieved by switching from gasoline or ethanol to natural gas are also generally modest. Therefore, the greatest potential benefit from additional natural gas usage in Brazil's transportation sector will accrue by focusing on heavy-duty buses and trucks that currently operate on diesel fuel.

Also, the increasing demand of higher engine efficiency and the need to reduce fuel consumption and meet the more and more stringent emission regulations lead to a deep investigation to make maximum use of the high potential of natural gas. Thus, technical solutions as the utilization of lean and ultra-lean NG/air mixture are widely studied. To efficiently burn a very lean mixture of natural gas and air, a much higher and widespread ignition source as to be provided rather than of having a localized spark-plug, and such an

enhancement can be obtained thanks to the combustion of a certain amount of diesel fuel injected into the cylinder.

According to the previous considerations, the Natural Gas/Diesel Dual-Fuel Engines can represent an interesting and useful solution to further spread the utilization of natural gas as the main fuel in the transportation field, thus reducing the dependence on imported petroleum, and to extend the lean limits of NG utilization. Such an approach could be successfully carried out as a new technology, but its proper strength consist in a powerful retrofit approach for the existing diesel engines which could not meet the increasing emission regulations in the future and could be easily, rapidly and at low-cost converted to dual-fuel operation.

Nevertheless, the dual-fuel technology is extremely complex, since two fuels characterized by different combustion processes are simultaneously burned within the cylinder. This study has the main target to investigate the dual-fuel conversion of a heavy-duty diesel engine and to analyze such a complicated combustion mechanism by means of a general (1-D) and detailed (3-D) numerical approach. The numerical results will be validated on the experimental data and discussed.

1.2 Natural Gas Engine Technology

1.2.1 Natural Gas Properties

Natural gas is commonly considered as the most inviting short-term fuel alternative for internal combustion engines applications. It should not be referred as an “alternative fuel” anymore, but its wide diffusion is not still satisfactory in comparison with its significant potential to ensure oil-like performance and reduced exhaust emissions. It also is largely available and characterized by low costs with respect to diesel fuel and gasoline. Natural gas is mostly composed by methane, even though its exact composition depends on its provenance, as can be observed in Table 1.2 [1].

COMPONENT	ITALIAN	RUSSIAN	DUTCH	ALGERIAN
Methane (%)	**99.62**	**98.07**	**91.01**	**83.28**
Ethane (%)	0.06	0.60	3.70	7.68
Propane (%)	0.02	0.22	0.88	2.05
Butane (%)	0.01	0.09	0.28	0.78
Pentane (%)	-	0.01	0.07	0.21
Hexane (%)	0.01	0.02	0.07	0.11
CO2 (%)	0.02	0.11	1.11	0.19
N2 (%)	0.26	0.87	2.84	5.52
He (%)	-	0.01	0.04	0.18

Table 1. 2 Natural gas distributed in Italy

Accordingly, the high potential of NG is referable to the remarkable chemical and physical properties of methane (Table 1.3). It is characterized by a high octane number (RON 120-130) and particularly suitable to be operated in high compression ratio engines, thus leading to high engine efficiency.

METHANE PHYSICAL PROPERTIES		
Density	(kg/Nm^3)	0.72
Flammability Limits	(% on air in volume)	5 ÷ 15
Auto-Ignition Temperature	(°C)	540
Lower Heating Value (LHV)	(MJ/kg)	50.0
Research Octane Number (NOR)		120 ÷ 130
Stoichiometric Air/Fuel Ratio (AFR)		17.2

Table 1. 3 Methane physical properties

Methane, the major component in natural gas, is generally believed to be the cleanest burning hydrocarbon as it produces less CO_2 and more H_2O than other fossil fuels because of its high H/C ratio. Another important aspect of methane combustion which contributed to its pristine image is the fact that its premixed flames with air do not soot, instead they are blown-out first because of flammability limit considerations. Furthermore, the formation of Polycyclic Aromatic Hydrocarbons (PAH) is widely reduced and a lower flame temperature limits NO_X emissions. With respect to gasoline

engines, reduced (-20%) emission of CO_2 can be obtained, as well as savings of at least 50% in the fuel cost per km. With respect to diesel engines it is possible to obtain reduced PM and NO_X emissions and savings of at least 30% in the fuel cost per km.

From a safety perspective, unlike diesel and gasoline engines, CNG is typically stored in gaseous form under high pressure (at 150 bar or more on light-duty vehicles and at 200 or more on heavy-duty vehicles). These elevated pressures can pose a significant hazard in the event of a valve or tank failure. Nevertheless, because natural gas is lighter than air, gas leaking in the open air will quickly rise and dissipate in the atmosphere to the point that there is no longer a danger of fire or explosion.

Despite of its significant characteristics, the wide diffusion on natural gas is limited by distribution and storage concerns, therefore it has been only partially introduced in the transportation field.

The major problem is represented by the low fuel autonomy. When stored in a vehicle, CNG provides about 1/4 the energy density of gasoline. The range of a CNG vehicle depends on the capacity to store fuel, but generally it is less than (about one-half) that of gasoline-fueled vehicles. Such an aspect obviously affects the design of NG engines, and a mixed gasoline/NG configuration is usually preferred from engine manufacturers, which is not able to properly exploit NG potential yet. Emerging methods of NG storage include Liquefied Natural Gas (LNG), which is already in commercial operation and Adsorbed Natural Gas (ANG), which is still in the developmental stage.

1.2.2 The Lean-Burn Concept

The wide flammability range of natural gas allows regular combustion for very lean mixtures with respect to gasoline engines, thus resulting in high efficiency (low specific fuel consumption) and low NO_X emissions. Moreover the utilization of lean mixtures, thus reducing brake torque, can be considered as a useful method to control the engine load without throttling, so minimizing the pumping losses.

The actual drawback is the reduction of the burning rate, mainly due to the lower flame speed, which results in an increase in combustion duration. Once the lean flammability limit is exceeded, the engine stability is affected by cyclic variation, the

engine performance drastically drop and the rapid increase in CO and HC emissions can be observed. Anyway it is still possible to fast and efficiently burn very lean mixtures, even though additional conditions have to be created as high turbulence, turbo-charging or high compression ratio as well (Figure 1.1).

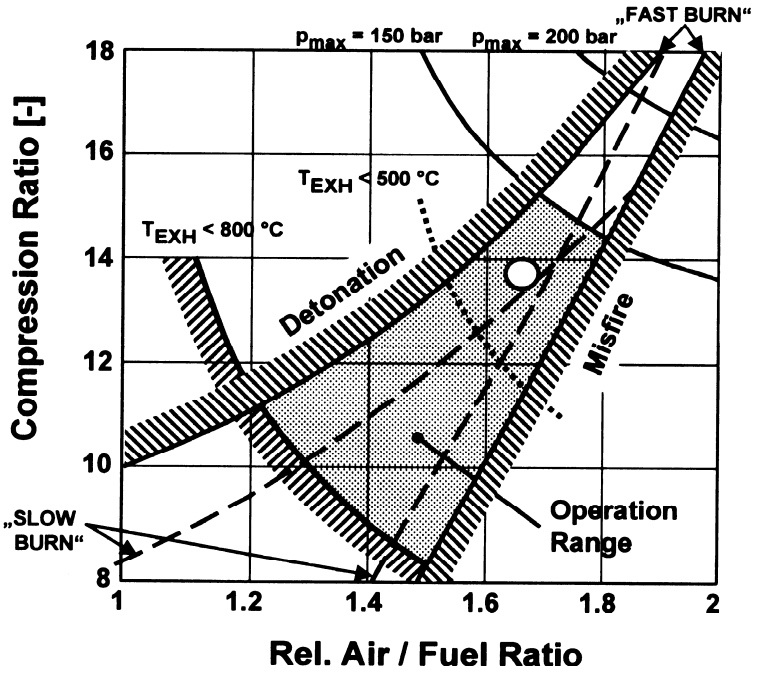

Figure 1. 1 Influence of CR on flammability limits

Table 1.4 shows the performance of a Fiat Mini-Van equipped with different engines [2]. The lean-burn approach allows operating with higher compression ratio and provides higher efficiency. This leads to performance comparable or even superior to diesel and gasoline ones, while reducing CO_2 emissions (Figure 1.2). Moreover, NO_X emissions can be sufficiently reduced to respect EURO 4 limits by the only use of EGR.

FUEL	**DIESEL**	**GASOLINE**	**CNG (λ=1)**	**CNG LB**
Displacement (l)	2.2	1.8	1.6	1.9
Compression Ratio	18.5	10.5	12.5	14.5
Turbocharging	Yes	No	No	Yes
Power (kW @ rpm)	92 @ 4000	92 @ 5600	71 @ 5800	100 @ 4000
Torque (Nm @ rpm)	280 @ 1500	170 @ 3800	145 @ 4000	300 @ 2000

Table 1. 4 Comparison among different fuelling configuration for a Fiat Mini-Van

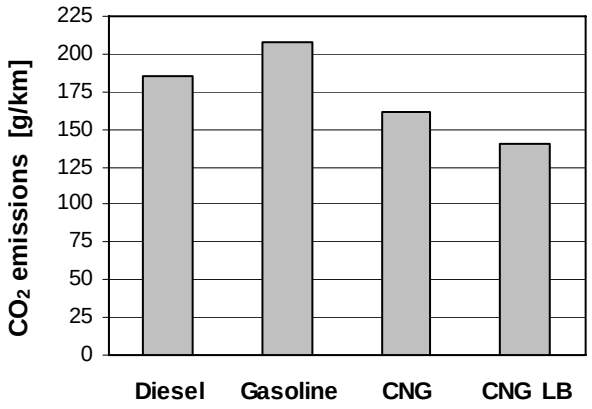

Figure 1. 2 Comparison among different fuelling configuration for a Fiat Mini-Van

As already stated, one possible solution to extend the lean flammability limit for natural gas application is to design more sophisticated high-turbulence level combustion chambers [3]. A well-known and successful approach is the “Partially Stratified-Charge” (PSC) concept, proposed by Evans et al. [4]. It consists of introducing an ultra-lean mixture (beyond the lean flammability limit) of air and NG within the cylinder. This main NG injection is then followed by a secondary NG direct injection, localized close the spark-plug, just before the spark timing. It is commonly known that the early stage of the flame growth (the development of the flame kernel) widely influences the overall combustion. To stabilize the whole process, a local enrichment of the mixture close the spark-plug can be provided (Figure 1.3).

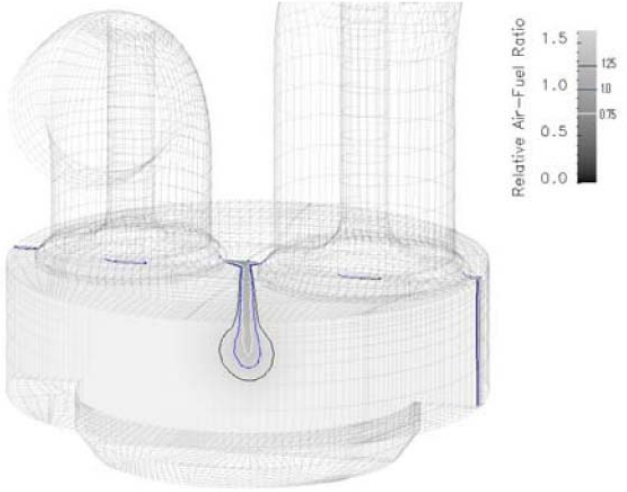

Figure 1. 3 Local enrichment close the spark-plug by NG direct injection [5]

Results on PSC test show an improved behavior of the engine up to $\lambda = 1.7$, while a homogeneous approach cannot ensure a regular combustion beyond $\lambda = 1.6$, as can be observed in Figure 1.4.

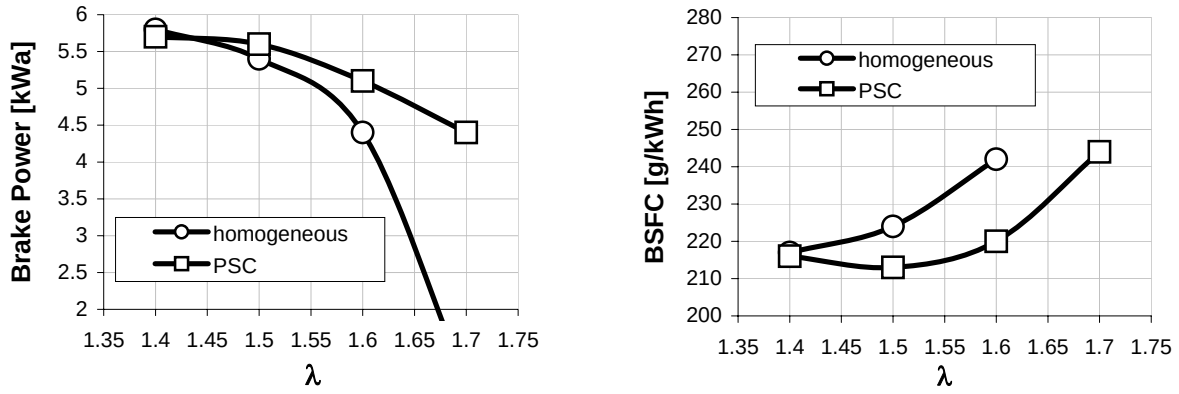

Figure 1. 4 Comparison between homogeneous and PSC operation

A further interesting solution is to feed the engine with an ultra-lean homogeneous NG/air mixture while enhancing the needed energy for the ignition and the regular development of the flame. As an example, a certain amount of diesel oil can be injected into the cylinder near the TDC. Its combustion provides the ignition source for the homogeneous mixture, thus leading to the presence of a large number of ignition points within the combustion chamber, instead of having a localized spark-plug. Such a technology is usually referred as “Dual-Fuel”.

1.2.3 The Natural Gas/Diesel Dual-Fuel Engine

Diesel/NG dual-fuel engines are one of the possible short-term solution to reduce emissions from traditional diesel engines (affected by the PM-NO_X trade-off) meanwhile utilizing an “alternative fuel” like natural gas as primary fuel. It consequently results in an interesting technology to meet future emissions regulations, but also a powerful solution to retrofit existing engines, so longing their life with consistently reduced global environmental impact.

In a dual-fuel natural gas/diesel engine the primary fuel (NG) is mixed with air in the intake manifold, just like a SI engine. The mixture is then compressed and

subsequently ignited by the combustion of a small amount of diesel fuel (the pilot), injected as the piston approaches the top dead centre (Figure 1.5).

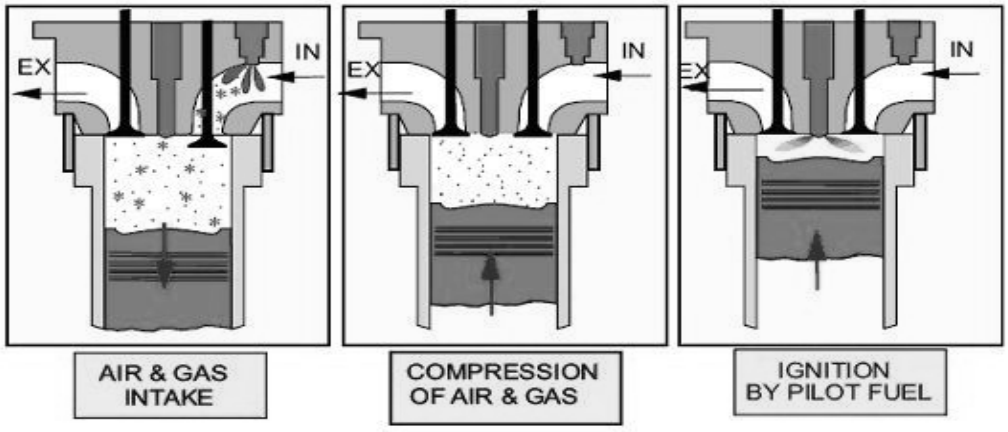

Figure 1. 5 Dual-Fuel technology

The wide zone of ignition, due to the presence of a large number of flame kernels in the chamber (Figure 1.6) instead of a localized spark plug, leads to a regular combustion of the whole charge into the cylinder also for very lean mixtures, thus extending the operating flammability limits of natural gas with respect to a spark-ignition solution.

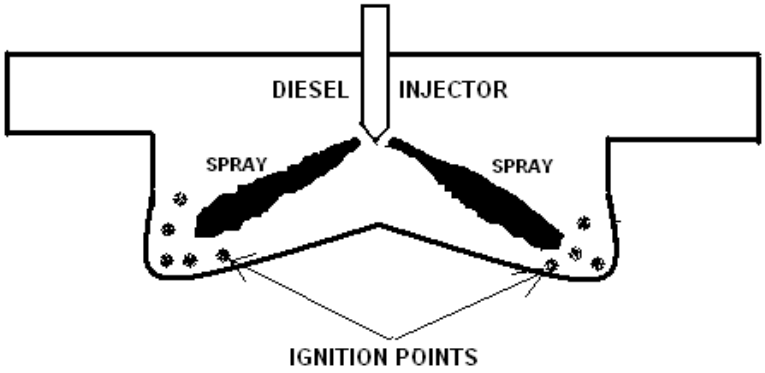

Figure 1. 6 A schematization of the “multi-point ignition” phenomenon

The use of very lean mixtures, together with the high octane number (NOR = 130) of the natural gas, also allows to prevent the occurrence of knock. Accordingly, the use of natural gas as primary fuel allows keeping the original compression ratio of the conventional diesel engine. Thus, the existing and already running on-road diesel engines can be easily converted to dual-fuel operation. In fact the only equipments that have to be

installed on the engine are the feeding system for the NG and the external device allowing to vary diesel injection flow rate. This results in great capital cost and time saving in comparison with other environmental low-impact solutions (fuel cells, hybrid vehicles).

A relevant aspect that has to be considered is the interaction between diesel oil and NG combustion, since they are characterized by different mechanisms. Karim et al. [6] schematized dual-fuel combustion as consisting of three main phases (Figure 1.7):

I. *Energy released from diesel combustion;*
II. *Energy released from combustion of natural gas surrounding diesel flames;*
III. *Energy released from combustion of overall natural gas.*

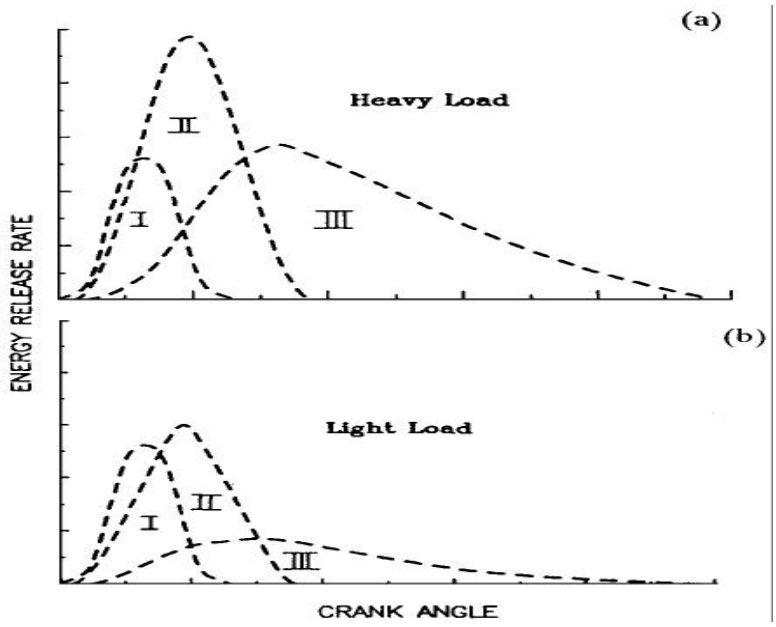

Figure 1. 7 Schematization of dual-fuel combustion

Accordingly, the correct propagation of the flame throughout the homogeneous mixture widely depends on the load, that is to say on the air/NG equivalence ratio. For too lean mixtures, the flame cannot completely propagate and only the natural gas in the vicinity of the diesel flames burns. When the mixture becomes richer, a more regular flame propagation is detected.

It is anyway complicated to establish the correct lean flammability limit in dual-fuel combustion. In fact, it is very similar to the PSC Concept, considering that the combustion of the diesel pilot locally reduces the air available for NG oxidation. Thus, the air/NG equivalence ratio near the diesel flames could be even close to the stoichiometric value. Moreover a large number of flames are expected to interact and join within the cylinder, and then a shorter path has to be covered by each flame.

1.2.4 Dual-Fuel Features and Strategies

Dual-fuel pilot-injected natural gas/diesel engines have a significant potential to reduce NO_X and PM emissions from the baseline diesel case, as shown from Papagiannakis and Hountalas [7] (Figure 1.8). Particulate emissions can be decreased with the substitution of a large amount of oil with NG. Moreover, the combustion of a homogeneous lean charge minimizes the local peaks of temperature and thus NO_X concentration in the exhaust gases.

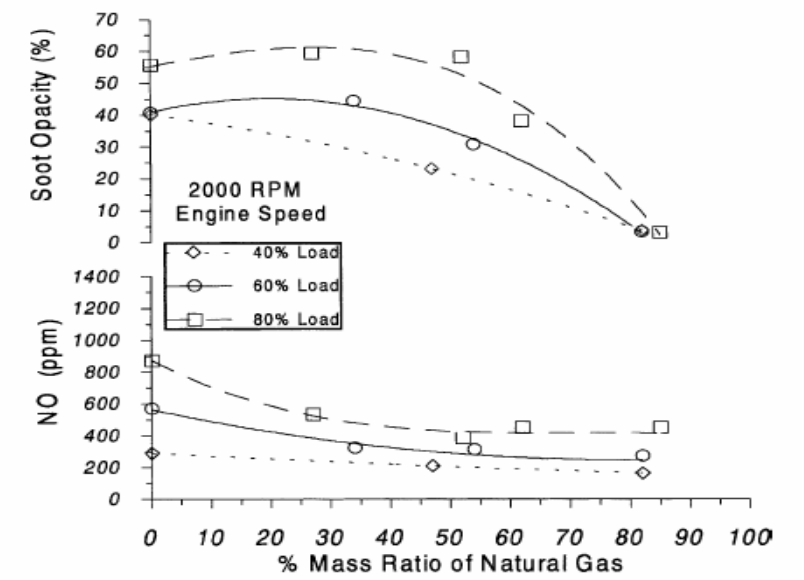

Figure 1. 8 Effect of NG percentage on soot and NO_X formation

Lower values of the fuel specific consumption and the low atomic ratio C/H of NG (mostly composed by methane) allow the reduction of CO_2 emissions, not yet ruled but considered as one of the most important cause of the greenhouse effect).

In the recent years the dual-fuel combustion system has been proposed [8-11], but has not reached a great diffusion. This can be explained considering that HC and CO emissions from a dual-fuel engine are higher than those of a conventional diesel engine, especially at part loads (Figure 1.9).

Dual-fuel engines, deriving from the conversion of conventional diesel engines, usually operate unthrottled, with the load regulated by the admission of natural gas in the intake manifold. The air-fuel mixture becomes leaner as the load is reduced, thus approaching the lean flammability limit of the mixture. The consequent combustion process is slow and this leads to the formation of incomplete combustion products (CO) and unburned hydrocarbons (HC). The increase in CO emissions is also due to the local mixture enrichment because the injected diesel pilot mixes with a carburated NG/air mixture instead of just air as in a conventional diesel engine.

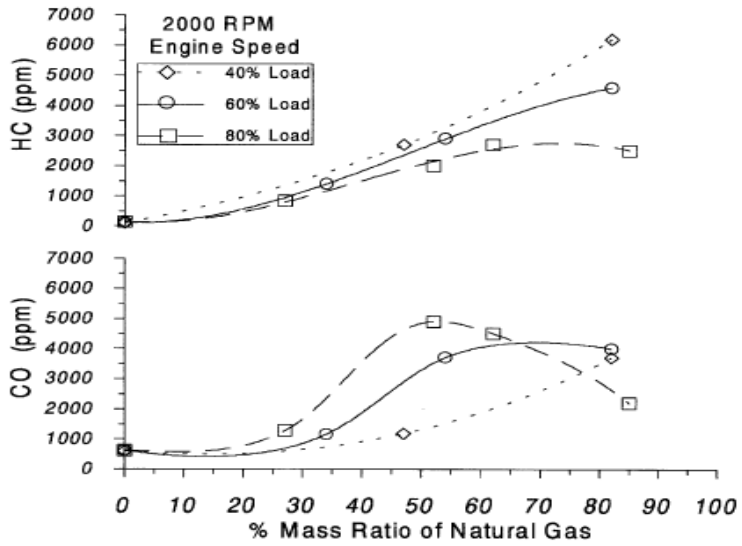

Figure 1. 9 Effect of NG percentage on HC and CO formation

Moreover other sources for high HC exhaust emissions are the scavenging phase and the crevice volumes. Unlike a conventional diesel engine, for dual-fuel operations the charge entering in the cylinder through the inlet valve is a mixture of air and natural gas: thus a fraction of the gaseous fuel is forced into crevice volumes during the compression stroke or escapes through the exhaust valve during the valve overlap period (usually

referred as “short-circuit effect”). This last aspect is particularly relevant when the overlap is great, as it is usual for turbo-charged diesel engines.

The low efficiency and the high emissions under part loads represent, together with the occurrence of knock at high loads (unavoidable for mixtures near to stoichiometric conditions), the major problems for the traditional dual-fuel conversions. Many possible solutions have been studied to improve the behavior of dual-fuel engines under part loads. A possible approach is the optimization of the pilot injection characteristics [12,13]: increasing pilot quantity and advancing injection timing a more regular combustion process can be observed, with higher efficiency and lower HC and CO emissions (Figures 1.10 and 1.11).

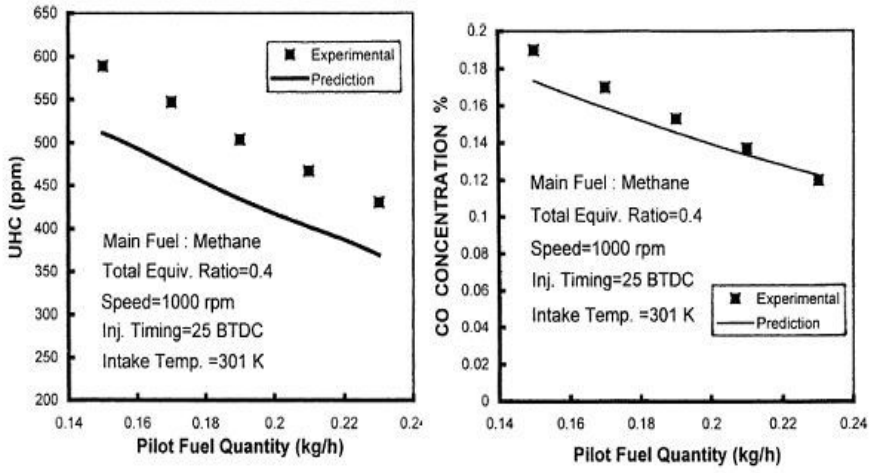

Figure 1. 10 Effect of the pilot quantity on HC and CO emissions

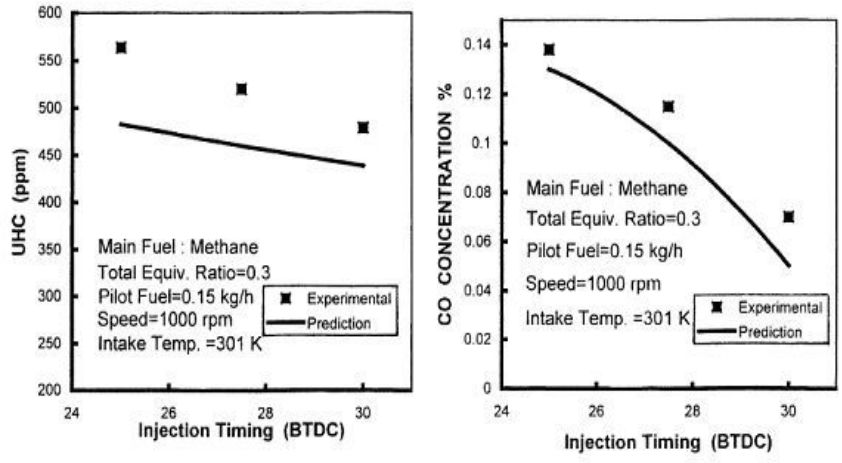

Figure 1. 11 Effect of the pilot injection timing on HC and CO emissions

Nevertheless these solutions can be responsible of an increase in NO_X emissions (Figure 1.12).

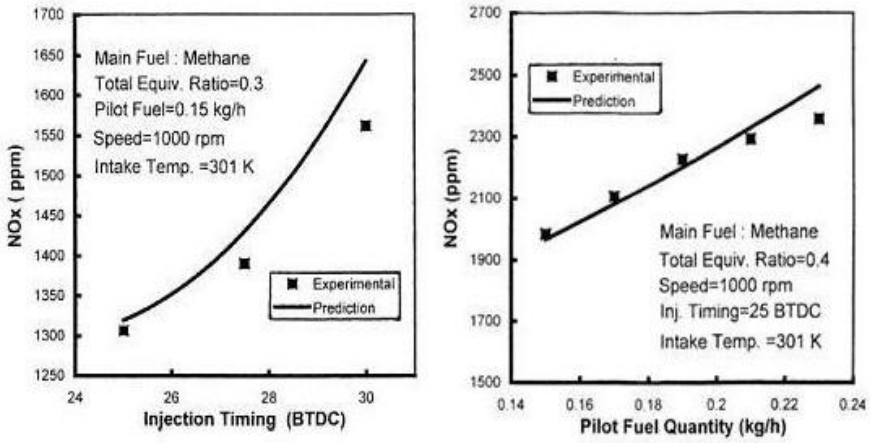

Figure 1. 12 Effect of the pilot quantity and injection timing on NO_X emissions

Another possible approach consists in reducing the amount of air and NG in the cylinder, by the introduction of intake throttling or varying intake valve timing. Nevertheless, these solutions can give high PM, CO and NO_X emissions. Recent studies [14] show that the use of low pilot quantities (about 2-3%), together with advanced pilot injection (45-60 CAD BTDC), permits to obtain very low NO_X emissions and "diesel-like" performance.

Daisho et al. [15,16] have carried out engine tests modifying some engine parameters as pilot injection timing advance, intake throttling and hot and cooled EGR (Figure 1.13). It was found that hot EGR is the best way to increase thermal efficiency and simultaneously reduce HC and NO_X emissions (Figure 1.14). With advanced injection timing a better thermal efficiency can be obtained, however NO_X emissions result to be higher (Figure 1.15). Intake throttling promotes better combustion, nevertheless increasing pumping losses.

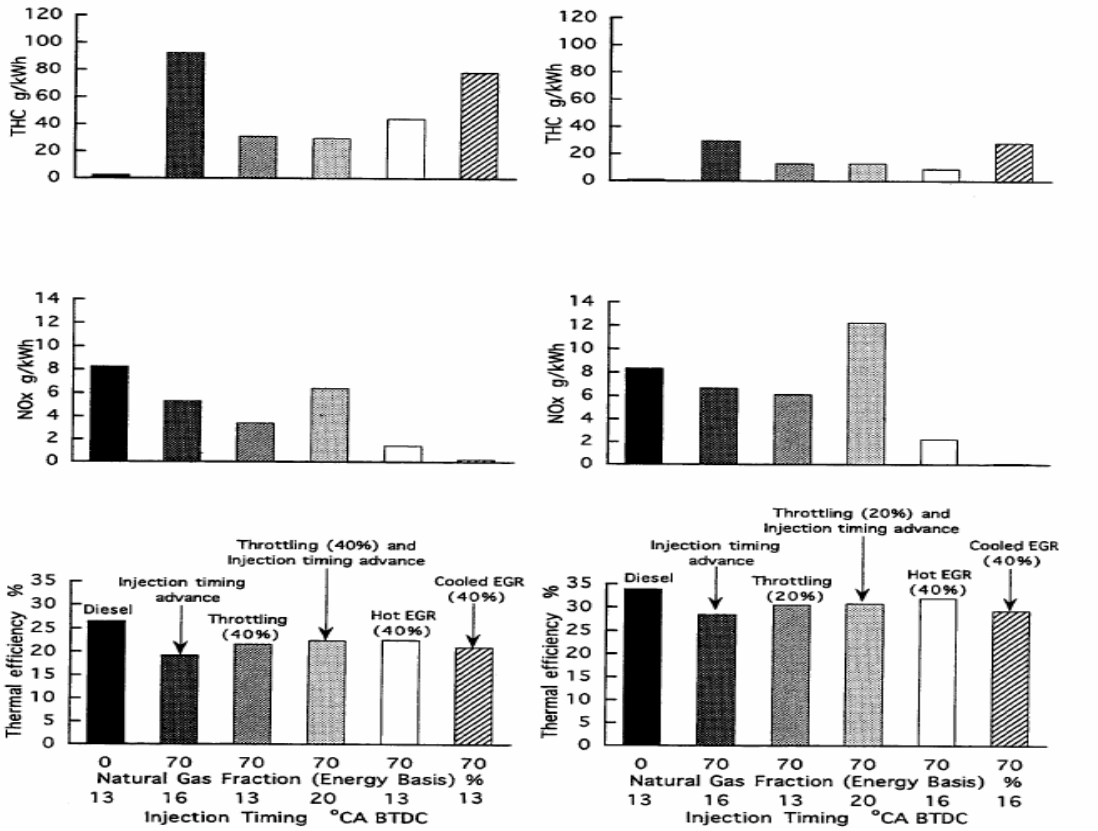

Figure 1. 13 Comparison among different solutions to improve part-load dual-fuel behavior

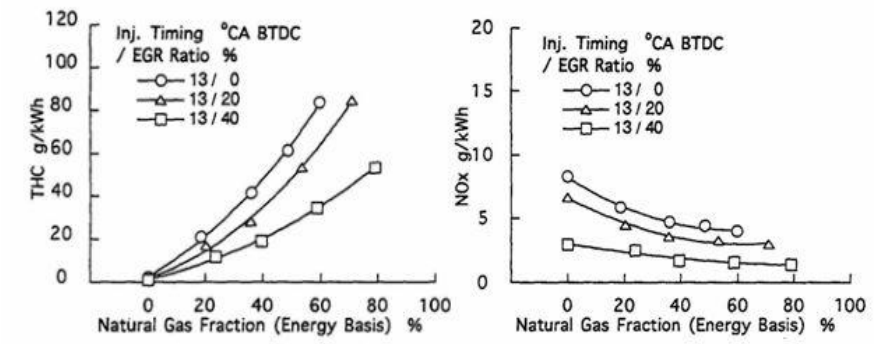

Figure 1. 14 Effect of EGR on HC and NO_X

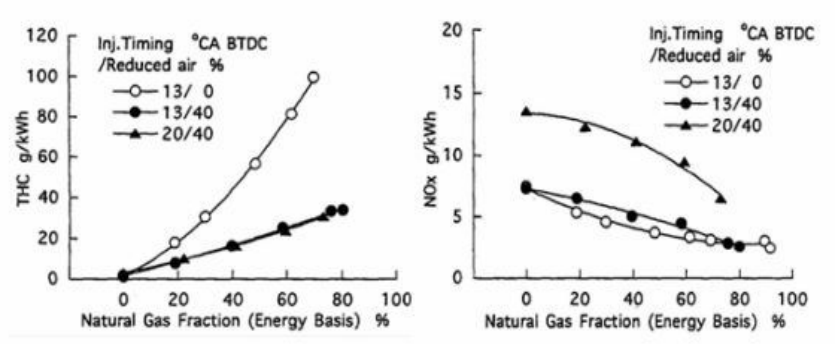

Figure 1. 15 Effect of throttling and injection timing on HC and NO_X

Chapter 2

THE NUMERICAL APPROACH

2.1 Modeling Turbulent Combustion

2.1.1 Turbulent Scales

A turbulent flow consists of large number of vortical structures of different sizes. The size of the largest vortices usually scales with the flow dimensions whereas the size of the smallest structures (Kolmogorov eddies) depends on the Reynolds number and decreases as the Reynolds number increases. The interaction between structures of different dimensions is best explained by the energy cascade concept [17]. It states that the kinetic energy produced by the velocity gradients is transferred from the large to smaller and smaller scales by an inviscid process down to the smallest scales where the energy is dissipated into heat (at the molecular level) by means of viscous motion.

The size of the large turbulence eddies can be calculated by the following expression:

$$L_I = \int_0^\infty R_x dx \tag{2.1}$$

L_I is also called integral length scale of turbulence, whereas R_X is the correlation coefficient, varying in the range of 0 to 1.

The smallest scale of turbulence is the Kolmogorov scale, expressed by:

$$L_k = \left(\frac{\nu^3}{\varepsilon}\right)^{1/4} = L_I \, \mathrm{Re}_T^{-\frac{3}{4}} \tag{2.2}$$

where ν is the kinematic viscosity and ε is the kinetic energy dissipation rate. It is defined using Kolmogorov hypothesis and it is strictly related to the concept of the energy cascade of the turbulent spectrum.

An intermediate length scale is the Taylor micro-scale L_M which is defined based on the velocity gradients as follows:

$$L_M^2 = -\frac{2}{\left(\partial^2 R_x / \partial x^2\right)_{x=x_0}} \tag{2.3}$$

In addition to the length scales it is possible to define analogous time scales, here neglected since they have similar expressions, apart from dimensional concerns.

2.1.2 Turbulent Combustion Regimes

Under turbulent combustion conditions, the interaction between the turbulent flow field and the flame front is described by means of characteristic dimensionless numbers. The most commonly used are the turbulent Reynolds number (Re_T), Damköhler (Da) and Karlovitz number (Ka) defined as:

$$\mathrm{Re}_T = \frac{u' L_I}{\nu} \qquad \mathrm{Da} = \frac{\tau_t}{\tau_c} = \frac{L_I}{u'}\frac{s_L}{\delta_L} \qquad \mathrm{Ka} = \frac{t_c}{t_k} = \left(\frac{\delta_L}{s_L}\right)\left(\frac{u'}{L_k}\right) \tag{2.4}$$

The turbulent Reynolds number describes the ratio of the momentum forces (destabilizing effects) to the viscous forces (stabilizing effect). Reacting flows at high turbulence Reynolds numbers are characterized by highly fluctuating flames. The Damköhler number relates the time scale of the turbulent mixing, defined as L_I/u', to the time scale of the chemical reaction defined as δ_L/s_L. When Da >> 1, the chemistry is fast

and the combustion is controlled by mixing processes. The resulting flame front is so thin as it can easily be distinguished and detected. Flame at small Damköhler numbers (Da < 1) are characterized by intense mixing. The reaction of combustion is controlled by chemical kinetics and flames referred to as well-stirred reactor are formed. The Karlovitz number relates the time scale of the chemical reaction (δ_L/s_L) to the smallest time scale of the turbulent flow, represented by the Kolmogorov scale (L_k/u'). Accordingly, it measures the flame front stretch. Using these three characteristic numbers (Re_T, Da and Ka), the turbulent premixed flames can be classified into groups (flame regimes), as postulated initially by Borghi [18] and later extended by Peters [19]. An example of Borghi/Peters diagram is shown in Figure 2.1.

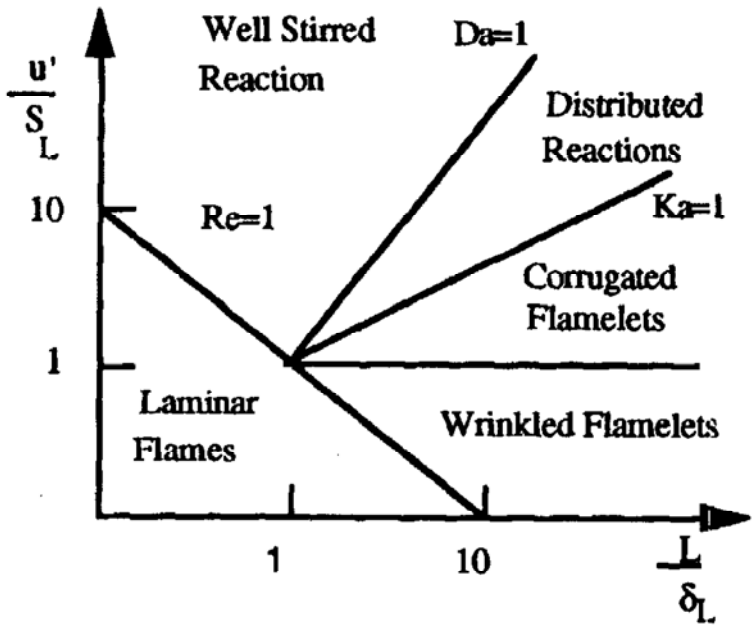

Figure 2. 1 The Borghi's diagram, modified by Peters

The x-axis in Figure 2.1 represents the size of the flame structures by means of the ratio of the integral length scale of turbulence L_I to the laminar flame thickness δ_L. The y-axis represents the ratio of the turbulence intensity u' to the laminar flame speed s_L.

The Borghi's diagram is represented again in Figure 2.2, together with the respective turbulent flame structures. Wrinkled flame regime is situated below the horizontal line of constant $u'/s_L = 1$. In that zone the laminar flame speed (s_L) is higher

than the turbulence intensity (u'). As a result the flame front propagating with the speed s_L is able to dump the turbulent fluctuations. The interaction between flame front propagation and the turbulent flow leads to creation of flame front wrinkles. The thickness of the wrinkled flame front is not changed by turbulence because the smallest turbulent structures (L_k) are larger than the laminar flame thickness (δ_L). Therefore the turbulence does affect the reaction zone and does not alter the chemical kinetics. In other words the interaction between the flame front and the turbulent flow field is purely kinematic (fluid-dynamic). The corrugated regime is situated above the line of constant $u'/s_L = 1$ and below the line of constant Ka = 1. Since u' is larger than s_L the flame front wrinkling of the corrugated flame regime is more intense than in the wrinkled flame regime and additionally the relatively intense turbulence is responsible for creation of "flame pockets" which are detached from the continuous flame sheet. The Kolmogorov eddies are still not able to penetrate the reaction zone because they are too big ($\delta_L < L_k$).

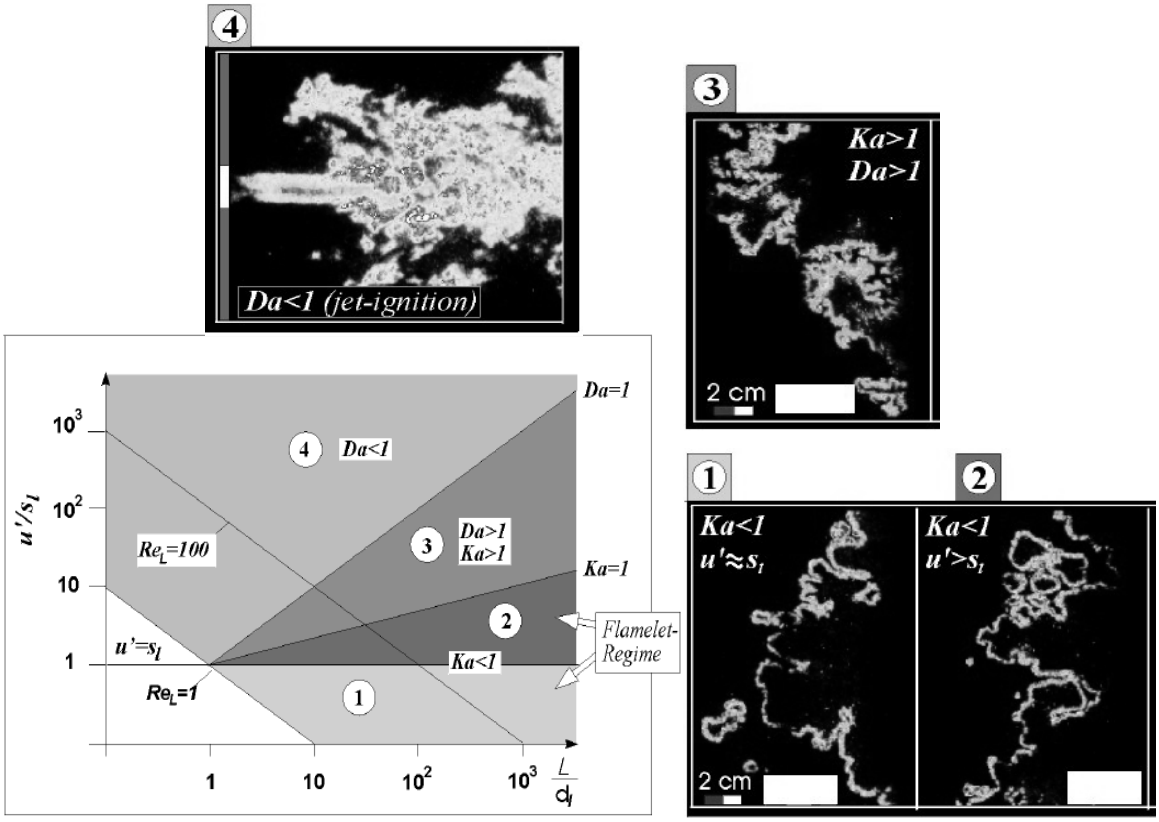

Figure 2. 2 The Borghi's diagram and the corresponding flame structures

In the regimes presented above the reaction layer is not disturbed by turbulence because $\delta_L < L_k$. Therefore the chemical kinetics can be described by the laminar flame properties (δ_L, s_L). Furthermore this offers a possibility to describe the turbulent flame in a simplified way where the turbulent flame front consists of laminar flamelets embedded in a turbulent flow. This simplification is the classical flamelet concept which is commonly used in modeling of turbulent premixed combustion. The well-stirred rector regime is characterized by Da << 1. Accordingly, the mixing time scale is much shorter than the chemical time scale and thus the combustion process is controlled by chemical kinetics. The intense mixing causes perfect mixing of the combustion products with reactants. As a consequence a classical flame front does not exist anymore, since there is no thin reaction where the combustion takes place. The intermediate distributed reactions regime is still characterized by the presence of a distinguishable flame front. Nevertheless, the Kolmogorov eddies are now able to penetrate the reaction zone and the latter results not so thin as to assume laminar flame properties to describe chemical reactions .

2.1.3 Turbulent Combustion Models

The Favre averaged system of equations describing turbulent flows, is generally expressed as follows:

- Conservation of Mass

$$\frac{\partial \overline{\rho}}{\partial t} + \frac{\partial \overline{\rho}\ \widetilde{u}_\alpha}{\partial x_\alpha} = 0 \tag{2.5}$$

- Conservation of Momentum

$$\overline{\rho}\frac{\partial\ \widetilde{u}_\alpha}{\partial t} + \overline{\rho}\ \widetilde{u}_\beta \frac{\partial\ \widetilde{u}_\alpha}{\partial x_\beta} = -\frac{\partial\ \overline{p}}{\partial x_\alpha} + \frac{\partial \overline{\tau}_{\alpha\beta}}{\partial x_\beta} + \overline{\rho}\ g_\alpha - \frac{\partial}{\partial x_\alpha}\left(\overline{\rho u''_\alpha u''_\beta}\right) \tag{2.6}$$

- Conservation of Energy

$$c_p\left(\bar{\rho}\frac{\partial\tilde{T}}{\partial t}+\bar{\rho}\,\tilde{u}_\alpha\frac{\partial\tilde{T}}{\partial x_\alpha}\right)=-\frac{\partial}{\partial x_\alpha}\bar{J}_{T,\alpha}+\frac{\partial\,\bar{p}}{\partial t}-\overline{\sum_{i=0}^{n}h_i\dot{m}_i}-\overline{q_r}-c_p\frac{\partial}{\partial x_\alpha}\left(\overline{\rho u_\alpha'' T''}\right) \qquad (2.7)$$

- Conservation of chemical species

$$\bar{\rho}\frac{\partial\tilde{Y}_i}{\partial t}+\bar{\rho}\,\tilde{u}_\alpha\frac{\partial\tilde{Y}_i}{\partial x_\alpha}=-\frac{\partial}{\partial x_\alpha}\bar{J}_{i,\alpha}+\overline{\dot{m}_i}-\frac{\partial}{\partial x_\alpha}\left(\overline{\rho u_\alpha'' Y_i''}\right) \qquad \text{i=1, n} \qquad (2.8)$$

- Equation of State (Perfect Gas)

$$\bar{p}=\bar{\rho}R\tilde{T}=(\gamma-1)\bar{\rho}\tilde{I} \qquad I = c_v T \qquad (2.9)$$

It is unclosed, due to the presence of two kinds of unknown terms. The first one is represented by the terms deriving from the mean operation of the product between two favre fluctuations $\left(\overline{\rho u_\alpha'' u_\beta''},\ \overline{\rho u_\alpha'' T''},\ \overline{\rho u_\alpha'' Y_i''}\right)$. Such terms have to be solved by the introduction of a proper turbulence model. Secondly, additional unknown quantities, $\dot{m}_i$ and $\overline{\sum_{i=0}^{n}h_i\dot{m}_i}$, derive from the presence of chemical reactions within the flow and cannot be represented by Arrhenius-type laws in a turbulent flow. Thus, the introduction of a proper combustion model is needed.

A turbulent combustion model calculates the reaction rate, $\dot{\omega}=\dot{m}_i=\frac{\partial[\ ]}{\partial t}$, which represent the rate of conversion of the generic chemical species. Since last years, several mathematical models have been introduced to describe the combustion process. A list and a brief description of them are here below reported:

- The *Zimont Model*, which describes the combustion process in terms of a single transport equation for a progress variable "c". The transport equation is

closed using a model to calculate the turbulent flame speed (s_T), derived using physically justified simplifications and dimensional analysis.

- The *Eddy-Break-Up (EBU) Model*, developed by Spalding [20], which calculates the mean reaction rate as only function of the turbulent quantities k (kinetic energy) and ε (kinetic energy dissipation rate). It was further developed by Magnussen e Hjertager [21] and referred to as *Eddy-Dissipation Model*.

- The *Abraham Model* [22], developed on the basis of EBU model, which calculates the mean reaction rate while taking into account for chemical reactions too. It is also commonly known as *Characteristic-Time Combustion (CTC) Model*.

- The *Bray-Moss-Libby (BML) Model* [23], which first introduces the two-zone hypothesis. The combustion chamber is divided into two separate regions (burned and unburned zone) by means of a flame front, which results to be so thin to assume laminar properties to model chemical reactions. The flame is corrugated by the action of the largest eddies but the smallest eddies cannot penetrate the flame (Ka < 1). Such a hypotesis follows the flamelet approach (Figure 2.2), that is why the BML model can be considered as the real ancestor of the flamelet models. It was further developed by Cant-AbuOrf [24] which introduced the progress variable "c" to describe the combustion process.

- The *flamelet models*, which follow the BML assumptions and describe the kinematic evolution of the flame front (*Coherent Flame Model*) or are based on a level set approach (*G-equation Model*).

- The *Pdf Models*, characterized by a statistical approach and wondering about the probability of the thermo-fluid-dynamic or chemical quantities having a certain value at a certain time, in a certain point of the computational domain.

- The *Eddy Dissipation Concept (EDC) Model*, assuming part of the fluid to be thoroughly mixed within a particular cell as well as to be the main driver for chemical reaction. These well mixed portions of a sub-volume, the so called "fine scales", are regarded to resemble a constant pressure reactor. That way the governing equations loose part of their complexity. Using the simplified equations for species conservation the corresponding source terms are derived from an Arrhenius-type reaction mechanism. It is particularly suitable to import detailed kinetic mechanisms.

The proper combustion model has to be chosen on the basis of the particular application field (Table 2.1).

<table>
<tr><th></th><th>Premixed Flames</th><th>Diffusive Flames</th><th>Partially Premixed Flames</th></tr>
<tr><td rowspan="3">Fast Chemistry</td><td>BML, Cant, CFM (Flamelet)</td><td rowspan="2">Mixture Fraction Model</td><td rowspan="2">Progress Variable
+
Mixture Fraction</td></tr>
<tr><td>Zimont (Progress variable)</td></tr>
<tr><td colspan="3">Eddy Break-Up Model (EBU)
Characteristic-Time Combustion (CTC)
Eddy Dissipation Model (EDM)</td></tr>
<tr><td>Finite Chemistry</td><td colspan="3">Eddy Dissipation Concept (EDC)
PDF Transport Model
G-Equation Model</td></tr>
</table>

Table 2. 1 Combustion models and their application field

If chemistry is infinitively fast in comparison with turbulent timescale, a model describing chemistry as a single-step reaction can be usefully considered. In particular, to simulate premixed flames, the flamelet approach is commonly followed. When chemistry is not infinitively fast or a more general model is required rather than the flamelet (i.e. for

the distributed reactions regime), PDF, EDC and G-equation Model are preferred. Such models allow taking into account for detailed kinetic mechanisms.

2.2 Overview on Dual-Fuel Combustion Simulation

First numerical activities on dual-fuel combustion and exhaust emissions, which are available on literature, have been mainly characterized by a multi-zone 0-dimensional (0-D) or quasi-dimensional approach [25-27].

In such studies the combustion chamber is usually divided into a certain number of zones representing the unburned and burned zones, or diesel premixed, diesel diffusive and NG combustion. Within each zone, no gradient of temperature, pressure or species concentration is considered and for the most simplified models no heat exchange between different zones is assumed. Even though such approaches well predict experimental data, they are not properly suitable to completely understand the dual-fuel combustion. Such a process is extremely complex and cannot avoid a locally-performed analysis of the interaction between diesel and natural gas combustion. Moreover the proper flow field has to be taken into account, since it widely influences the whole process, starting from the pilot injection and passing through the mixture formation and ignition up to the overall combustion.

In the last years, due to the improved calculation capability, a multi-dimensional CFD approach has been carried out on dual-fuel engines to analyze the in-cylinder processes.

Basic 3D analyses of dual-fuel combustion are reported in the literature. Reitz et al. [28,29] have used KIVA-3V code to simulate diesel ignition by means of the Shell Model and dual-fuel combustion by the CTC model. It is commonly utilized to describe diesel combustion but has been properly modified to take into account for NG as fuel in addition to oil. They have realized that, when the amount of NG increase (i.e. NG $\geq$ 90% of the total energy available), the CTC is not able to describe the flame propagation throughout the charge. Therefore they subsequently introduced a G-equation model to simulate overall combustion [30].

2.3 Modeling, Experiments and Interaction

The numerical activity performed during the present study has been mainly based on a multi-dimensional (3-D) approach. This choice is due to the complex phenomena involved in dual-fuel combustion, which is strongly characterized by the local interaction between the main fuel (NG) and its ignition source (the diesel pilot). Moreover, the actual 3-D flow field within the cylinder has to be considered to well describe all the physical processes occurring during a dual-fuel operation (diesel pilot injection, breakup, evaporation, auto-ignition, and overall combustion).

Nevertheless, a preliminary analysis of the behavior of the whole engine (here referred as "diagnostic" strategy) has been carried out by means of a 1-D approach, to get useful information on the dual-fuel combustion process, just having as input the experimental in-cylinder pressure traces. The calculated heat release curves have been then analyzed with the aim to detect and distinguish the single contribution of diesel fuel and NG to the overall combustion. The 1-D approach can also be considered a useful tool to put into evidence fluid-dynamic processes like the "short-circuit effect" and it also has been utilized to provide the correct pressure boundary condition for the subsequent 3-D analysis.

The latter has been carried out by analyzing three fundamental steps (flow field evolution, diesel spray evolution, diesel auto-ignition and overall combustion) and the numerical results have been compared with the experimental ones. Once the model is validated, the predictive approach can be undertaken. The engine key-parameters can be varied, their influence on engine performance can be easily put into evidence, and important guidelines can be provided for the future experimental procedures. In such a way, the interaction loop between experiments and modeling can be finally executed.

The present activity on dual-fuel engines has been performed in the framework of a collaboration between the Univesity of Rome Tor Vergata (UTV) and the Istituto Motori of the Italian National Research Council (IM-CNR), where the experimental tests have been carried out.

Chapter 3

COMPUTATIONAL TOOLS

3.1 Analysis of Overall Engine: the FW2001 Code

3.1.1 General Description

The integrated 0-D / 1-D framework FW2001 is an in-house developed code, since it has been entirely developed at UTV. It represents a simple and useful tool to simulate the behavior of the whole engine, from the intake to the exhaust, while being characterized by good predictive ability and reduced calculation time. The overall engine schematization leads to the definition of 0-D and 1-D elements (Figure 3.1).

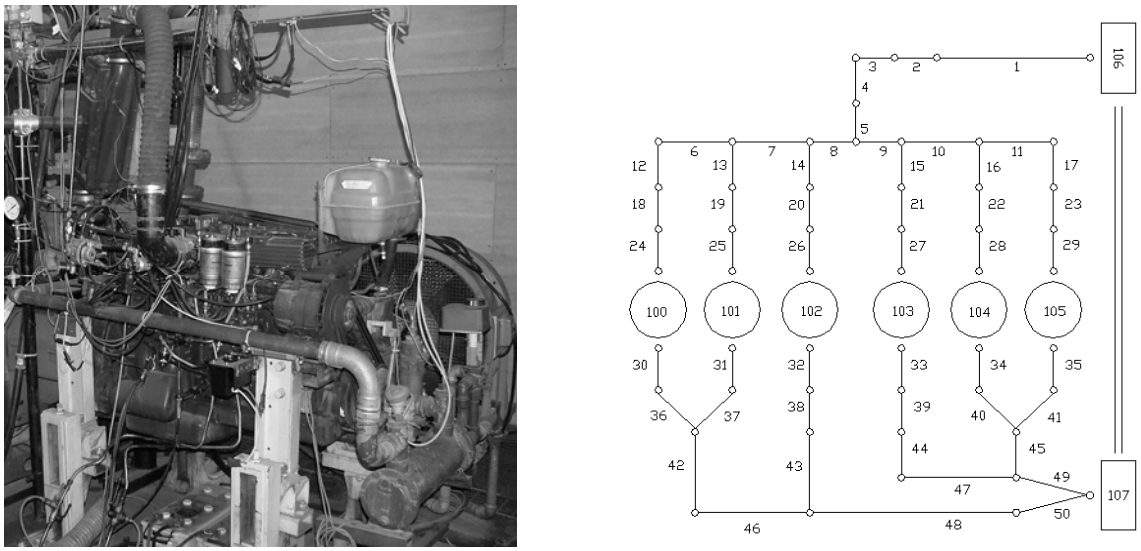

Figure 3. 1 The real engine and its schematization

Main feature of the 0-D elements is the uniformity of the thermo-fluid-dynamics properties. Accordingly, they are used to model capacities, cylinder-piston and all the elements characterized by uniform thermodynamic properties (Figure 3.2).

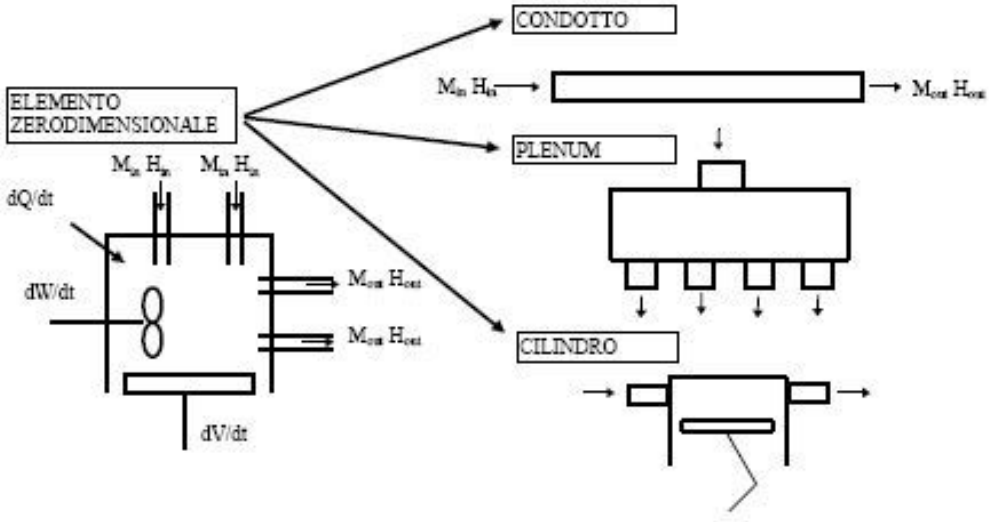

Figure 3. 2 0-D elements: an example

0-D elements are modeled as open system allowing the exchange of mass and energy with the external environment. Mass and enthalpy exchanges occur through the permeable sections characterized by flow velocities greater than zero. The study of a 0-D element needs the energy and mass conservation equations, as well as the knowledge of the following quantities:

- Volume variation and work
- Input and output exchange of mass and enthalpy
- Heat exchange at the cylinder walls
- Chemical Heat Release

Main feature of the 1-D elements is that the thermo-fluid-dynamics properties change along the element main direction, while keeping a constant value along the orthogonal section. Ducts and heat exchangers can be successfully represented by 1-D elements (Figure 3.3). The study of a 1-D element needs the energy, momentum and mass conservation equations.

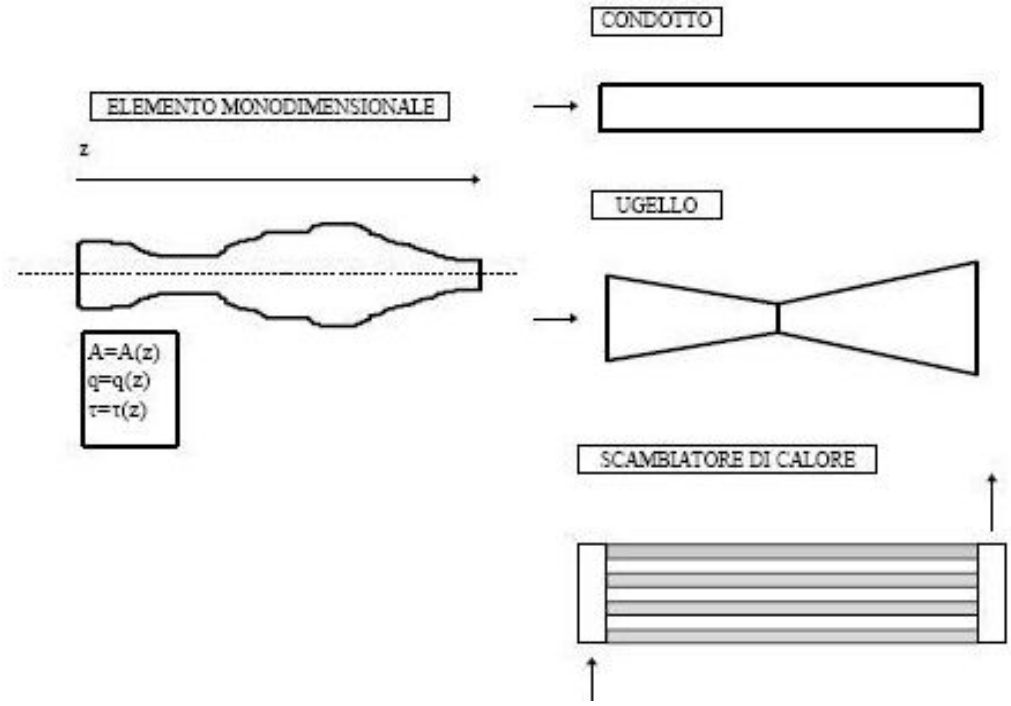

Figure 3. 3 1-D elements: an example

0-D and 1-D elements are coupled by means of joint elements, which allow for the information exchange between the elements. A coupling can be realized between 1-D elements, or between 0-D elements, as well as between different types of elements. A multiple joint can be realized as well (Figure 3.4).

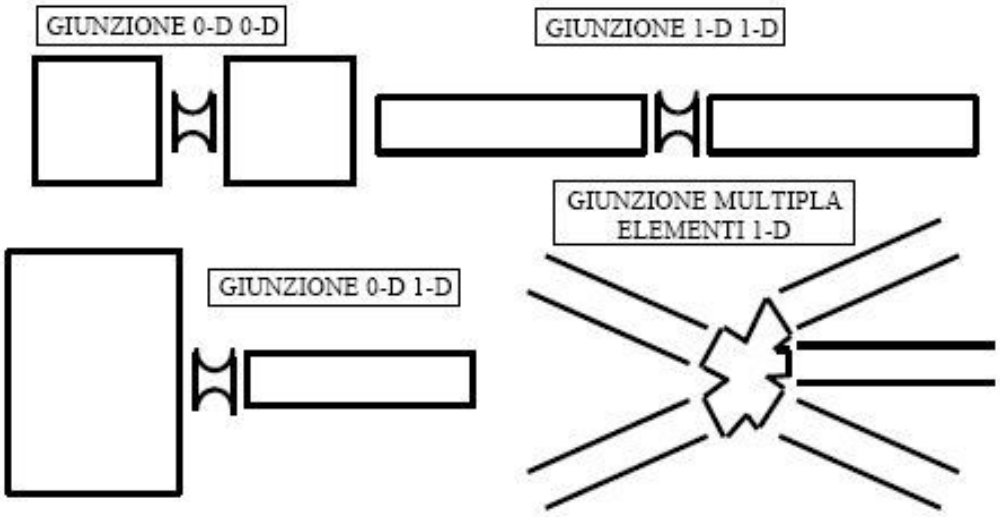

Figure 3. 4 Joint elements: an example

3.1.2 Solving Method

The sequence of operation that has to be followed is here below reported:

- Time-step calculation
- Crossing section updating
- Velocity updating
- Source terms updating
- Solution of 0-D joints
- Solution of 0-D 1-D joints
- Solution of multiple 1-D joints
- Solution within 1-D elements
- 1-D boundary conditions updating
- Solution within 0-D elements

In such a way the code structure results to be widely flexible. In fact, each element is individually handled and it is possible to utilize different solving methods for the same types of element or joint. Accordingly, more complex algorithm can be used to solve the most critical elements.

The basis equations that describe the mass, momentum and energy balance within the 1-D elements can be expressed in a compact differential form as follows:

$$\frac{\partial W}{\partial t} + \frac{\partial F}{\partial x} + S = 0 \tag{3.1}$$

$$W = \begin{pmatrix} \rho \\ \rho u \\ \rho \dfrac{u^2}{2} + \dfrac{p}{\gamma - 1} \end{pmatrix} \quad F = \begin{pmatrix} \rho u \\ \rho u^2 + p \\ \left(\rho \dfrac{u^2}{2} + \dfrac{kp}{\gamma - 1} \right) u \end{pmatrix} \quad S = \begin{pmatrix} \rho u \\ \rho u^2 \\ \left(\rho \dfrac{u^2}{2} + \dfrac{\gamma p}{\gamma - 1} \right) u \end{pmatrix} \frac{dA}{dx} \frac{1}{A} + \begin{pmatrix} 0 \\ \rho g \\ -\rho q \end{pmatrix} \tag{3.2}$$

where ρ, u, p, γ, A, g, q are respectively density, velocity, pressure, c_p/c_v ratio, section area, friction coefficient and thermal exchange coefficient. The set of differential

equations is solved through the two-step Lax-Wendroff scheme. This scheme is particularly reliable and describes optimally the propagation of pressure waves within ducts. The 0-D objects are analyzed solving the mass and energy conservation for open systems. The main hypotheses are:

- Space uniformity of the thermodynamic variables and the chemical species concentration within the 0-D element
- Mass flows incoming in the element instantaneously reach the stagnation conditions
- The flow field within the element is everywhere zero

Under these assumptions, the 0-D elements are analyzed through a filling-emptying model, based on the following equations:

$$\frac{d(X_i \rho V)}{dt} - \sum_k X_{k,i} \dot{m}_k = 0 \tag{3.3}$$

$$\frac{dE}{dt} = Q^* + \sum_k \dot{m}_k h_k - pV^* \tag{3.4}$$

where X_i, m, V*, E, Q* ,h_k, are respectively mass fraction, mass, volume variation, energy, heat rate, enthalpy. The joint elements represent the most critical elements of all fluid-dynamics sections. The calculation of the mass and energy fluxes is solved by means of characteristic lines and semi-empirical systems are to account for the loss coefficients. Each joint is characterized by two nodal points, which are connected through calculated loss coefficient. They are fixed through compatibility equations until attainment of the inlet and outlet mass balance. Once obtained mass balance, the objects extremities are fixed by characteristics lines, finding their thermodynamic parameters. The location of loss coefficients is obtained through experimental analysis, which characterizes the dependency on joint geometrical parameters and velocity values.

3.1.3 1-D Approach for Internal Combustion Engines

The proposed 1-D approach allows both predictive and diagnostic analysis of combustion.

A diagnostic approach, based on the heat release calculation can be utilized to analyze the experimental in-cylinder pressure data. To this aim, a single zone model [31], based on the First Law of Thermodynamics, can be used with the following assumptions:

- There is no distinction between burned and unburned zones
- Cylinder temperature and pressure are assumed to be uniform throughout the combustion chamber
- The charge composition does not vary during combustion
- The sensible enthalpy from fuel injection is negligible in comparison with the other terms
- The contents of the cylinder are modeled as an ideal gas
- The effect of the crevice regions, fuel heating and evaporation is negligible

Under the previous assumptions the First Law equation becomes:

$$dQ_{ghr} = \frac{\gamma}{\gamma - 1} pdV + \frac{1}{\gamma - 1} Vdp + dQ_{wall} \tag{3.5}$$

where dQ_{ghr} is the "gross" heat release, dQ_{wall} is the wall heat transfer, p is the measured cylinder pressure, V is the cylinder volume and γ is the ratio of the specific heats of the considered gas. The sum of the first and second terms on the right-hand member is usually referred as "net heat release" too. Heat transfer through cylinder walls is usually modeled by means of semi-empirical correlations:

$$\frac{dQ_{wall}}{dt} = h_c S(T_g - T_{wall}) \tag{3.6}$$

where S is the heat transfer, T_g is the charge temperature and T_{wall} is the wall temperature. The heat transfer coefficient h_c (W/m^{2}K) can be determined by the Woschni's correlation [32]:

$$h_c = 3.26 B^{-0.2} p^{0.8} T^{-0.5} w^{0.8} \tag{3.7}$$

where B is the cylinder bore and p, T and w are the cylinder pressure, temperature and mean velocity respectively. Mean velocity is defined as:

$$w = C_1 \overline{S}_p + C_2 \frac{V_d T_{rif}}{p_{rif} V_{rif}} (p - p_m) \tag{3.8}$$

where $\overline{S}_p$ represents the piston speed, V_d is the volume displaced, p_r, T_r and V_r are the cylinder pressure, temperature and volume at the reference state respectively, p is the cylinder pressure, whereas p_m is the cylinder pressure of the corresponding motored cycle. C_1 and C_2 constants are expressed as follows:

- $C_1 = 2.28$ and $C_2 = 0$ during compression stroke
- $C_1 = 2.28$ and $C_2 = 3.24 \cdot 10^{-3}$ during combustion and expansion stroke

The ratio of the specific heats $\gamma = c_p/c_v$, accordingly with the above assumptions, was considered as a function of the temperature only. The following equations are utilized to describe the dependence from temperature:

$$\gamma = \left(\frac{\overline{c_p}}{\overline{c_p} - R} \right) \tag{3.9}$$

$$\overline{c_p} = 3.636 - 1.337 \frac{T}{1000} + 3.294 \frac{T^2}{10^6} - 1.911 \frac{T^3}{10^9} + 0.275 \frac{T^4}{10^{12}} \quad (\mathrm{T} < 1000\ \mathrm{K}) \tag{3.10}$$

$$\overline{c_p} = 3.045 + 1.338\frac{T}{1000} - 0.488\frac{T^2}{10^6} + 0.085\frac{T^3}{10^9} - 0.006\frac{T^4}{10^{12}} \quad \text{(T > 1000 K)} \tag{3.11}$$

After the diagnostic approach has been carried out, a Wiebe's functions analysis can be performed to reproduce the calculated heat release rate curves, with the aim to identify the influence of the engine key-parameters on combustion. Secondly, a predictive strategy can be carried out by means of the FW2001. In this case, the numerical code needs the proper input data (a burning mass fraction law) required for the calculation of engine performance. Wiebe's functions are commonly used in the analysis of the combustion process of diesel engines. The rate of heat released from the combustion of diesel fuel is usually expressed as [33]:

$$\frac{dQ}{d\vartheta} = \frac{dQ_p}{d\vartheta} + \frac{dQ_d}{d\vartheta} \tag{3.12}$$

$$\frac{dQ_p}{d\vartheta} = 6.908\frac{M_p}{\theta_p}\left(f_p + 1\right)\left(\frac{\theta - \theta_0}{\theta_p}\right)^{f_p} exp\left[-6.908\left(\frac{\theta - \theta_0}{\theta_p}\right)^{f_p+1}\right] \tag{3.13}$$

$$\frac{dQ_d}{d\vartheta} = 6.908\frac{M_d}{\theta_d}\left(f_d + 1\right)\left(\frac{\theta - \theta_0}{\theta_d}\right)^{f_d} exp\left[-6.908\left(\frac{\theta - \theta_0}{\theta_d}\right)^{f_d+1}\right] \tag{3.14}$$

where the index *p* is referred to the fraction of diesel fuel injected that burns in premixed conditions while the index *d* is referred to the diffusive phase of combustion. Wiebe's functions are characterized by the presence of four main parameters, the crank angles duration of combustion θ_p and θ_d, and the shape factors f_p and f_d. M_p and M_d are the amounts of diesel oil that burn under premixed and diffusive conditions respectively. θ_0 represents the crank angle at the start of combustion. Typical values for a direct injection diesel engine are [34]:

$$\theta_p = 6.5 \div 7 \text{ CAD} \qquad m_p = 3 \qquad m_d = 0.5 \tag{3.15}$$

In order to simulate the heat release rate for a dual-fuel engine, a further Wiebe's function, similar to the previous ones, was introduced for the combustion of natural gas:

$$\frac{dQ_{gas}}{d\vartheta} = 5\frac{M_{gas}}{\theta_{gas}}\left(f_{gas}+1\right)\left(\frac{\theta-\theta_0}{\theta_{gas}}\right)^{f_{gas}} exp\left[-5\left(\frac{\theta-\theta_0}{\theta_{gas}}\right)^{f_{gas}+1}\right] \tag{3.16}$$

Accordingly, the eq. 3.12 becomes:

$$\frac{dQ}{d\vartheta} = \frac{dQ_p}{d\vartheta} + \frac{dQ_d}{d\vartheta} + \frac{dQ_{gas}}{d\vartheta} \tag{3.17}$$

A typical value for a spark ignition engine is $f_{gas} = 2$, while θ_{gas} mainly depends on the equivalence ratio of the air/natural gas mixture. In Figure 3.5, typical heat release rate curves, obtained by means of the Wiebe's functions, are reported for both (full-diesel and dual-fuel) cases. The standard Wiebe analysis allows to fit the heat release rate curves only for limiting full-diesel and natural gas spark ignition conditions. In dual-fuel modality, Wiebe's parameters are widely modified by the contemporaneous presence of oil and gas into the combustion chamber.

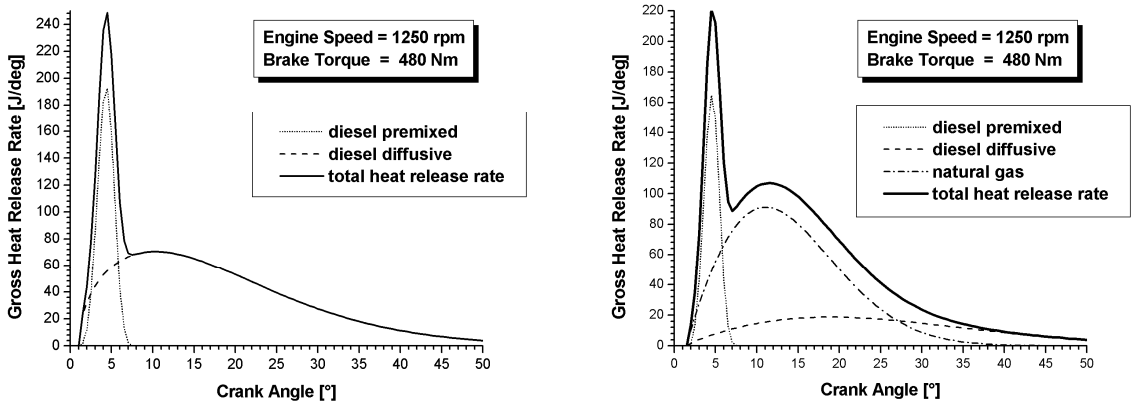

Figure 3. 5 Wiebe's function approximation of the heat release rate curve for diesel and dual-fuel case

FW2001 has been successfully used to predict SI engine performance with regard to simple combustion chamber geometries [35-37]. However, when complicated geometries are concerned, a more detailed (3D) approach is desirable to take into proper account non-axial-symmetric chambers. Nevertheless, FW2001 can be successfully used to simulate the presence of the overall engine ducts and devices, in order to provide, starting from the experimental pressure trace, the actual and time dependent boundary conditions to the 3D code, which in turn computes the 3D chamber and intake-exhaust duct fluid dynamics.

3.2 Analysis of In-Cylinder Processes: the KIVA-3V Code

3.2.1 General Description

The multi-dimensional CFD (Computational Fluid-Dynamics) KIVA-3V code, developed at the Los Alamos American National Laboratory, solves the conservation of mass, momentum, energy and species equations for turbulent and reacting flows.

It follows a Finite Volume Method (FVM), and is able to manage structured and moving grids. In this way it is possible to reproduce the real motion of piston and valves. Temporal and spatial differencing is managed by using semi-implicit quasi second order up-winding approaches with the Arbitrary Lagrangian Eulerian (ALE) algorithm. A KIVA's inviting characteristic is that it is an "open sources" code, which can be modified as the user likes.

The first public release [38] of KIVA was made in 1985 through the American National Energy Software Center, at Argonne National Laboratory, which served at the time as the official distribution center for DOE-sponsored software. The Los Alamos team and other users worldwide soon began testing KIVA in a broad variety of applications. Over time a significant number of papers were presented, each focusing on some aspect of the model and often offering extensions and improvements. The model itself was gradually being made more efficient and realistic, resulting in the public release in 1989 of the improved version previously mentioned, called KIVA-II [39].

KIVA-II extends and enhances the earlier KIVA-II code, improving the computational accuracy and efficiency and its ease of use. The KIVA-II equations and numerical solution procedure are very general and can be applied to laminar or turbulent flows, subsonic or supersonic flows, and single-phase or dispersed two-phase flows. Arbitrary numbers of species and chemical reactions are allowed. A stochastic particle method is used to calculate evaporating liquid sprays, including the effects of droplet collisions and aerodynamic breakups. Although the initial and boundary conditions and mesh generation have been written for internal combustion engine calculations, the logic for these specifications can be easily modified for a variety of other applications.

The KIVA computer program consists of a set of subroutines controlled by a short main program. The general original structure of KIVA-II is illustrated in Figure 3.6, showing a top-to-bottom flow encompassing the entire calculation. Beside each box in the flow diagram appears the name(s) of the primary subroutines(s) responsible for the associated task. In addition to the primary subroutines, Figure 3.6 also identifies a number of supporting subroutines that perform tasks for the primaries.

A cycle is performed in three phases. Phases A and B together constitute a Lagrangian calculation in which computational cells move with the fluid. Phase A is an explicit calculation of spray droplet collision and oscillation/breakup terms and mass and energy source terms due to the chemistry and spray. Phase B calculates in a coupled, implicit fashion the acoustic mode terms (namely the pressure gradient in the momentum equation and velocity dilatation terms in mass and energy equations), the spray momentum source term, and the terms due to diffusion of mass, momentum, and energy. Phase B also calculates the remaining source terms in the turbulence equations. In Phase C (Eulerian calculation), the flow field is frozen and rezoned or remapped onto a new computational mesh.

Such a mixed (Lagrangian - Eulerian) approach allows to well manage moving grid, since the rezone (C) eulerian phase allows to avoid the excessive cell deformation, taking place during the lagrangian phase. Thus, internal combustion engines (characterized by the motion of the piston) can be easily simulated.

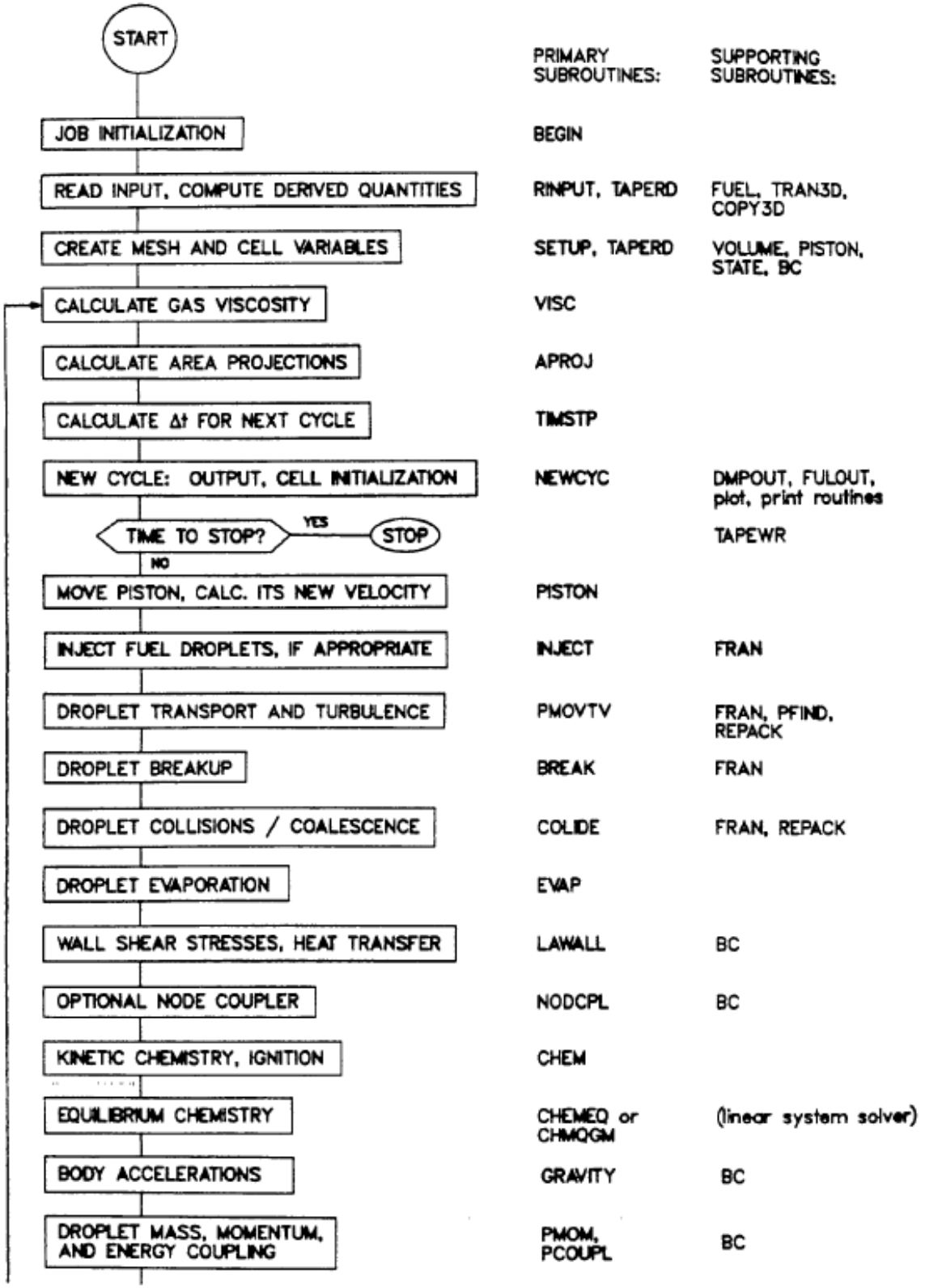

Figure 3. 6 General flow diagram for the KIVA program

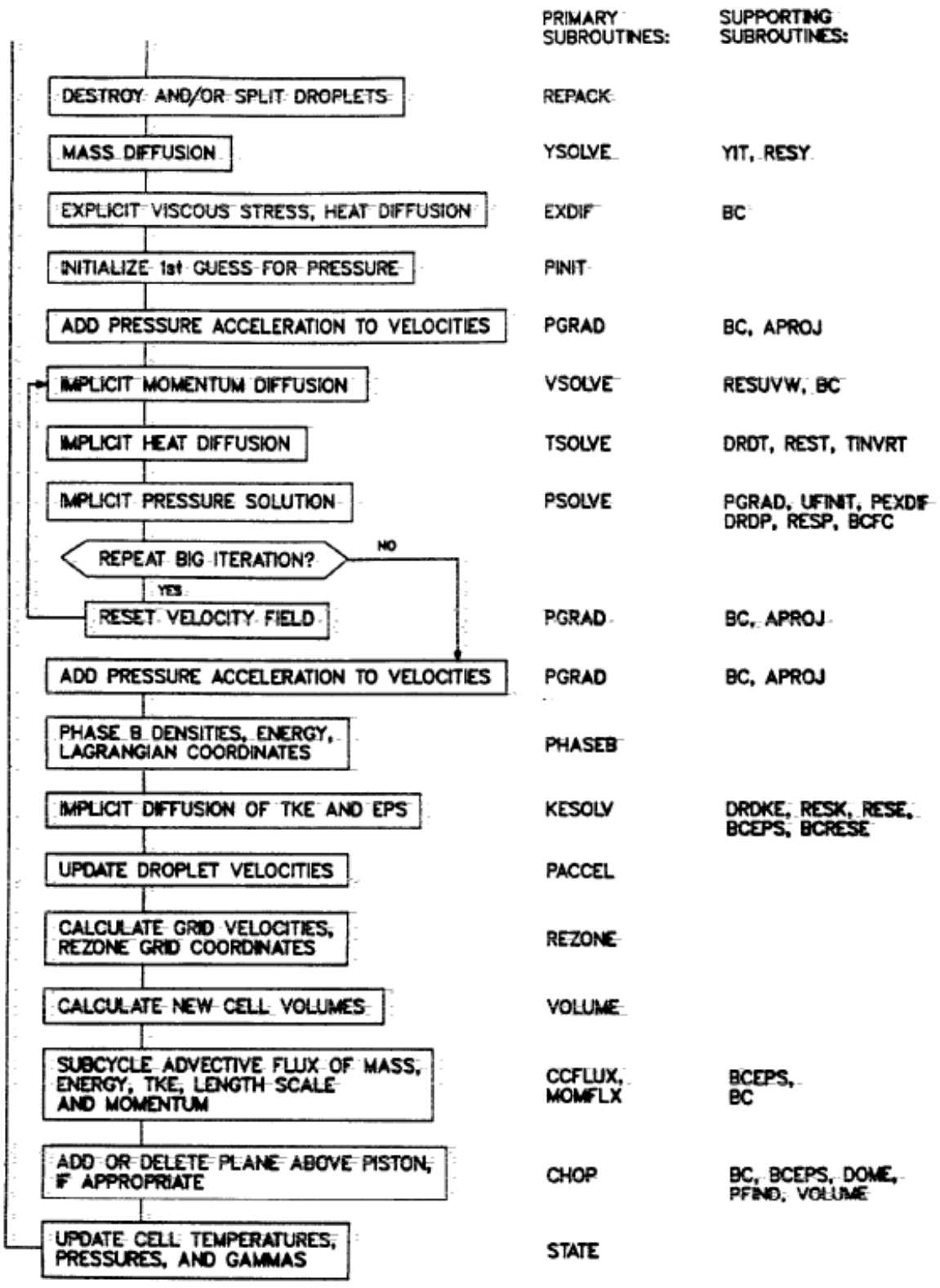

Figure 3. 6 continued

The two earlier versions of KIVA lend themselves well to confined in-cylinder flows and to a variety of open combustion systems, but they can become quite inefficient to use in complex geometries that contain such features as inlet ports and moving valves, diesel pre-chambers, and entire transfer ports. In these code versions, the entire domain of interest must be encompassed by a single block of computational zones, which may require that a significant number of zones be deactivated.

The latest version of KIVA, known as KIVA-3, is intended to overcome this deficiency [40]. It differs from KIVA-II in that it uses a multi-block structured grid, which allows complex geometries to be modeled with far greater efficiency than KIVA-II, because discrete blocks of zones can now be coupled together to build the required structure. Figure 3.7 shows a computing mesh for a KIVA-3 model of a two-stroke engine.

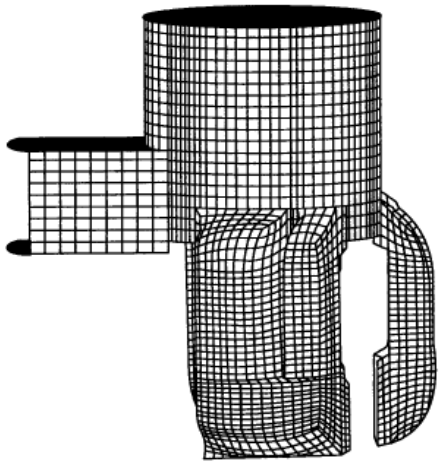

Figure 3. 7 An example of a multi-block structured grid

The last extended version of KIVA-3, known as KIVA-3V [41], also can model any number of vertical or canted valves in the cylinder head of an internal combustion engine (Figure 3.8). The valves are treated as solid objects that move through the mesh using the familiar "snapper" technique used for piston motion in KIVA-3.

The only difference is that during the piston motion, some planes in the mesh are activated (with the piston moving down) or deactivated (piston moving up). On the contrary, when the valve moves through the mesh, the planes are simply passed from the bottom valve face to the top one (valve moving down) and vice versa.

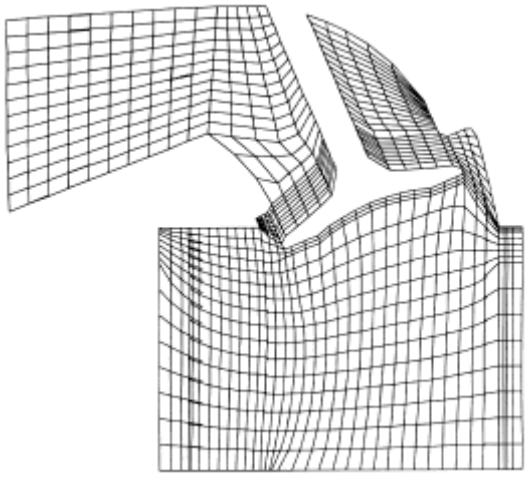

Figure 3. 8 The introduction of valves in the KIVA-3V version

Because the valve motion is modeled exactly, and the valve shapes are as exact as the grid resolution will allow, the accuracy of the valve model is commensurate with that of the rest of the program.

Other new features in KIVA-3V include a particle-based liquid wall film model, a new sorting subroutine that is linear in the number of nodes and preserves the original storage sequence, a mixing-controlled turbulent combustion model, and an optional RNG k-ε turbulence model. All features and capabilities of the previous KIVA-3 and KIVA-II versions have been retained.

KIVA-3V has been used to successfully model gasoline, diesel and NG fuelled engines since its inception, and still represents the best code to simulate in cylinder processes. Nevertheless, some modifications are needed to improve its predictive capabilities.

Once again, the reader has reminded that the KIVA code is fully open sources. Thus, every subroutine can be easily modified and any sub-model can be directly introduced within the main program. One the contrary, the commercial programs are sold for profit, and the original source code is generally unavailable to the user. What is being marketed is the object code, a “black box” that has been tailored to the user’s requirements, backed up with service and consultation. In contrast to commercial programs, the relatively low cost and ready availability of the source code has created a wide KIVA user community, particularly through the engineering schools and

universities. What the KIVA user forfeits is service and consultation, because the Los Alamos team has few resources and therefore must work primarily with its direct collaborators. The KIVA user also has to contend with a basic research tool that cannot be treated as a black box. Its use requires a non-trivial level of sophistication and experience with CFD modeling, along with a good grasp of spray and combustion theory, but these same abilities are also required if one is to make the best use of a commercial program.

According to the previous consideration, within the present work, a modified version of the KIVA-3V code is proposed. An improved rezoning algorithm [42] has been utilized to ensure a regular mesh during the overall piston and valve motion, and the original k-ε approach of KIVA has been utilized to model the in-cylinder turbulence. Moreover, with the aim to simulate the combustion process in the dual-fuel engines, further models have been introduced to better represent the spray breakup, the diesel pilot ignition and the overall combustion. A description of the main utilized sub-models is here below reported.

3.2.2 Turbulence Modeling

In this study, the standard k-ε model [43] was utilized to model the unknown terms $\left(\overline{\rho u_\alpha'' u_\beta''},\ \overline{\rho u_\alpha'' T''},\ \overline{\rho u_\alpha'' Y_i''}\right)$ of the conservation equations of momentum, energy and chemical species (eq. 2.6, 2.7, 2.8). The k-ε model is already implemented in the original version of the KIVA code. It is based on the assumption of a newtonian proportional relation between the turbulent stresses and a fictitious turbulent viscosity $\mu_t = \rho \nu_t$:

$$\overline{\rho u_\alpha'' u_\beta''} = \begin{cases} -\overline{\rho}\ \widetilde{\nu}_t \left[2\dfrac{\partial\ \widetilde{u}_\alpha}{\partial\ x_\beta} - \dfrac{2}{3}\dfrac{\partial\ \widetilde{u}_\gamma}{\partial\ x_\gamma} \right] & \text{if } \alpha = \beta \\ -\overline{\rho}\ \widetilde{\nu}_t \left[2\dfrac{\partial\ \widetilde{u}_\alpha}{\partial\ x_\beta} - \dfrac{2}{3}\dfrac{\partial\ \widetilde{u}_\gamma}{\partial\ x_\gamma} \right] & \text{if } \alpha \neq \beta \end{cases} \tag{3.18}$$

$$\overline{\rho u_\alpha'' T''} = -\overline{\rho}\frac{\widetilde{\nu}_t}{\sigma_t}\frac{\partial\ \widetilde{T}}{\partial\ x_\alpha} \tag{3.19}$$

$$\overline{\rho u_\alpha'' Y_i''} = -\overline{\rho}\frac{\widetilde{\nu}_t}{\sigma_t}\frac{\partial\ \widetilde{Y}_i}{\partial\ x_\alpha} \tag{3.20}$$

The eddy viscosity ν_t is modeled as:

$$\widetilde{\nu}_t = c_\mu \frac{\widetilde{k}^2}{\widetilde{\varepsilon}} \tag{3.21}$$

$$c_\mu = 0.09 \tag{3.22}$$

Accordingly, two new quantity are introduced, the kinetic energy $\widetilde{k} = \frac{\overline{u_\alpha'' u_\alpha''}}{2}$ and its dissipation rate $\widetilde{\varepsilon} = c_\mu^{\frac{3}{4}} \frac{\widetilde{k}^{\frac{3}{2}}}{L_I}$, which need to be solved by means of two further transport equations:

$$\overline{\rho}\frac{\partial \widetilde{k}}{\partial t} + \overline{\rho}\widetilde{u}_\beta \frac{\partial \widetilde{k}}{\partial x_\beta} = -\frac{\partial}{\partial x_\alpha}\left(\overline{\rho}\widetilde{\nu}_t \frac{\partial \widetilde{k}}{\partial x_\alpha}\right) - \overline{\rho u_\alpha'' u_\beta''}\frac{\partial \widetilde{u}_\alpha}{\partial x_\beta} - \overline{\rho}\widetilde{\varepsilon} - \widetilde{\nu}_t \frac{\partial \ln \overline{\rho}}{\partial x_\alpha}\frac{\partial \overline{p}}{\partial x_\alpha} \tag{3.23}$$

$$\overline{\rho}\frac{\partial \widetilde{\varepsilon}}{\partial t} + \overline{\rho}\widetilde{u}_\beta \frac{\partial \widetilde{\varepsilon}}{\partial x_\beta} = -\frac{\partial}{\partial x_\alpha}\left(\overline{\rho}\frac{\widetilde{\nu}_t}{\sigma_\varepsilon}\frac{\partial \widetilde{k}}{\partial x_\alpha}\right) - c_{\varepsilon 1}\frac{\widetilde{\varepsilon}}{\widetilde{k}}\overline{\rho u_\alpha'' u_\beta''}\frac{\partial \widetilde{u}_\alpha}{\partial x_\beta} - c_{\varepsilon 2}\overline{\rho}\frac{\widetilde{\varepsilon}^2}{\widetilde{k}} - c_{\varepsilon 3}\widetilde{\nu}_t \frac{\partial \ln \overline{\rho}}{\partial x_\alpha}\frac{\partial \overline{p}}{\partial x_\alpha} \tag{3.24}$$

where the following values are assumed for the model constants:

$$\sigma_\varepsilon = 1.3 \qquad c_{\varepsilon 1} = 1.44 \qquad c_{\varepsilon 2} = 1.92 \qquad c_{\varepsilon 3} = 1.0 \tag{3.25}$$

3.2.3 Spray Breakup Modeling

In the present work, the WAVE model, developed by Reitz and Bracco [44,45], has been introduced and implemented within the KIVA code to represent both the primary breakup (liquid atomization) and the secondary breakup (drop breakup) processes.

Main assumption of the WAVE model is that atomization of the injected liquid is the result of the aerodynamic interaction between the liquid jet and the surrounding gas. Such interaction leads to the propagation of unstable waves on the surface (Figure 3.9) of the liquid jet, which is supposed to be infinite in the axial (z) direction. The analysis starts by imposing on the surface an infinitesimal disturbance.

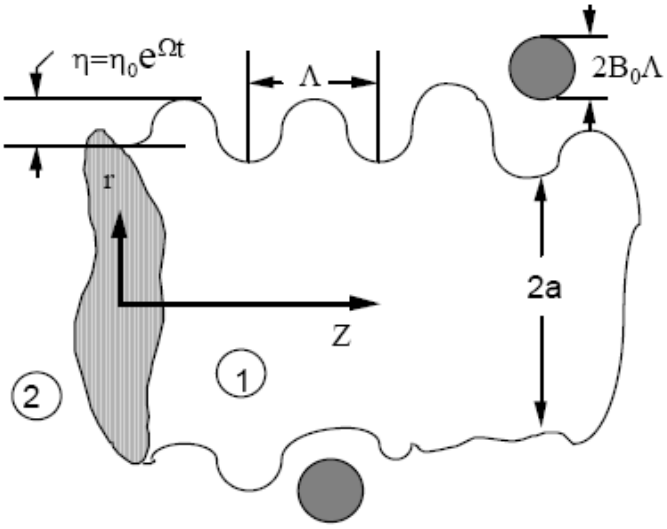

Figure 3. 9 A schematization of the atomization process

The WAVE model computes breakup by using results from a stability analysis. The results indicate that there is a maximum wave growth rate, Ω, that occurs at a wave length of Λ. The maximum wave growth rate and the corresponding wavelength characterize the fastest growing (or most probable) waves on the liquid surface which are thought to be eventually responsible for the breakup. Accordingly, the breakup time is equal to:

$$\tau = \frac{3.788 B_1 a}{\Omega \Lambda} \tag{3.26}$$

Where B_1 is the breakup time constant, a is the undisturbed jet radius and the following relations are valid:

$$\Omega \left(\frac{\rho_l a^3}{\sigma} \right)^{0.5} = \frac{0.34 + 0.38\,\mathrm{We}_g^{1.5}}{(1+\mathrm{Z})(1+1.4\mathrm{T}^{0.6})} \tag{3.27}$$

$$\frac{\Lambda}{a} = 9.02 \frac{(1+0.45\mathrm{Z}^{0.5})(1+0.4\mathrm{T}^{0.7})}{(1+0.87\,\mathrm{We}_g^{1.67})^{0.6}} \tag{3.28}$$

where $\mathrm{Z} = \mathrm{We}_l^{0.5}/\mathrm{Re}_l$ is the Ohnesorge number and $\mathrm{T} = \mathrm{Z}\cdot\mathrm{We}_g^{0.5}$. The indexes *l* and *g* are referred to the liquid jet and the surrounding gas respectively. As it can be seen, the maximum wave growth rate increases and the corresponding wavelength decreases rapidly with increasing Weber number. The effect of viscosity which appears in the Ohnesorge number is seen to reduce the wave growth rate and increase the wave length significantly as the liquid viscosity increases.

Reitz and Diwakar [46] applied the “wave” atomization theory to drop breakup modeling. The injection of liquid jet is simulated through the introduction of a sequence of liquid discrete parcels (blobs) having size equal to the diameter of the nozzle hole (Figure 3.10).

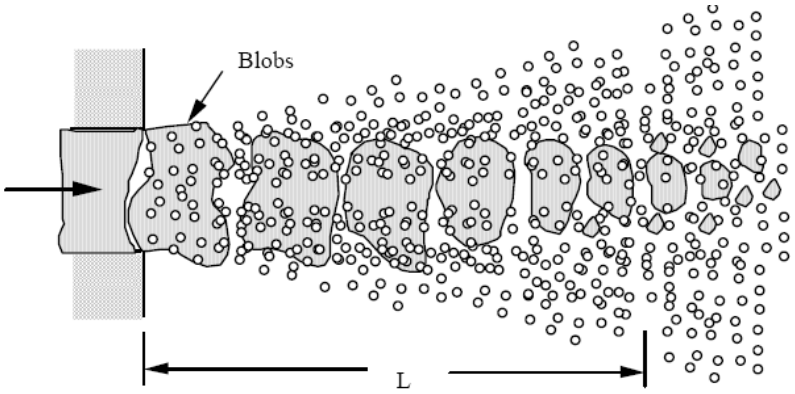

Figure 3. 10 "Blob" injection breakup model (Reitz and Diwakar)

The previous assumption allows to reduce the uncertainties bound up with the initial size of the droplets. The mass of new droplets formed due to breakup is subtracted from the parent drop. The change of parent drop radius is:

$$\frac{da}{dt} = -\frac{(a-r)}{\tau} \tag{3.29}$$

The WAVE model assumes that the new droplets generated from the parent drop have a radius *r* equal to:

$$\begin{cases} r = B_0 \Lambda & \text{if } (B_0 A \le a) \\ r = \min \begin{cases} (3\pi a^2 U / 2\Omega)^{0.33} \\ (3a^2 \Lambda / 4)^{0.33} \end{cases} & \text{if } (B_0 A > a, \textit{only one time}) \end{cases} \tag{3.30}$$

The recommended value for B_0 is set equal to 0.61 for diesel sprays, whereas the breakup time constant B_1 is related to the initial disturbance level in the breakup process and to wall impingement effects. Suggested values are B_1 = (10 ÷ 60) when low turbulence and low wall impingement are expected and $B_1 < 10$ vice versa.

In addition to the aerodynamic interaction, other possible sources of liquid atomization are cavitation (Arcoumanis model) and turbulent flow (Huh and Gosman model) in the nozzle. The present study does not consider such effects because they are particularly relevant for high speed breakup (high injection pressure, like in modern common rail systems), while the examined engine is characterized by a mechanical diesel injection (the injection pressure is about 240 bar).

For the same reason the contribution of drop distortion to breakup process was also neglected, and the authors decided to not completely test other available breakup models like TAB [47] (the original breakup model implemented in KIVA-3V) and DDB (a modified version of TAB developed by Ibrahim et al. [48]).

3.2.4 Ignition Modeling

The Shell model, developed by Halsted et al. [49], was originally drawn up to describe knock phenomenon in gasoline engines, even though it subsequently was successfully used to simulate ignition in diesel engines [50,51]. It describes the auto-ignition of hydrocarbon fuels by means of a simplified reaction mechanism, characterized by eight single-step reactions involving five generic species:

Initiation:

$RH + O_2 \rightarrow 2R^*$ kinetic coeff. K_q (3.31)

Propagation:

$R^* \rightarrow R^* + P + Heat$ kinetic coeff. K_p (3.32)

$R^* \rightarrow R^* + B$ kinetic coeff. $f_1 * K_p$ (3.33)

$R^* \rightarrow R^* + Q$ kinetic coeff. $f_4 * K_p$ (3.34)

$R^* + Q \rightarrow R^* + B$ kinetic coeff. $f_2 * K_p$ (3.35)

Branching:

$B \rightarrow 2R^*$ kinetic coeff. K_b (3.36)

Termination:

$R^* \rightarrow inert$ kinetic coeff. $f_3 * K_p$ (3.37)

$2R^* \rightarrow inert$ kinetic coeff. K_t (3.38)

The term RH represent the hydrocarbon fuel (C_nH_{2m}). N-heptane (C_7H_{16}) was utilized as the vaporizing species representing diesel fuel. R* is the radical formed from the fuel, B is the branching agent, Q is an intermediate specie, while P represents the oxidized products (CO, CO_2 and H_2O).

The premise of the Shell model is that degenerate branching plays an important role in determining the cool flame and two-stage ignition phenomena that are observed during the auto-ignition of hydrocarbon fuels. Some interpretations of these generic species have

been proposed. The branching agent B is related to hydroperoxides (RO_2H) at low temperatures and to hydrogen peroxides (H_2O_2) at high temperatures. The intermediate species Q is related to aldehydes (RCHO) during the first induction period and to the alkylperoxy radical (HO_2) and its isomerization products during the second induction period. The formation of intermediate species is the crucial reaction leading to the production of branching agent, which in turn induces hot ignition.

The rate constants in Eqs. (3.31-3.38) are defined as follows:

$$f_i = A_{fi}\exp\left(-E_{fi}/RT\right)[\mathrm{O_2}]^{xi}[\mathrm{RH}]^{yi} \tag{3.39}$$

$$K_j = A_j\exp\left(-E_j/RT\right) \tag{3.40}$$

$$K_p = \left[\frac{1}{K_{p1}[\mathrm{O_2}]} + \frac{1}{K_{p2}} + \frac{1}{K_{p3}[\mathrm{RH}]}\right]^{-1} \tag{3.41}$$

where j stands for p_1, p_2, p_3, q, b and t. Details on Shell implementation and the utilized values for A_{fi}, E_{fi}, x_i, y_i, A_j and E_j can be found in previous papers. [49,50]

Ignition process was assumed to occur in the local diesel/air equivalence ratio range between 0.5 and 3.0 [52]. The Shell model can be considered as a reliable tool to describe only the low-temperature chemistry of hydrocarbon fuels and its validity range usually goes up to temperature values close to 1000÷1100 K. Once exceeded such value, the Shell model has to be switched off. Within the present work the switch temperature was set as 1000 K.

The Shell model simulates diesel auto-ignition, thus only n-heptane was considered as fuel. Once diesel fuel ignited, a proper combustion model has to be introduced. A possible approach is to extend the validity of a typical diesel combustion model (CTC) to dual-fuel operations.

When a low amount of diesel oil is utilized (high NG percentage), also a flame propagation model (CFM) can be used to describe NG combustion only, starting from the ignition zones.

3.2.5 Combustion Modeling

CTC Model. The Characteristic-Time Combustion (CTC) model was originally introduced for SI engine modeling [53] and subsequently extended to study diesel combustion [51]. It involves seven species (fuel, O_2, N_2, CO_2, CO, H_2 and H_2O), and assumes that the rate of change of the mass fraction Y_m of the generic species m is given by:

$$\frac{dY_m}{dt} = -\frac{Y_m - Y_m^*}{\tau_c} \tag{3.42}$$

where Y_m^* is the local and instantaneous thermodynamic equilibrium value of Y_m and τ_c is the characteristic time, given by:

$$\tau_c = \tau_l + f\tau_t \tag{3.43}$$

where τ_l and τ_t are the laminar and the turbulent timescales respectively. The coefficient *f* accounts for the influence of turbulence on combustion and works as a switch between laminar and turbulent combustion after ignition. The laminar timescale is calculated from the one-step reaction rate and is equal to:

$$\tau_l = \mathrm{A}^{-1}\left[\mathrm{C_7H_{16}}\right]^{0.75}\left[\mathrm{O_2}\right]^{-1.5}\exp\left(E/RT\right) \tag{3.44}$$

where $A=2.868\cdot10^9$ (SI unit) is the pre-exponential factor and E=125.6 kJ/mol is the activation energy. The turbulent timescale is modeled as:

$$\tau_t = \mathrm{C}_2 \frac{k}{\varepsilon} \tag{3.45}$$

where the standard k-ε model is used to describe turbulence into the cylinder and to calculate k and ε and C_2 is the CTC model constant. The switch factor *f* varies from 0 to 1 according with the ratio of combustion products r as follows:

$$f = \frac{1 - e^{-r}}{0.632} \tag{3.46}$$

$$r = \frac{Y_{CO_2} + Y_{H_2O} + Y_{CO} + Y_{H_2}}{1 - Y_{N_2}} \tag{3.47}$$

Thus the early combustion lies on laminar regime, while turbulence becomes more important later on, when combustion products are not negligible. In this study, the CTC model was modified to account for dual-fuel combustion. Both fuels (n-heptane and NG) are considered to compute the equilibrium mass fraction of each species and are burnt according to their proportions. Also the respective values of lower heating value are considered for diesel and NG combustion.

CFM Model. The Coherent Flame Model (CFM) was first introduced by Marble and Broadwell [54] and later extended [55,56]. Its formulation is based on the hypothesis of flamelet combustion, originally developed by Williams [57], Peters [58] and Mantel and Borghi [59]. The generalized flamelet assumption requires that chemical reactions take place in thin sheets which propagate at the laminar flame speed. The chemical reaction of fuel oxidation is supposed to occur in this very thin layer separating the burned and unburned gases. Although the flame thickness increases once the mixture is in a certain lean range, the role of chemical kinetics is more important. By examining flames at different equivalence ratios, it was shown that combustion can still occur in laminar flamelets. This implies that the chemical time scale is short in comparison with

the turbulent time scale, and therefore the chemistry can be decoupled from the turbulence. The mean reaction rate then can be expressed by:

$$\omega = \rho_u Y_{F,u} S_L \Sigma \tag{3.48}$$

In the mean reaction rate model two unknown parameters appear: the flame laminar speed S_L and the flame surface per unit volume Σ. The former depends strictly on local thermo-chemical variables, even if its modeling recently received considerable attention to take into account stretch and curvature effects by using DNS [60-63]. In this paper it is calculated through the following equations [24]:

$$S_L(T_u, p, \varphi) = S_{L0}\left(\frac{T_u}{T_0}\right)^{\alpha_k}\left(\frac{p}{p_0}\right)^{\beta_k} \tag{3.49}$$

where $S_{L,0}$ is the unscratched laminar burning velocity at room temperature and pressure expressed as a function of the equivalence ratio as:

$$S_{L0}(\phi) = a_k \phi^{b_k} \exp\left[-c_k(\phi - d_k)^2\right] \tag{3.50}$$

where a_k, b_k, c_k, d_k, α_k and β_k are constants depending on the fuel. Values are given for methane and other fuels in [64] The latter term Σ can be described by an exact transport equation:

$$\frac{\partial \Sigma}{\partial t} + \nabla \cdot v_F \Sigma = (\nabla \cdot v_F - nn : \nabla v_F)\Sigma \tag{3.51}$$

where v_F is the velocity of the flame surface, given by the sum of the velocity and the flame propagation speed in the normal direction, and n is the unit normal vector to the flame surface. In a turbulent flow field the Σ equation becomes:

$$\frac{\partial \overline{\Sigma}}{\partial t} + \nabla \cdot \overline{v}\overline{\Sigma} + \nabla \cdot v'\overline{\Sigma} + \nabla \cdot \left(S_L n\right)\overline{\Sigma} = k_S \overline{\Sigma} \tag{3.52}$$

where $\overline{\Sigma}$ is the mean surface value, $\overline{\nu}$ and ν' the Favre mean and fluctuating velocities, k_S is the turbulent flame stretch. The basic physical processes are represented by three transport terms on the LHS (mean flow, turbulence and flame propagation), while on the RHS production and destruction terms depend on flame stretch. Modeling assumptions are needed for turbulent transport and flame-stretch terms. A general form of the modeled transport equation is here reported:

$$\frac{\partial \overline{\Sigma}}{\partial t} + \nabla \cdot \overline{v}\overline{\Sigma} = S - D + \nabla \cdot \left(\frac{\nu_t}{\sigma_\Sigma} \nabla \cdot \overline{\Sigma} \right) \tag{3.53}$$

where S represents the source term corresponding to the flame stretch induced by the turbulent eddies, and D represents the destruction term which comes from the burnout of the flame. Substituting the CFM modeling assumptions, the final equation gives:

$$\frac{\partial \overline{\Sigma}}{\partial t} + \nabla \cdot \overline{v}\overline{\Sigma} = \alpha e \overline{\Sigma} - \frac{\beta \rho_u S_L \overline{\Sigma}^2}{\rho Y_F} + \nabla \cdot \left(\frac{\nu_t}{\sigma_\Sigma} \nabla \cdot \overline{\Sigma} \right) \tag{3.54}$$

where e represents the mean strain rate (equal to $c_e\varepsilon/k$, c_e being a constant equal to 5), and α and β are the model constants. Normally a further term $-\nabla \cdot \overline{\nu}\ \overline{\Sigma}$ is added to take into account the compressibility effects.

Since the flamelet assumption leads to a separation between flame and turbulent scales, all the chemical reactions can be summarized into the S_L quantity, and this model can behave satisfactorily by keeping track of two species: the unburned and the burned mixtures.

The CFM model has been applied successfully [65,66] to model combustion by means of flame propagation mechanism and has provided significant results in terms of predictive reliability and results accuracy.

Chapter 4

EXPERIMENTS ON DUAL-FUEL ENGINES

4.1 Experimental Apparatus

For the experimental activities, a dedicated test bed has been prepared at the Istituto Motori of the Italian National Research Council in Naples, where the dual-fuel conversion of the IVECO 8360.46R heavy-duty diesel engine, used for public transportation, has been carried out by means of the ETRA equipment.

Main characteristics of the engine are listed in Table 4.1.

Item	**Specification**
Engine	IVECO 8360.46R
Type	4 Stroke CI
Number of Cylinders	6 Inline
Stroke	130 mm
Bore	112 mm
Volume Displacement	7.8 l
Compression Ratio	17.6 : 1
Maximum Power	166 kW @ 2050 rpm
Maximum Torque	965 Nm @ 1250 rpm
Diesel Injection System	Mechanical Direct (240 bar)
Turbo-Charging	Yes
Maximum TC Pressure	1.3 bar @ 2050 rpm
Maximum IMEP	15.8 bar @ 2050 rpm

Table 4. 1 Main specification of the analyzed engine

The schematic layout of the test installation is shown in Figure 4.1.

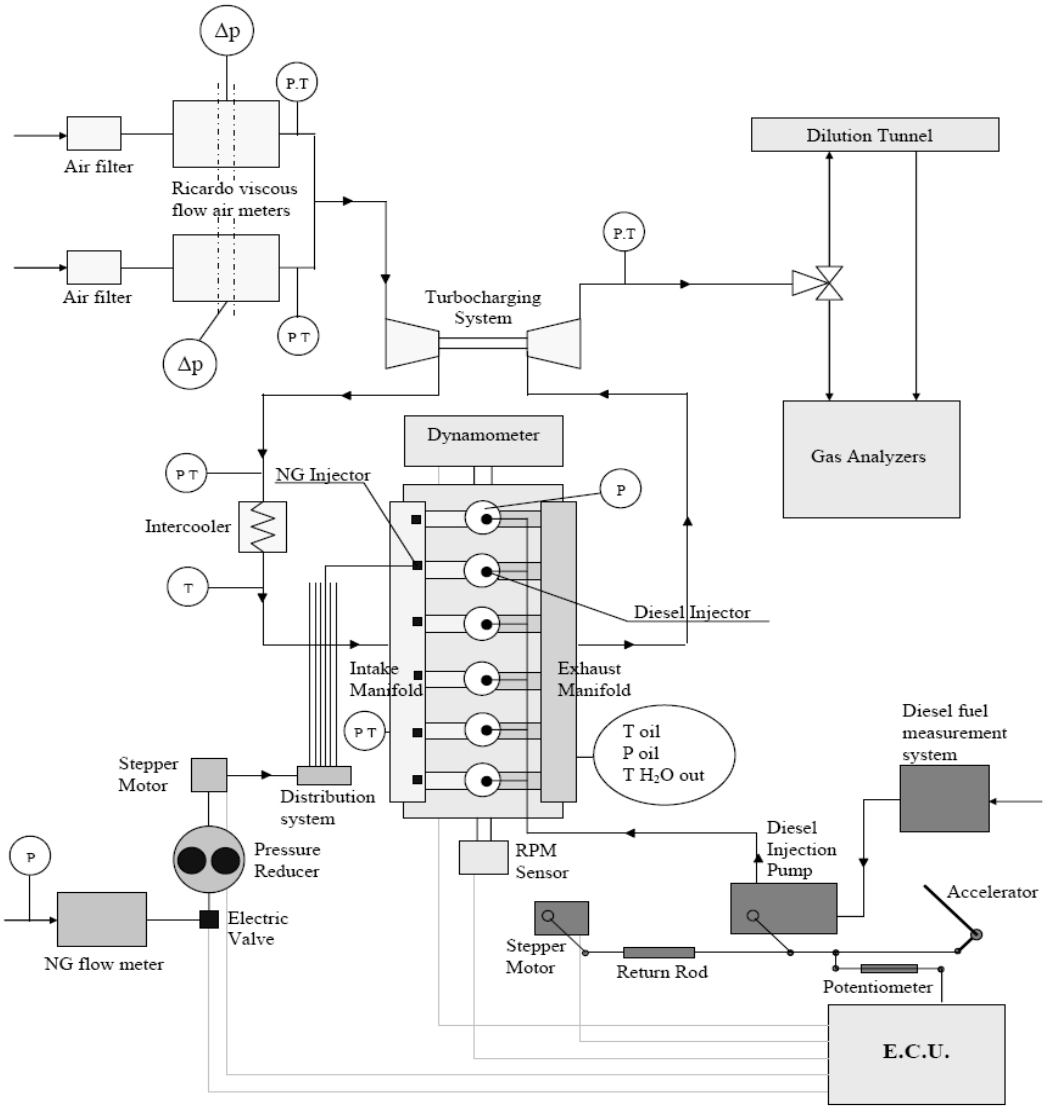

Figure 4. 1 The schematic layout of the test installation

The engine has been connected to a BORGHI & SAVERI FE 350 S eddy currents dynamometric brake. The air flow has been determined by two RICARDO viscous meters in parallel. The pressure cycle in the combustion chamber has been measured and acquired by means of a quartz transducer and AVL INDISKOP. Diesel fuel consumption has been measured by an electronic integrated gravimetric system AVL MOD 730. Natural Gas flow has been measured by a MICRO MOTION RFT 9739 flow meter.

The ETRA dual-fuel system is characterized by the installation of the following devices on the conventional diesel engine:

- An electronic control unit (ECU)
- A transducer of linear shifting to remark the position of the accelerator. In operation with the measured shifting, the ECU regulates the quantity of diesel fuel and natural gas
- A stepper motor to control the diesel injection pump. It adjusts the position of the injection pump lever and is controlled by the ECU
- An adjustable stop, which acts on a telescopic rod between the above stepper motor and the diesel injection pump lever, limiting the maximum excursion (Figure 4.2), according to the required load but allowing the return to idle position.
- An elastic element which allows the accelerator to move without a direct effect on diesel injection pump. It acts on the transducer of linear shifting in order to give information to the ECU about the required load
- A two-stages pressure reducer, which stabilize natural gas feeding pressure
- A stepper motor which regulates natural gas admission (volumetric control) by ECU order. It acts on a shutter, modifying the passage section for the natural gas
- A distribution system which feeds the natural gas injectors in continuous manner
- A security electric valve, which can achieve cut-off function for the natural gas feeding
- The natural gas nozzles, one for each cylinder (continuous low pressure multi-point admission), installed near the intake valve, connected to the above stepper motor by gum pipes.

A detail of diesel quantity regulation system is given in Figure 4.2. The ECU software sets diesel fuel and natural gas quantities on the basis of the values of two principle variables: the engine speed and the accelerator position. Dual-fuel modality can be activated only at idle speed condition.

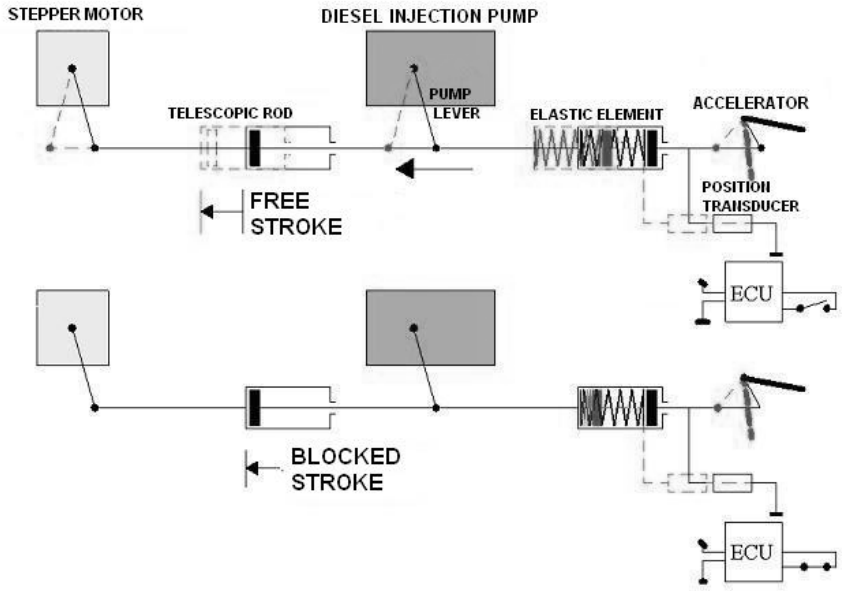

Figure 4. 2 A detail of the regulation system for diesel fuel quantity

From this point, the ECU controls the diesel stepper motor, which reduces the quantity of diesel fuel admitted, acting against the diesel injection pump lever. Moreover ECU controls the NG stepper motor. The desired quantity of natural gas can thus be admitted in the intake manifold.

For the experimental tests, the admission of natural gas and the quantity of the pilot has also been varied by manual control, in order to optimize the amounts of both fuels on the basis of pollutant emissions, for each operating condition.

During the engine tests a large number of data have been measured by using pressure transducers and J-type thermocouples and a PC based data acquisition system has been realized. The exhaust emissions measurement has been performed by the following analyzers:

- BECKMANN HFID MOD 404 for HC emissions
- BECKMANN HCLA MOD 955 for NO_X emissions
- BECKMANN NDIR MOD 880 for low CO emissions
- HARTMAN & BRAUN URAS 10E for NO, CO_2, O_2 and high concentration for CO emissions

Concerning with the particulate matter emissions, a partial-flow and partial-sampling dilution tunnel has been used according to the sampling procedure.

Cylinder pressure data have been averaged over 256 engine cycles to account for cycle-to cycle variations and the resulting medium pressure cycle has been utilized for numerical applications. Three repetitions for each measurement have been carried out.

Properties of natural gas used for experimental test are reported in Table 4.2. The lower heating value of the utilized diesel oil is 42.6 MJ/kg vs. 49.0 MJ/kg of NG.

Component	**Volumetric concentration**	
Methane	96.7	% vol
n-Butane	0.30	% vol
Ethane	0.11	% vol
i-Butane	0.20	% vol
Propane	0.20	% vol
Alifatic C_6-C_8	0.11	% vol
n-Pentane	720	ppm
i-Pentane	650	ppm
Benzene	60	ppm
Toluene	19	ppm
Xylenes	10	ppm
Propine	9.6	ppm
CO	7	ppm
Acetylene	3.1	ppm
Propylene	2.2	ppm
Ethylene	1.2	ppm
N_2	1.10	% vol
CO_2	0.16	% vol
Stoichiometric AFR	17.1	kg/kg
Lower heating value	49.0	MJ/kg
Density	0.74	kg/Nm^3

Table 4. 2 NG composition and properties

4.2 Experimental Procedure

4.2.1 Diesel Baseline Characterization

The engine behavior has been first analyzed under full-diesel operation. In table 4.3 the emission data resulting from the 13-mode (ECE R49) test are reported. The diesel injection has been delayed from 14 CAD BTDC to 10 CA BTDC to ensure EURO 2

limits concerning NO_X emissions. Nevertheless PM emission has resulted widely beyond the EURO 2 regulation.

	HC g/kWh	**CO g/kWh**	**NO_X g/kWh**	**PM g/kWh**
EURO 2 LIMITS	1.1	4.0	7.0	0.15
FULL-DIESEL	0.7	2.6	6.3	0.285

Table 4. 3 Full-diesel baseline case: pollutant emissions on a 13-mode test

4.2.2 Dual-Fuel Conversion and Comparison with Diesel Baseline Case

The IVECO 8360.46R has been subsequently converted to dual-fuel operation by the ETRA dual-kit described in § 4.1. No internal modification has been introduced to the engine. The only external additional devices have consisted in the NG feeding system (Figure 4.1) and in the regulation system for diesel injection (Figure 4.2). First experimental test have been carried out with the target to analyze the general engine behavior under dual-fuel mode.

A first comparison between dual-fuel and full-diesel configuration has provided encouraging results. The engine can easily ensure diesel-like performance along the overall range of loads. This is a fundamental result, since it represents a mandatory aspect for a dual-fuel conversion of already existing diesel engines. Moreover, the total fuel consumption can be reduced at medium-high loads and a significant reduction of CO_2 can be observed, due to the lower C/H ratio of NG (Table 4.4).

Nevertheless, a general increase in CO and HC emissions can be detected. In particular, the progressive increase in HC emissions, while reducing the engine load, can be observed. It is probably due both to the short-circuit effect of the charge (higher loads) and to poor combustion (lower loads). Accordingly, the numerical analysis of the short-circuit effect is suggested.

Also, an increase of NO_X emissions at higher loads can be observed. This is the only result which differs from other studies available on dual-fuel engines (§ 1.2.4) and can be explained by considering the extremely delayed diesel injection (10 CAD BTDC), which widely reduce the heat released from diesel fuel under premixed conditions. In such a

condition, the increase of NO_X emissions, while introducing NG into the cylinder, overcomes the reduction of NO_X, due to substituting diesel fuel with NG.

Operating Condition	RPM	TORQUE Nm	BSFC kg/h	BSEC MJ/kWh	HC ppm	NO_X ppm	CO ppm	CO_2 %vol
FD 70% load	1250	700	19.5	9.0	65	1030	1000	9.6
DF 70% load	1250	700	18.1	9.4	1160	2520	960	8.5
FD 50% load	1250	480	13.8	9.3	77	885	200	7.3
DF 50% load	1250	480	13.8	10.1	1560	881	1200	6.4
FD 25% load	1250	260	7.8	9.9	95	520	100	5.0
DF 25% load	1250	300	9.9	11.8	2690	440	2000	4.6

Table 4. 4 A first comparison between full-diesel (FD) and dual-fuel (DF) performance and emissions

First experimental results have also provided interesting results on PM emissions (Table 4.5).

Operating Condition	RPM	TORQUE Nm	DIESEL kg/h	NG kg/h	PM mg
FD 50% load	1250	480	13.7	-	0.85
DF 50% load 1	1250	480	6.7	7.1	0.37
DF 50% load 2	1250	480	3.6	10.0	0.31
FD 30% load	1250	300	9.1	-	0.65
DF 30% load	1250	300	2.6	7.4	0.40

Table 4. 5 PM emission under FD and DF operation

PM data at medium-high loads are here not reported, since the engine has not been initially run at higher loads under dual-fuel mode for a long time, due to the possible occurrence of knock, while the PM sampling procedure requires some time to be well performed. Nevertheless, experimental data under medium and light load conditions suggest that a significant reduction of PM emission at higher loads has to be expected.

Also, the further substitution of diesel with NG at a fixed load, allows for a further reduction in PM emissions. According to the above results and considerations, the subsequent experimental tests have been focused on the engine behavior at partial loads, characterized by reduced efficiency and high HC emissions, and the effect of substitution of diesel oil with natural gas has first been analyzed.

4.2.3 Effect of NG Percentage

The effect of NG percentage on performance and emissions has been studied at 50% of the maximum load. In Table 4.6, the characteristics of the examined test cases are reported.

Test Case	**FD**	**MF1**	**MF3**	**MF6**
Engine Speed	1250 RPM	1250 RPM	1250 RPM	1250 RPM
Load	480 Nm	480 Nm	480 Nm	475 Nm
Intake throttle	WOT	WOT	WOT	WOT
EGR	No	No	No	No
Three-way Catalyst	No	No	No	No
Diesel flow rate	13.7 kg/h	6.7 kg/h	4.6 kg/h	1.64 kg/h
NG flow rate	-	7.1 kg/h	9.0 kg/h	12.1 kg/h
NG/air λ	-	3.14	2.48	1.84
% NG (Energy basis)	0%	55%	70%	90%
Injection start	10 CAD BTDC	10 CAD BTDC	10 CAD BTDC	10 CAD BTDC
Injection duration	33 CAD BTDC	16.5 CAD BTDC	11 CAD BTDC	4 CAD BTDC

Table 4. 6 Main specifications of the examined test cases

Under dual-fuel mode the engine can still ensure diesel-like performance, even for high degrees of diesel/NG substitution (480 Nm at full-diesel vs. 475 Nm at 90% NG).

Moreover, the 90% NG test case is characterized by very lean homogeneous mixtures ($\lambda = 1.84$), rather beyond the lean flammability limit of natural gas. In such a lean operating condition, regular NG combustion can also be obtained, due to the spread ignition of the diesel pilot. The increase of the NG/air AFR (λ), thus leading to much leaner mixtures, requires a higher ignition energy, that is to say much larger diesel injection. Anyway, at every percentage of NG utilization, the engine provide for the same torque as the full-diesel case.

The same result can be further confirmed by observing the experimental in-cylinder traces in Figure 4.3.

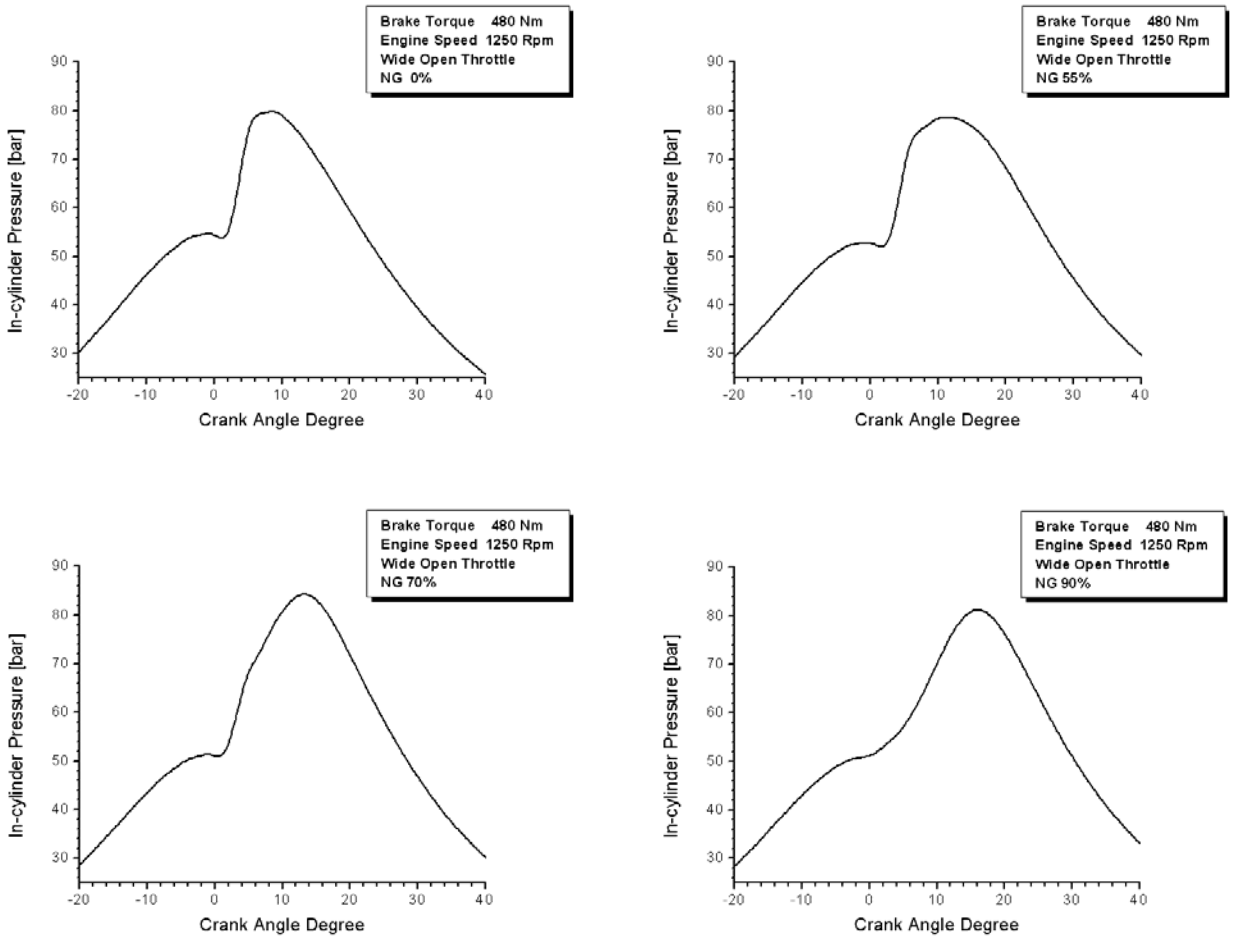

Figure 4. 3 Experimental in-cylinder pressure data (1250 RPM, 50% load)

Despite of the different rise rates of pressure, the value of the peak pressure is basically unchanged, even though it moves toward higher crank angle degrees.

Accordingly, the combustion process results as widely modified by the prevalence of NG instead of oil, as can be also confirmed by means of the experimental heat release rate curves (Figure 4.4), calculated by means of the FW2001 code described in § 3.1.3.

Main combustion is delayed with respect to full-diesel operations, due to the flame propagation throughout the chamber, while the diesel contribution to combustion is reduced. In particular the last case in Figure 4.4 (90% of NG utilization) seems to be a typical SI-engine heat release curve, with the only exception of a short initial stage,

consisting in the combustion of the diesel pilot. Accordingly, such an operating condition could be even simulated as a SI-NG operation, by considering diesel pilot only as the ignition source. The extreme cases (diesel and 90% NG) are thus well defined, while great uncertainty remains when approaching the intermediate cases. In Figure 4.3 (55% and 70%NG) the net change of pressure rise rate is evident just passing from diesel to NG combustion. Such an aspect is still confirmed by Figures 4.4 (55% and 70%NG again) where the prevalence of one (diesel or NG) combustion process, with respect to the other one, cannot be put into evidence.

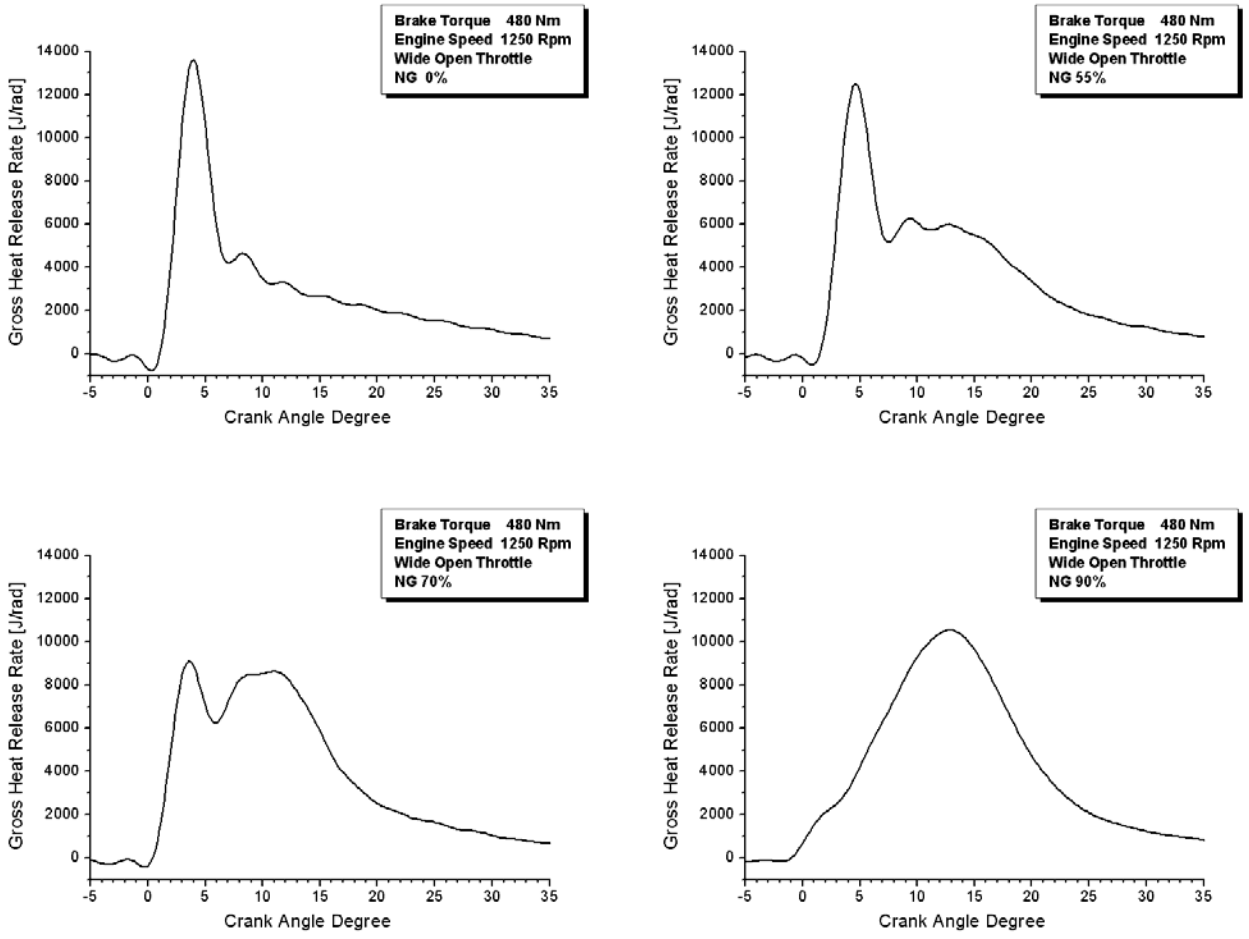

Figure 4. 4 Heat release rate curves (1250 RPM, 50% load)

The previous diagnostic approach highlights the need of an accurate analysis of the interaction between diesel and natural gas combustion. Also, it is not properly clear if flames propagate throughout the homogeneous air/NG mixture or the only NG entrained

within the zones surrounding diesel flames is burned. Accordingly, to correctly simulate dual-fuel engines, at every operating condition, a locally-performed analysis is mandatory. Therefore, a multi-dimensional detailed simulation is required to well represent the overall combustion.

The effect of NG percentage on exhaust emissions can be observed in Figure 4.5. CO_2 emissions are progressively reduced while increasing NG, as expected from the low value of the C/H ratio for NG. NO_X and CO seem to be stable during the progressive substitution of diesel with NG. The increase of HC is evident instead, due to the increase of NG mass trapped into the cylinder. Such an effect overcomes the beneficial effect of the reduction of air/NG AFR λ (from 3.14 to 1.84).

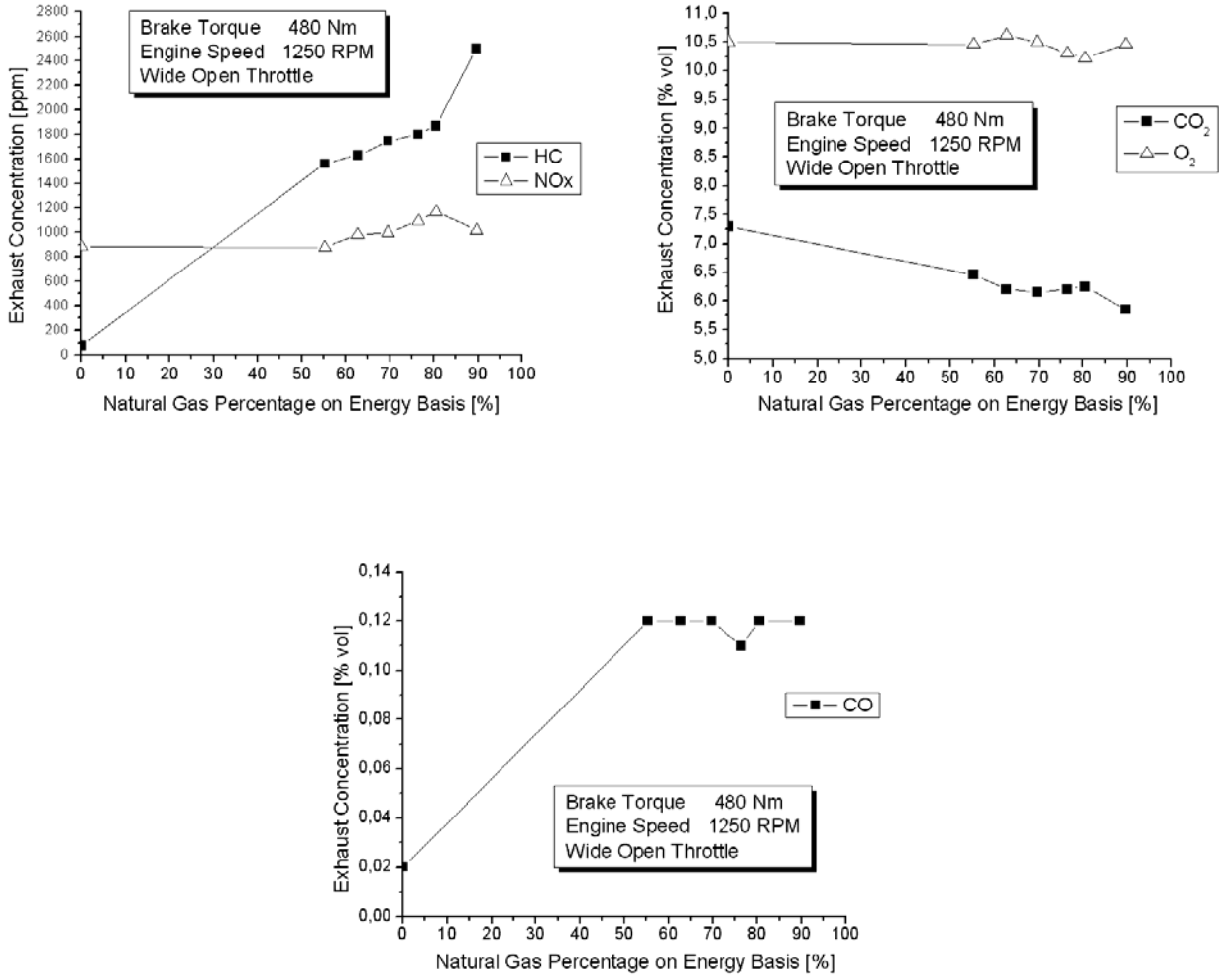

Figure 4. 5 Effect of NG percentage on exhaust emissions

A significant quantity of O_2 is still available for oxidation. This means that combustion occurs in too lean conditions and the ignition energy due to pilot combustion is not large enough to fully sustain the overall flame propagation. It is worth noting that the last DF test case (90 % NG) is quite similar to a typical SI-NG lean burn operation, but characterized by reduced ignition timing advance. In fact, the pilot injection starts at 10 CAD BTDC and, due to the diesel ignition delay, combustion starts around the TDC. Therefore, a SI engine characterized by such a low ignition timing advance and by lean homogeneous mixtures is clearly expected to suffer from instability, cyclic variation and high HC emissions.

4.2.4 Introduction of Further Devices like Throttling, EGR and Catalyst

The IVECO 8360.46 R engine is characterized by a mechanical injection system for diesel fuel, as reported in Table 4.1. Accordingly, the optimization of pilot characteristics is only partially feasible. In fact, the pilot injection timing advance cannot be varied during the engine running, unlike its quantity. This is a hard shortage, since light-loads and high-NG operating conditions would require higher ignition timing advance to reduce engine instability and HC emissions.

Thus, throttling has been introduced, just before the intake manifold, as first considerable modification to the engine. Figure 4.6 shows the effect of throttling percentage on exhaust emissions. Significant beneficial effects on HC emissions can be obtained by reducing the available air (O_2 is reduced). Nevertheless, the increase in NO_X and CO_2 emissions are the unavoidable drawbacks. For high-throttled conditions, the rapid increase in CO emissions has been also observed.

Introducing a three-way catalyst (Table 4.7) has not allowed for the simultaneous reduction of NO_X, CO and HC emissions. NO_X can be reduced only by a considerable throttling, thus also reducing engine efficiency and increasing the total BSFC and BSEC. A promising strategy consists in introducing EGR to simultaneously reduce HC and NO_X emission upstream of the catalyst. Nevertheless a limited throttling has still to be provided to limit the air excess.

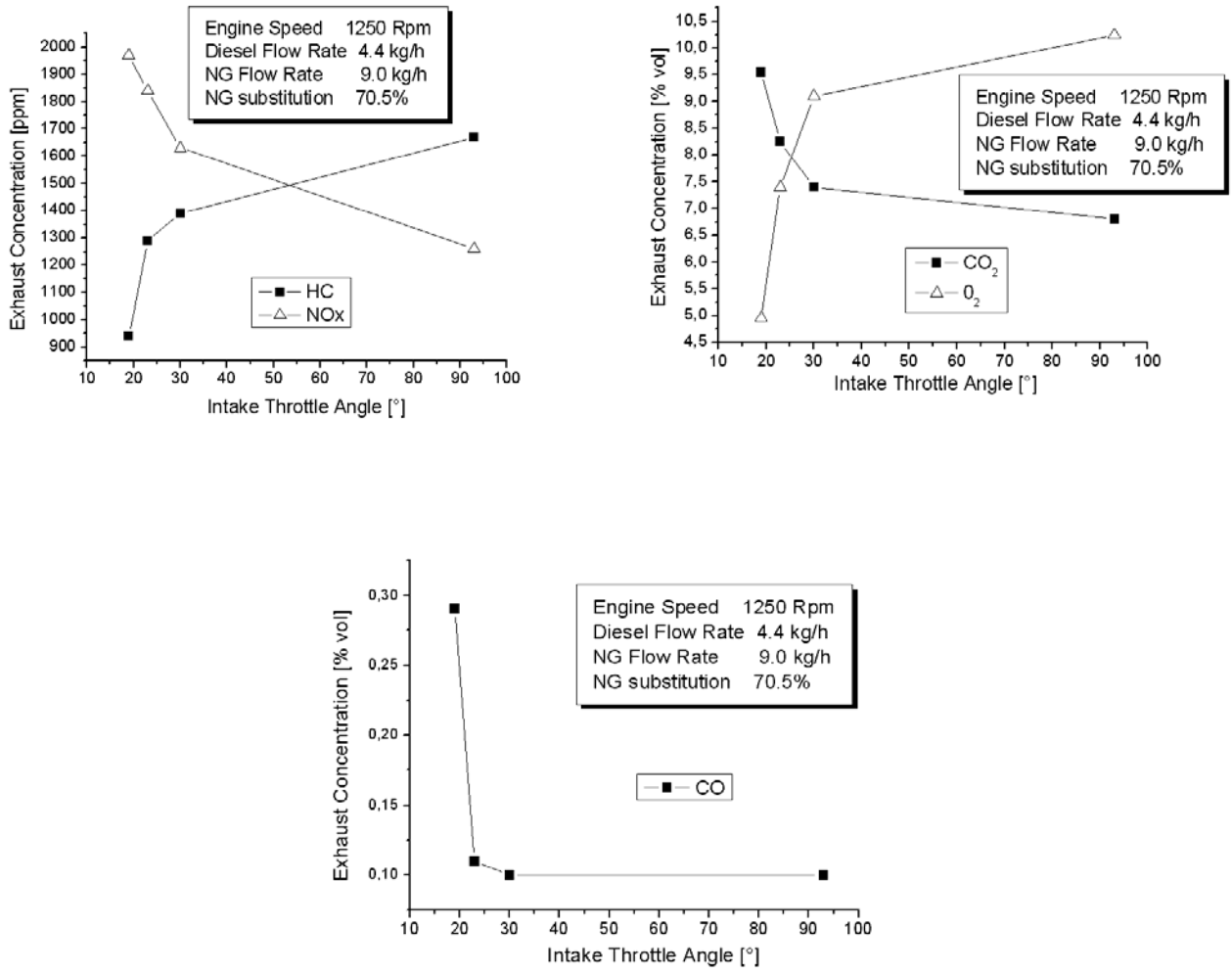

Figure 4. 6 Effect of throttling percentage on exhaust emissions

Operating Condition	THROT.	RPM	TORQUE Nm	DIESEL kg/h	NG kg/h	HC ppm	NO_X ppm	CO ppm	CO_2 %vol.
Upstream	WOT	1254	488	3.5	10	1750	1000	1225	6.3
Downstream	WOT	1254	488	3.5	10	1200	990	2	6.59
Upstream	WOT	1249	304	2.6	7.5	2820	346	2100	4.1
Downstream	WOT	1249	304	2.6	7.5	2650	340	4	4.36
Upstream	17	1248	488	3.7	11.4	640	1811	17100	10.0
Downstream	17	1248	488	3.7	11.4	61	11	200	12.4
Upstream	13	1250	260	2.5	7.8	820	960	13700	10.0
Downstream	13	1250	260	2.5	7.8	19	900	2	11.8

Table 4. 7 Effect of throttling percentage on exhaust emissions

4.2.5 Definition of the Optimized Strategy for Steady Tests

According to the previous remarks, the engine has been operated at very-light loads on full-diesel mode (FD), as well as for idle speed. On the contrary, at middle and high load, apart for maximum torque, the engine operation has been dual-fuel throttled with EGR. As previously stated, throttling is necessary to reduce oxygen excess (typical of diesel engine) and to obtain a good performance of the three-way catalyst. The EGR has been further introduced to improve the diesel pilot ignition and NG combustion (higher temperatures before combustion) while controlling NO_X formation (higher inert mass).

EGR quantity in each point has been carefully chosen with the aim to obtain a right compromise between the necessity to feed the cylinder with an inert gas mixture, and the necessity to have the right air quantity for a good flame front propagation without quenching, in order to avoid high pollutant production (especially HC, CO and PM). Furthermore EGR, together with throttle valve, has allowed to reduce knocking probability and therefore to operate with more safety at high load. In DF mode, only at maximum torque the engine has been operated unthrottled and without EGR. Moreover in this condition all the regulated emissions, PM including, has resulted very low.

On the basis of the above considerations two 13-mode cycles (ECE R49) have been performed, in the following way: the points 1, 2, 3, 7, 11, 12 and 13 in full diesel operation (1, 7 an 13 are at idle speed); the points 4, 5, 8, 9, 10 have been performed throttled dual-fuel with EGR. Only the point 6 (maximum torque) has been performed unthrottled dual-fuel operation without EGR. The main remark regards the relatively high tendency to knock at higher loads, especially maximum power, in spite of EGR and intake air reduction. This could be an issue for further tests, to evaluate the possibility to control knocking better on dual-fuel mode.

4.2.6 Final Experimental Results

In the Table 4.8, the 13-mode cycle emissions for the dual-fuel engine IVECO 8360-ETRA are reported. The results have been obtained running some points in full diesel and others in dual-fuel, according to the above description. The test cycle has been performed two times and the results have been compared with those of a traditional

EURO 2 diesel engine. Considerable differences can be appreciated, especially between CO and NO_X emissions of the two tests in DF. This is due to the presence of the catalyst. In fact a small variation in air fuel control (λ) can hugely affect the catalyst conversion efficiency. Anyway, average emission values are also reported in the table. The good strategy adopted for the dual-fuel operation has been evidenced by the great global emissions reduction in comparison with the diesel version. In particular NO_X-PM trade-off is largely influenced. In fact both NO_X and PM resulted lower in DF (respectively 75% and 73%) and far from EURO 2 limits, while those of the diesel engine were much higher. As expected, lower differences in comparison with the diesel have been found for HC and CO. Anyway also for these two pollutants, a reduction has been obtained with dual-fuel operation, (33% and 32% respectively). In the Table 4.8 the BSEC is also reported. The dual-fuel engine efficiency is slightly lower with respect to the diesel (about 10%) baseline case. This result can be easily explained with throttled operation and slightly lower combustion efficiency in dual-fuel operation.

	HC	**CO**	**NO_X**	**PM**	**BSEC**
	g/kWh				MJ/kWh
European R49 limits (EURO2)	**1.1**	**4.0**	**7.0**	**0.15**	-
Full Diesel	**0.6**	**2.2**	**6.5**	**0.26**	**9.8**
Dual-Fuel 1	0.5	2.8	1.2	0.07	11.1
Dual-Fuel 2	0.3	0.1	3.9	0.07	11.1
Dual-Fuel average	**0.4**	**1.5**	**1.6**	**0.07**	**11.1**

Table 4. 8 13-mode cycle emissions for the dual-fuel engine IVECO 8360-ETRA

Maximum torque and power in dual-fuel mode have resulted slightly lower than full diesel (respectively 780 Nm vs. 840 Nm both at 1250rpm, and 143 kW at 1950 rpm vs. 154 kW 2050 rpm). Such small difference can be attributed to the modifications of:

- The intake manifold with a throttle valve
- The exhaust pipe with EGR and a catalyst

Chapter 5
NUMERICAL RESULTS AND DISCUSSION

5.1 Introduction

Experimental tests have put into evidence the influence of the main engine parameters on dual-fuel performance and emissions, but have not allowed for a complete analysis of the engine to explore all the potential of dual-fuel technology. As an example, the effect of injection timing advance (which also means ignition timing advance) on engine performance and emissions has not been investigated, due to the mechanical injection system, which does not allow for the complete optimization of the diesel pilot characteristics. Also, a deep investigation of important phenomena like short-circuit effect, diesel pilot ignition delay and flame propagation has to be carried out for a correct understanding of dual-fuel combustion.

Accordingly, an accurate numerical analysis has been carried out, in parallel with the experimental activity, with the aim of developing a dedicated model for dual-fuel combustion simulation. The numerical analysis has been developed on both the whole engine and the in-cylinder scale. In fact, being the dual-fuel combustion highly depending on local fluid-dynamics, a detailed evaluation of the flow field in the engine is required. This task has been performed by using a mixed 1-D / 3-D approach. 1-D tools can be used to compute realistic time-dependent 3-D code boundary conditions (at the ends of the intake and exhaust ducts), by means of which the presence of the overall engine ducts and devices can be taken into account. Moreover, the fluid-dynamics of the whole engine can be simply and carefully represented. 3-D tools are mainly used to model the in-

cylinder thermo-fluid dynamic processes. Thus, a detailed description of the phenomena occurring into the combustion chamber can be performed.

5.2 1-D Simulation of Overall Engine

The heat release rate curves showed in § 4.2.3, calculated from the experimental pressure data, have also been fitted by means of the Wiebe's functions approach described in § 3.1.3, to identify and separate the single contribution of each fuel (diesel and NG) to overall combustion. The results are shown in Figure 5.1.

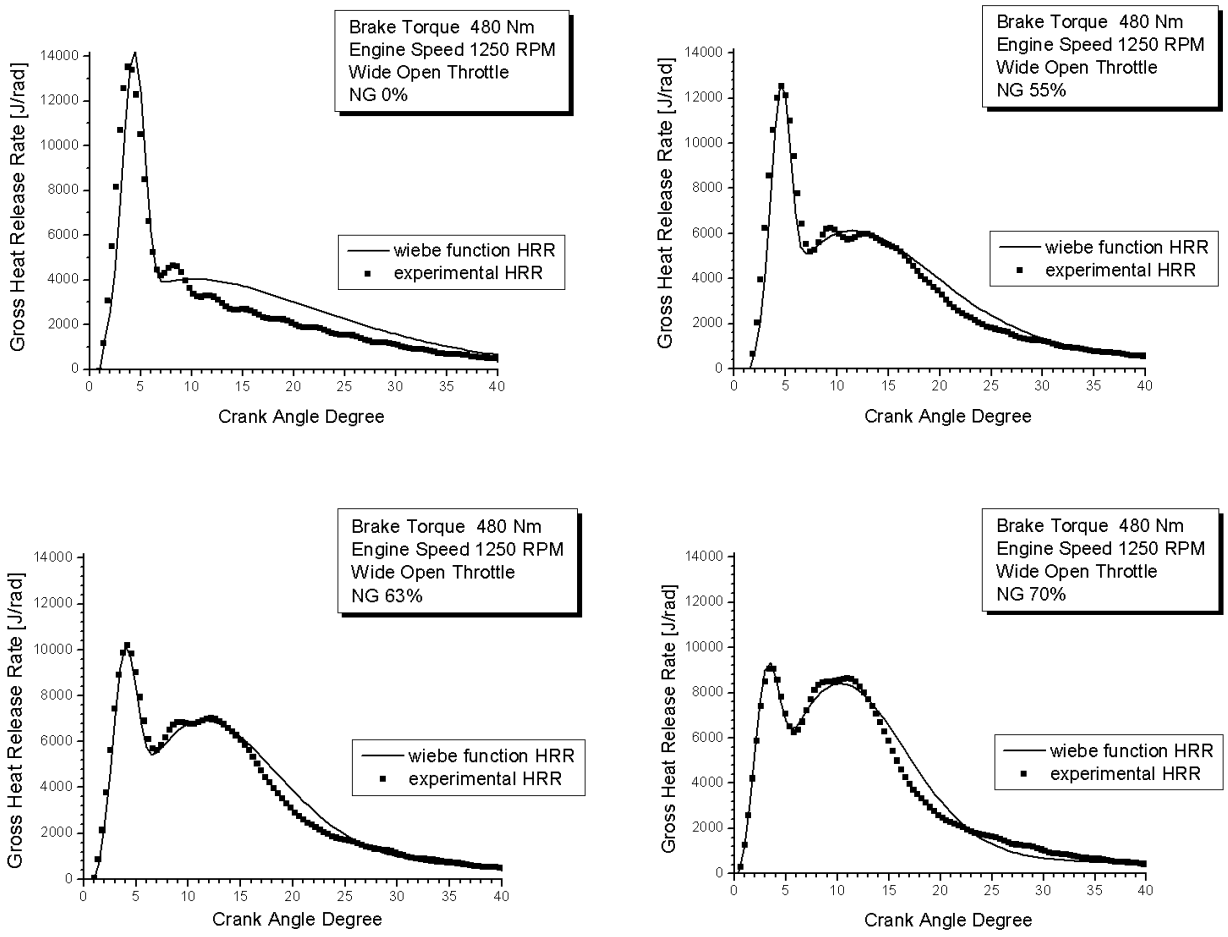

Figure 5. 1 The analysis of the calculated heat release rate curves by the Wiebe's functions approach

The duration of diesel premixed combustion has been observed to be almost constant increasing the NG content, while the durations of diesel diffusive and natural gas

combustion has resulted to be respectively increased and decreased. Natural gas combustion is enhanced by the increase of natural gas quantity injected into the intake manifold. In fact, the homogeneous mixture becomes richer and the flame propagation through the combustion chamber is faster. The increase of the shape factor f_{gas} from 0.9 (0% NG) to 1.7 (90% NG), suggests that the NG combustion is getting similar to that occurring in a SI engine ($f_{gas} = 2$).

The actual mass burning or heat release rate can be provided as an input to the 1-D FW2001 code to obtain a complete evaluation of the engine behavior. The detailed analysis of the fluid-dynamic processes occurring during the cylinder filling can then be carried out, for different operating conditions. Under dual-fuel operations, short-circuit effect can also be detected at medium-high loads (dot line in Figure 5.2a), while an appreciable internal EGR may be observed at part-loads (straight line in Figure 5.2b).

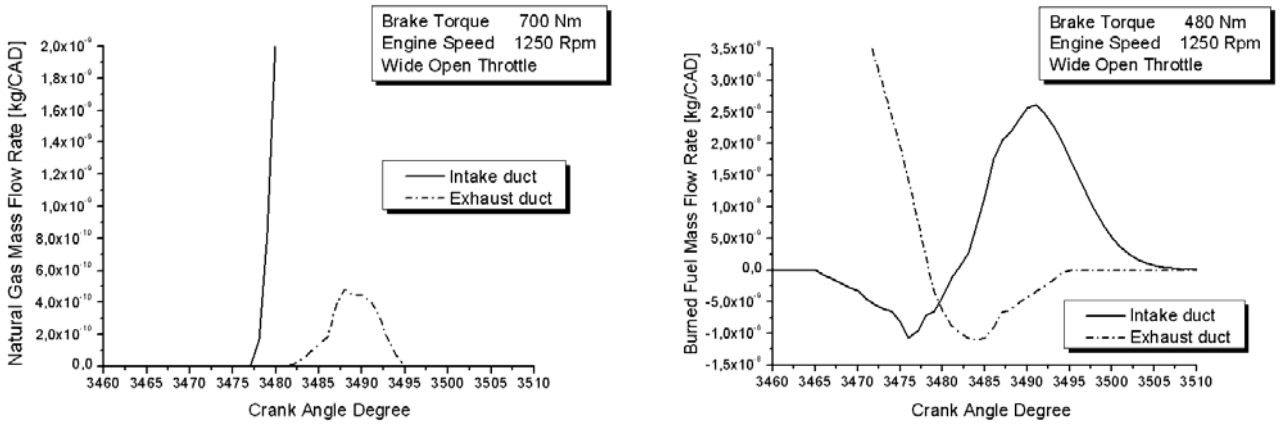

Figure 5. 2 a) Short-circuit effect of the fresh mixture, which escapes through the exhaust duct during the overlap **b)** Internal EGR of the burned products, which re-circulates within the intake duct

Accordingly, the short-circuit effect could be considered as a possible source for HC emissions on dual-fuel mode, especially at higher loads. Nevertheless, it cannot be considered as the main explanation for the high HC emissions at partial load. Under these conditions, the increase in HC is mainly due to the irregular combustion, which occurs when the air/NG mixture is too lean, and to the low injection timing advance.

The 1-D approach has been performed for the initial understanding of dual-fuel combustion and for the analysis of the behavior of the overall engine, from the intake to the exhaust. A more detailed multi-dimensional (3-D) approach has been then performed

to better analyze the dual-fuel in-cylinder processes. Nevertheless, the 1-D code has been utilized once again, to provide the correct pressure boundary conditions for this latter approach.

5.3 Multi-Dimensional Simulation of In-Cylinder Processes

The multi-dimensional approach has been carried out by means of the KIVA-3V code described in § 3.2. The computational grid related to the IVECO 8360.46R engine, sketched in Figure 5.3, consists of about 150,000 nodes.

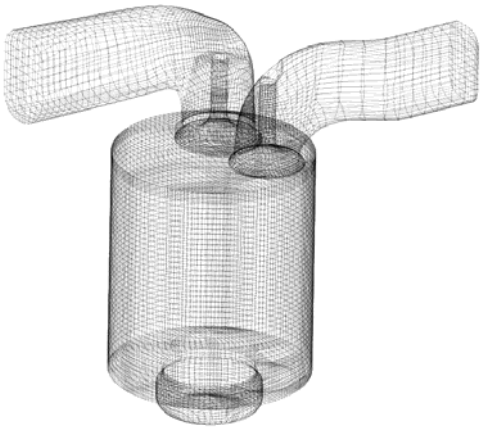

Figure 5. 3 The computational mesh of the IVECO 8360.46R engine

First, the influence of the flow field on the evolution of the diesel spray has been studied. Secondly, the pilot-ignition and overall combustion have been analyzed and the numerical results have been compared with the experimental data.

5.3.1 The In-Cylinder Flow Field

The simulation of the whole working cycle allows accounting for the real flow field in the engine. Concerning the present analysis, numerical simulations start from the BDC of exhaust stroke, thus the whole scavenging phase can be represented together with the effects of the real geometry on the resulting flow field at BDC of the compression stroke. Figure 5.4 shows the flow field on a frontal section through the axis of both valves and on a cross-section located near the cylinder head during intake and compression stroke (MF6 test case).

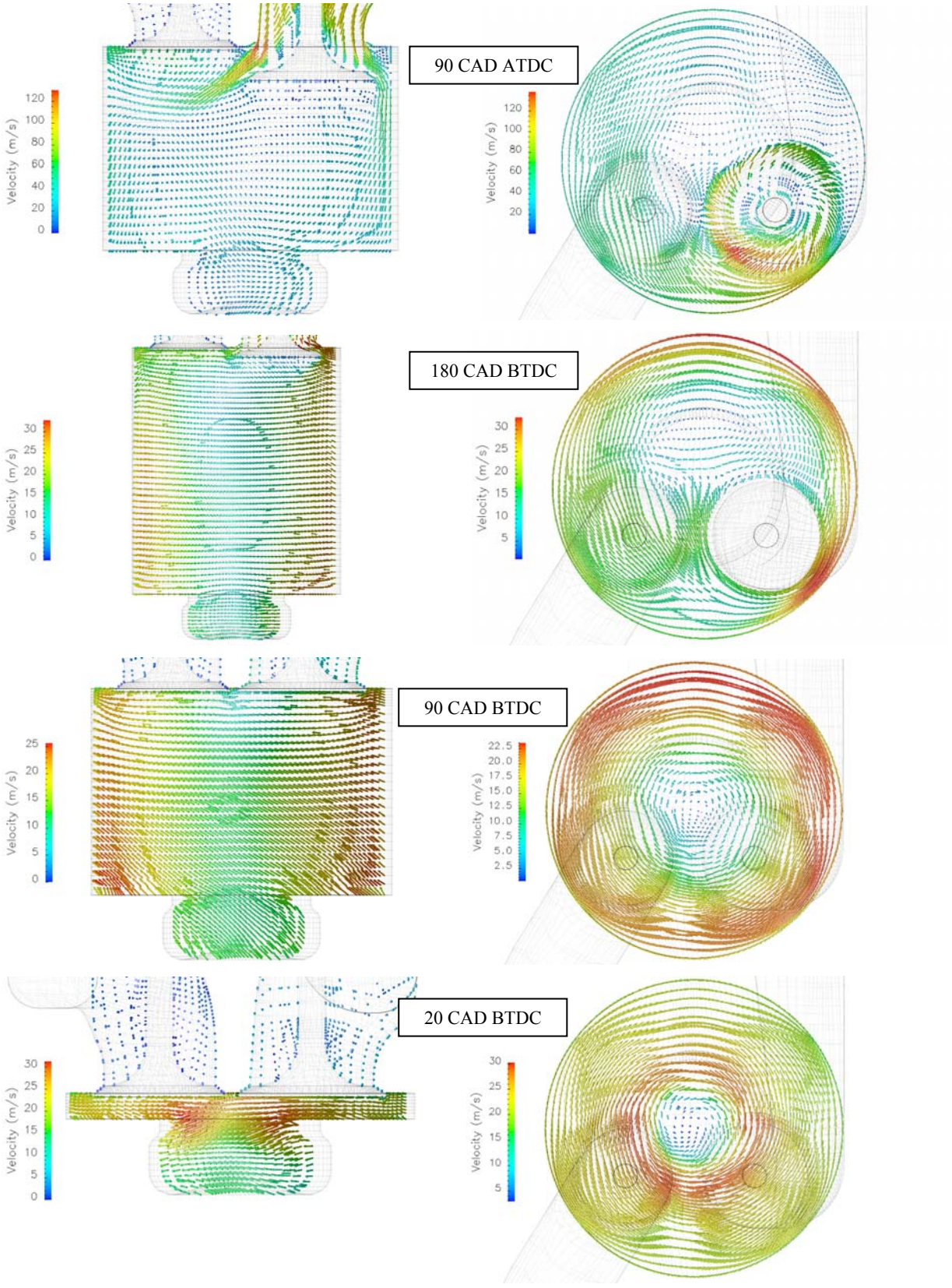

Figure 5. 4 Flow field on a frontal section and on a cross-section close the cylinder head (MF6)

A strong swirl motion can be clearly observed, related to the shape of the intake duct. Moreover, the swirl intensity results to be larger than tumble and squish effects.

An appreciable swirl motion can still be recognized at the end of compression stroke, just few CAD before the injection start.

From that point, the evolution of the spray into the cylinder, its evaporation and auto-ignition, and the subsequent flame propagation throughout the overall combustion chamber will be widely influenced from it. Accordingly, the role of this information cannot be underestimated.

5.3.2 The Evolution of the Spray

The high swirl motion widely influences the evolution of the spray within the chamber, as can be observed in Figure 5.5, reporting a sequence of images (step = 2 CAD) that illustrate the diesel spray evolution and the mass fraction distribution of the vaporized diesel on a frontal section and on a cross-section within the piston bowl (FD case). The effect of swirl on the droplet path is highlighted, in particular for the droplets which are located near the walls of the piston bowl, where the tangential velocity is higher and the droplets have a small size with respect to the injected size (injection droplet radius = 100μm, equal to the nozzle radius). Within the present work, the WAVE constant B_1 has been set as 30.

Most of diesel fuel vaporizes near the walls of the bowl, and the zones of main evaporation are quite far from the nozzle direction. As previously stated in § 3.2.3, N-heptane (C_7H_{16}) has been considered as the chemical species representing diesel vapor.

Figure 5.6 shows the diesel spray and the C_7H_{16} mass fraction at 2 CAD ATDC, immediately after the auto-ignition of the pilot, which occurs around the TDC. A large amount of vaporized diesel fuel can be observed for FD, MF1 and MF3 cases, while the MF6, as already reported, is characterized by low diesel admission (10% of the total energy introduced into the cylinder). That is why the initial combustion stage is characterized by a slight rise in the cylinder pressure and temperature.

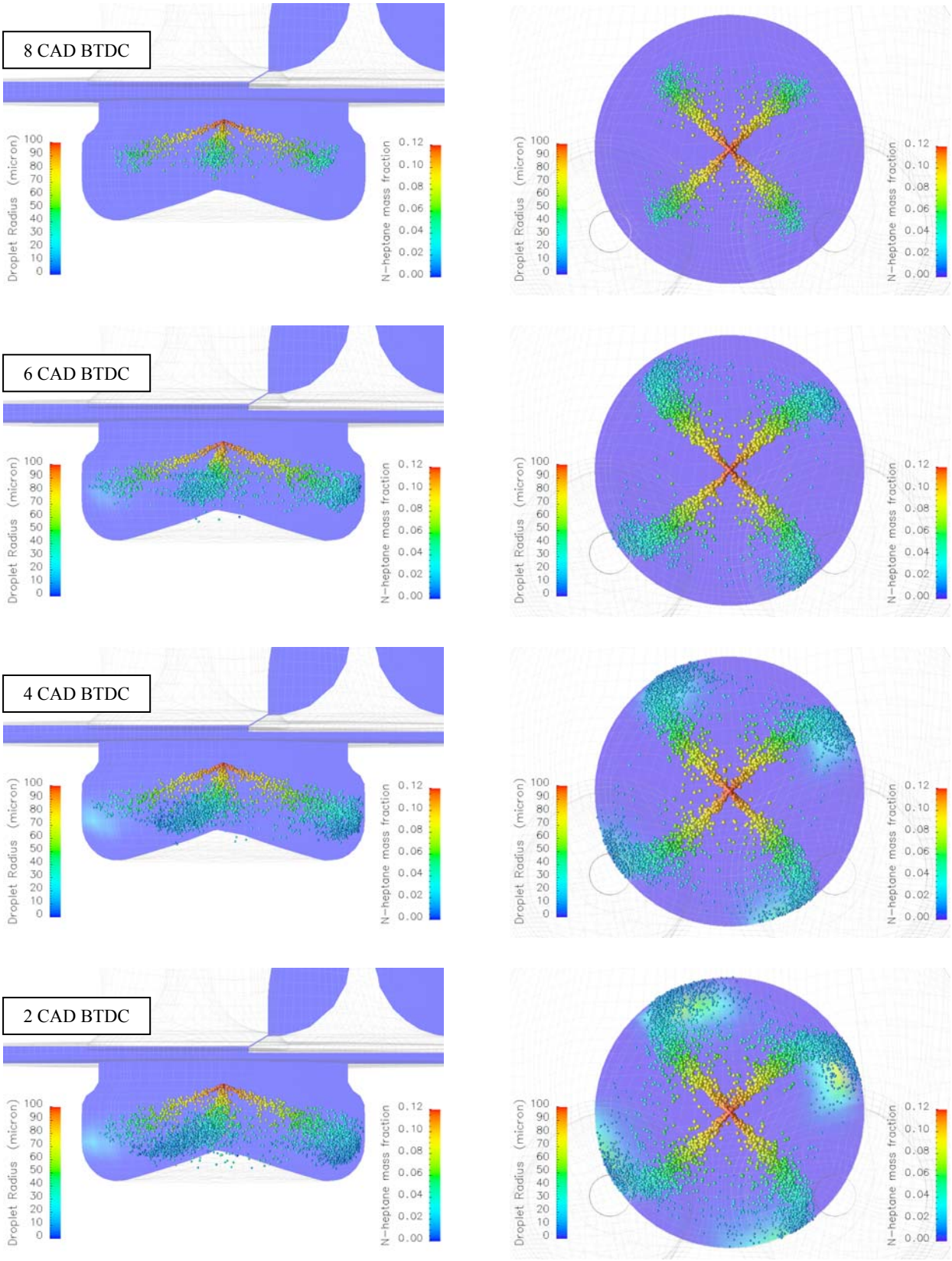

Figure 5. 5 Spray droplets and vaporized diesel on a frontal section and on a cross-section of the piston bowl (FD)

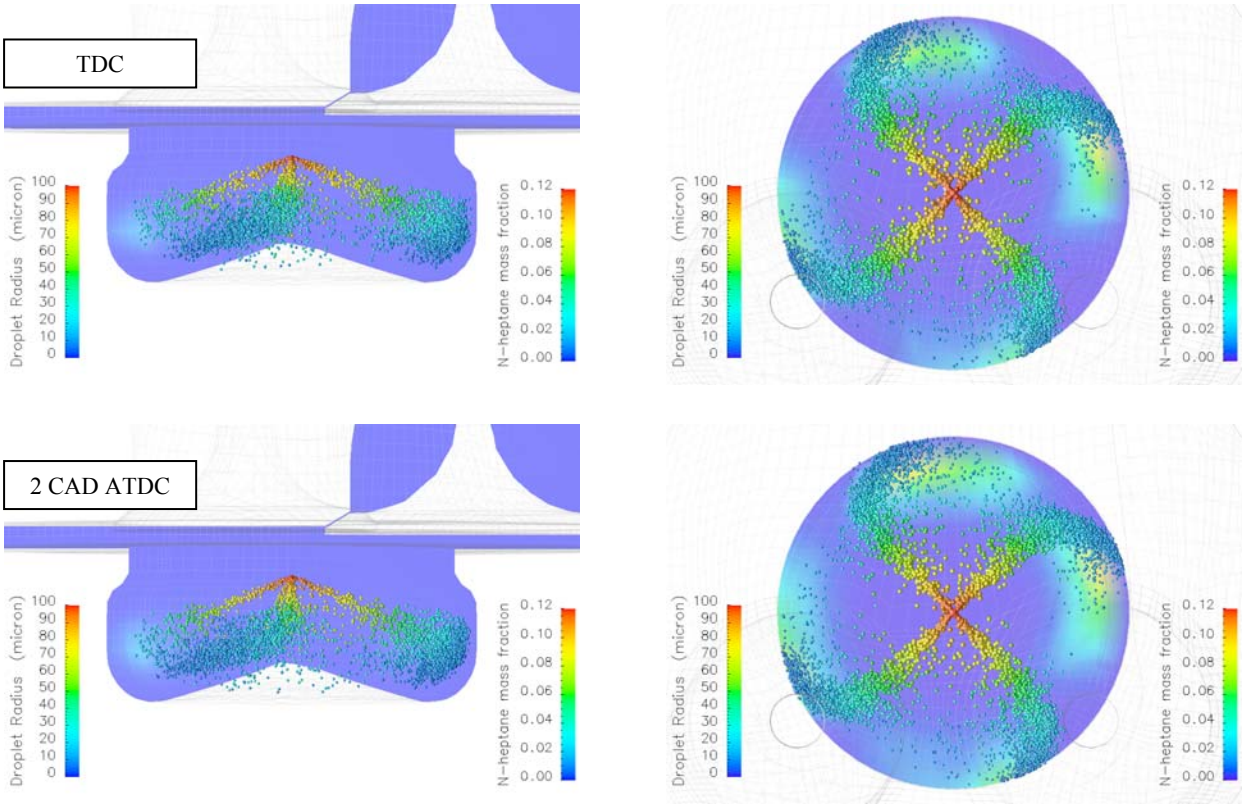

Figure 5.5 Continued

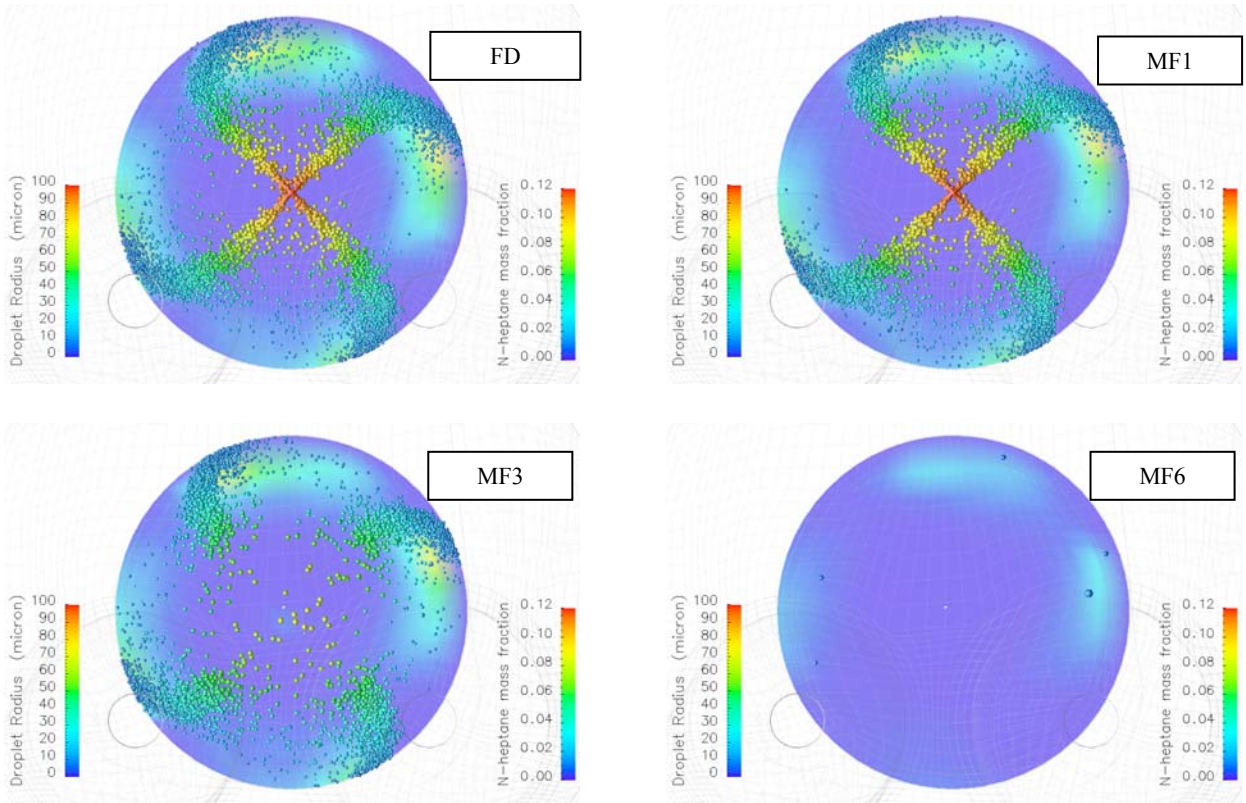

Figure 5. 6 Spray and vaporized diesel at 2 CAD ATDC

5.3.3 The Dual-Fuel Combustion

As already mentioned, an operating condition characterized by high NG percentage could be even simulated as a SI-NG operation, thus neglecting the contribution of the diesel fuel to combustion and considering it as the ignition source for NG combustion only. Accordingly, the attention has been initially focused on the test case characterized by highest percentage of NG utilization (MF6, 90% NG). The CFM model has been used to simulate the flame propagation throughout the homogeneous mixture, starting from the pilot auto-ignition points.

Results show that pilot auto-ignition first occurs around the TDC. The strategy to switch from the Shell auto-ignition model to CFM combustion model is quite simple: when diesel pilot auto-ignites and the temperature in a computation cell becomes greater than 1000 K, the Shell Model is switched-off and a value of Σ different from zero is initialized in those zones of the computational domain (Figure 5.7).

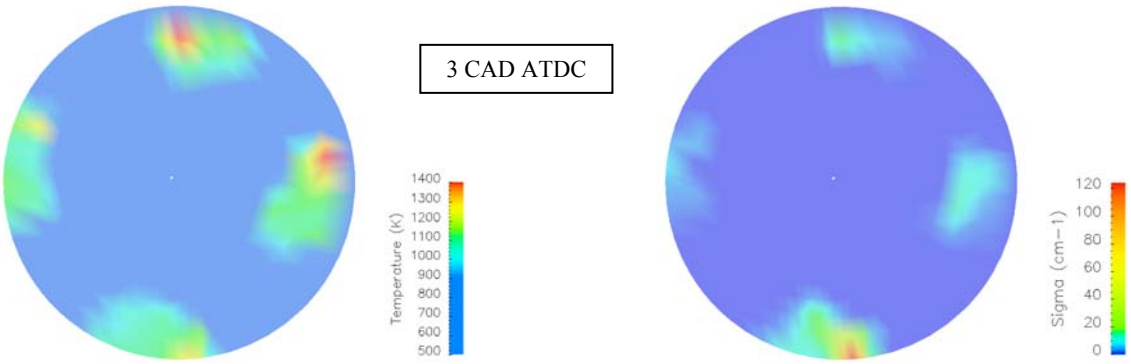

Figure 5. 7 An example of the switch procedure between Shell and CFM models (MF6)

Once a $\Sigma \neq 0$ is set, the Σ transport equation (Eq. 3.54, § 3.2.5) accounts for the flame propagation throughout the chamber.

Figures 5.8 and 5.9 show the flame propagation mechanism. Four main flames move from the ignition points, which are located near the walls of the piston bowl, toward the centre of the chamber and interact (Figure 5.8). The corresponding temperature field is shown in Figure 5.9.

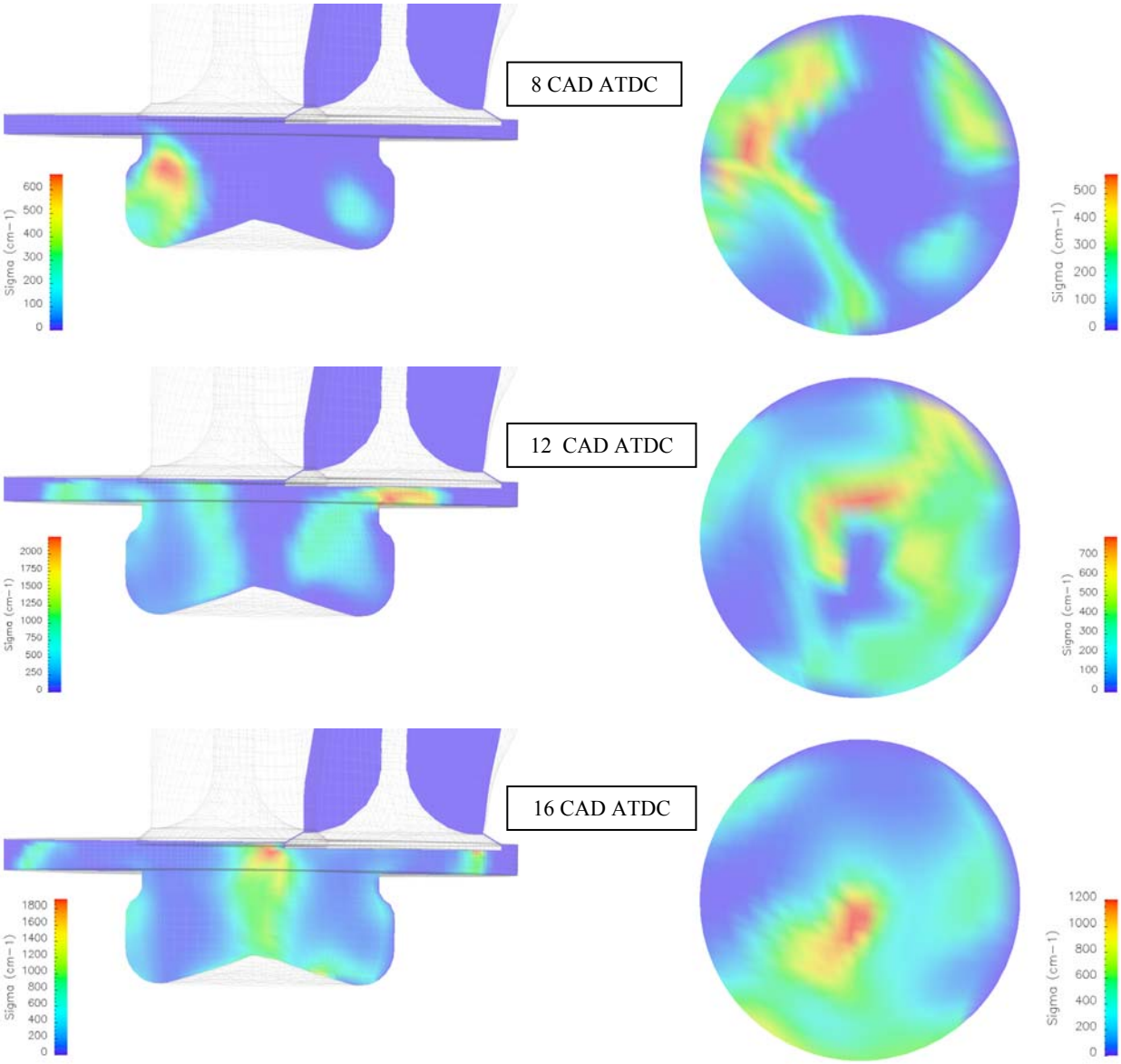

Figure 5. 8 Σ map on a frontal section and on a cross-section of the piston bowl (MF6)

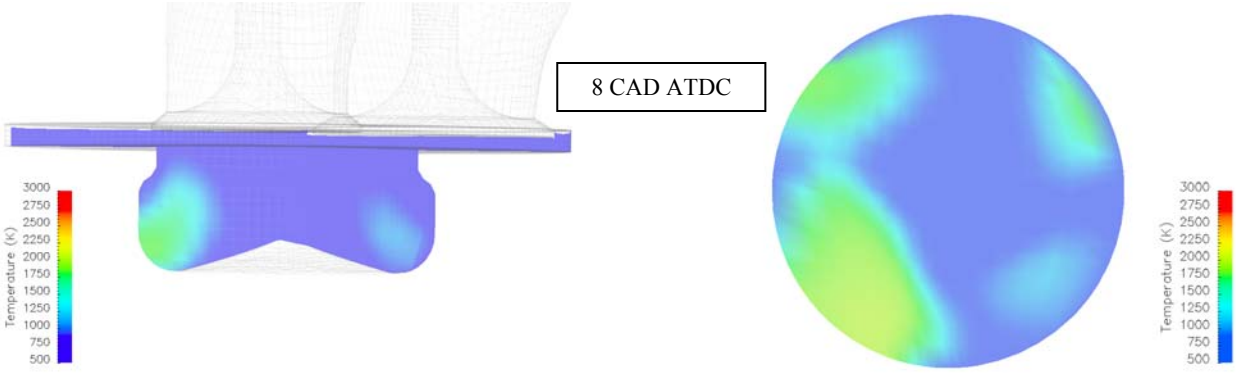

Figure 5. 9 Temperature map on a frontal section and on a cross-section of the piston bowl (MF6, CFM model)

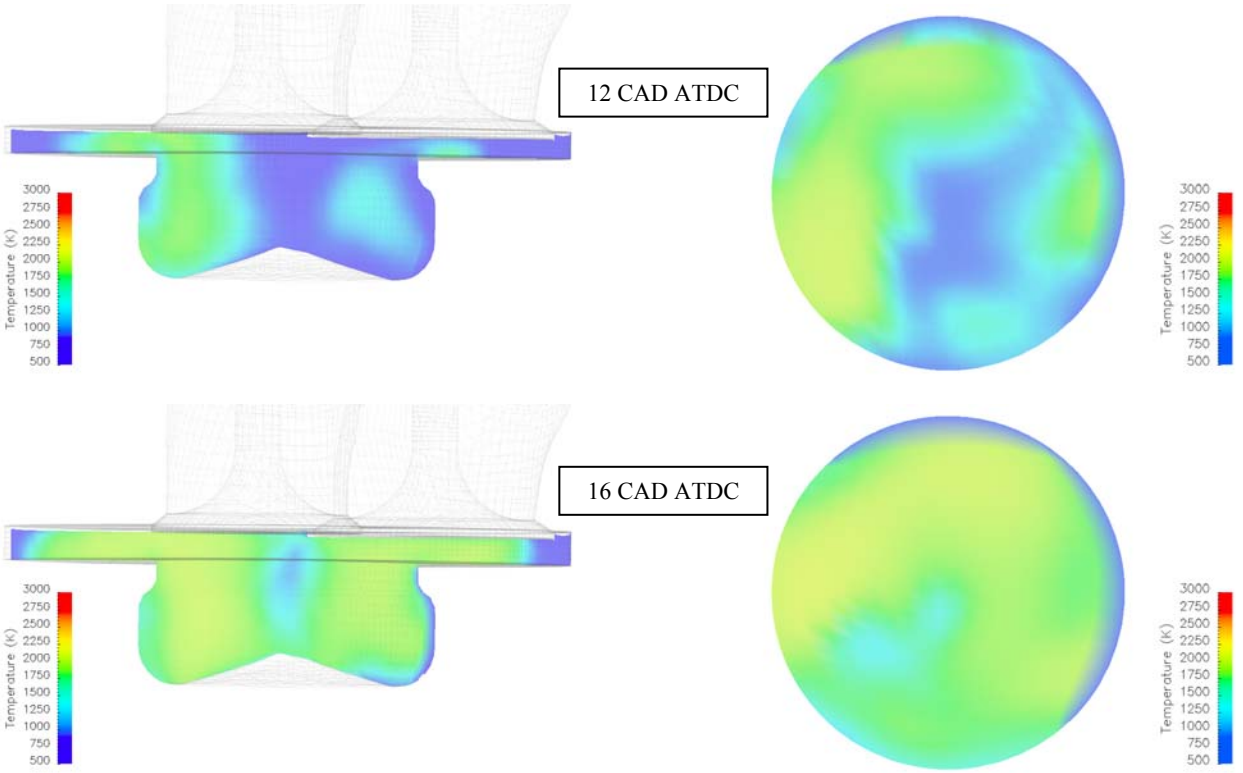

Figure 5. 9 Continued

The comparison between experimental and numerical data is reported in Figure 5.10.

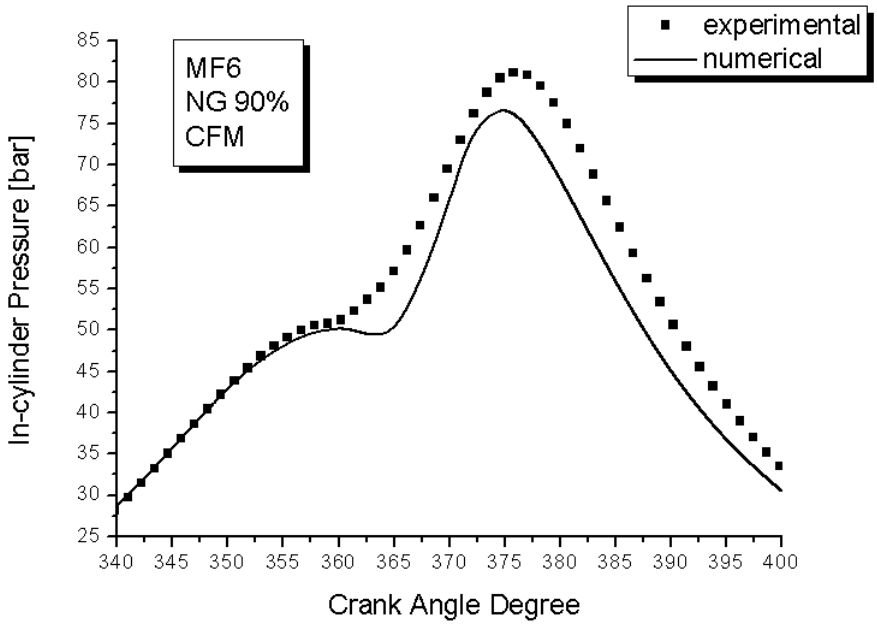

Figure 5. 10 Comparison between experimental and numerical pressure data (MF6, CFM model)

A good agreement can be observed up to the ignition crank angle ($CAD_{ign} \approx$ TDC = 360 CAD), as well as during the latter phase of combustion. Nevertheless, the numerical data undervalues the experimental pressure traces, mainly due to the assumption of having neglected the energy contribution of the diesel pilot to combustion. In fact, such an undervaluation is mostly localized immediately after the pilot ignition and affects the overall heat release.

To the aim of simulating diesel combustion too, the modified CTC model described in § 3.2.5 has been introduced within the KIVA code. In such a way it is possible to account for the total energy introduced into the cylinder. The comparison with the experimental (Figure 5.11) data shows a better general agreement.

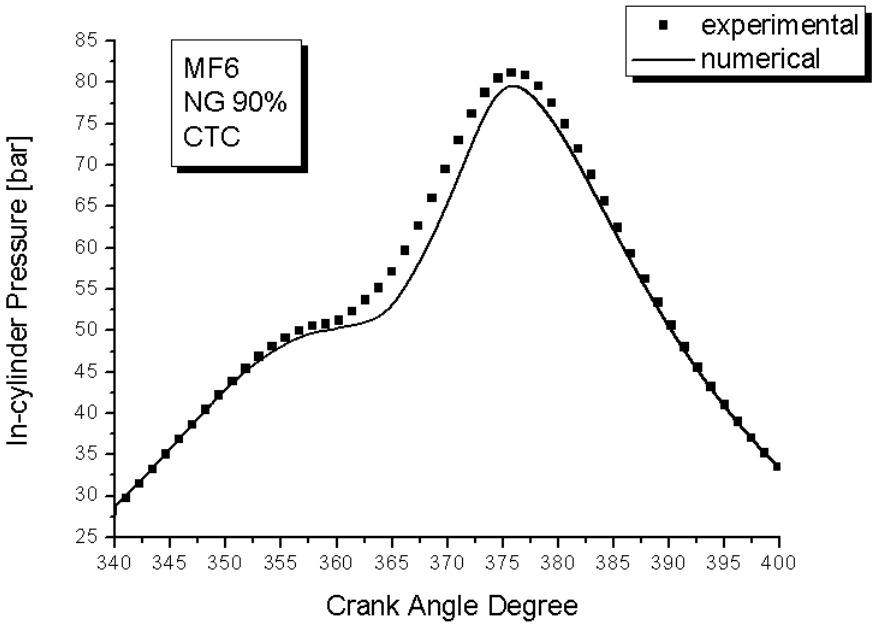

Figure 5. 11 Comparison between experimental and numerical pressure data (MF6, CTC model)

Figure 5.12 reports the temperature maps during combustion. The comparison with Figure 5.9 can be considered as a useful tool to analyze the different behavior of both models. By means of CTC model, the combustion of the whole vaporized diesel fuel and the overall NG can be represented, even though the flame remains localized near the ignition points and the unburned mixture is drawn towards the flame by diffusion. On the contrary, by CFM model, flame develops from an ignition point and propagates rapidly

throughout the chamber. That is why a flamelet approach is preferred for SI engine simulations and the CTC model is usually utilized for diesel applications.

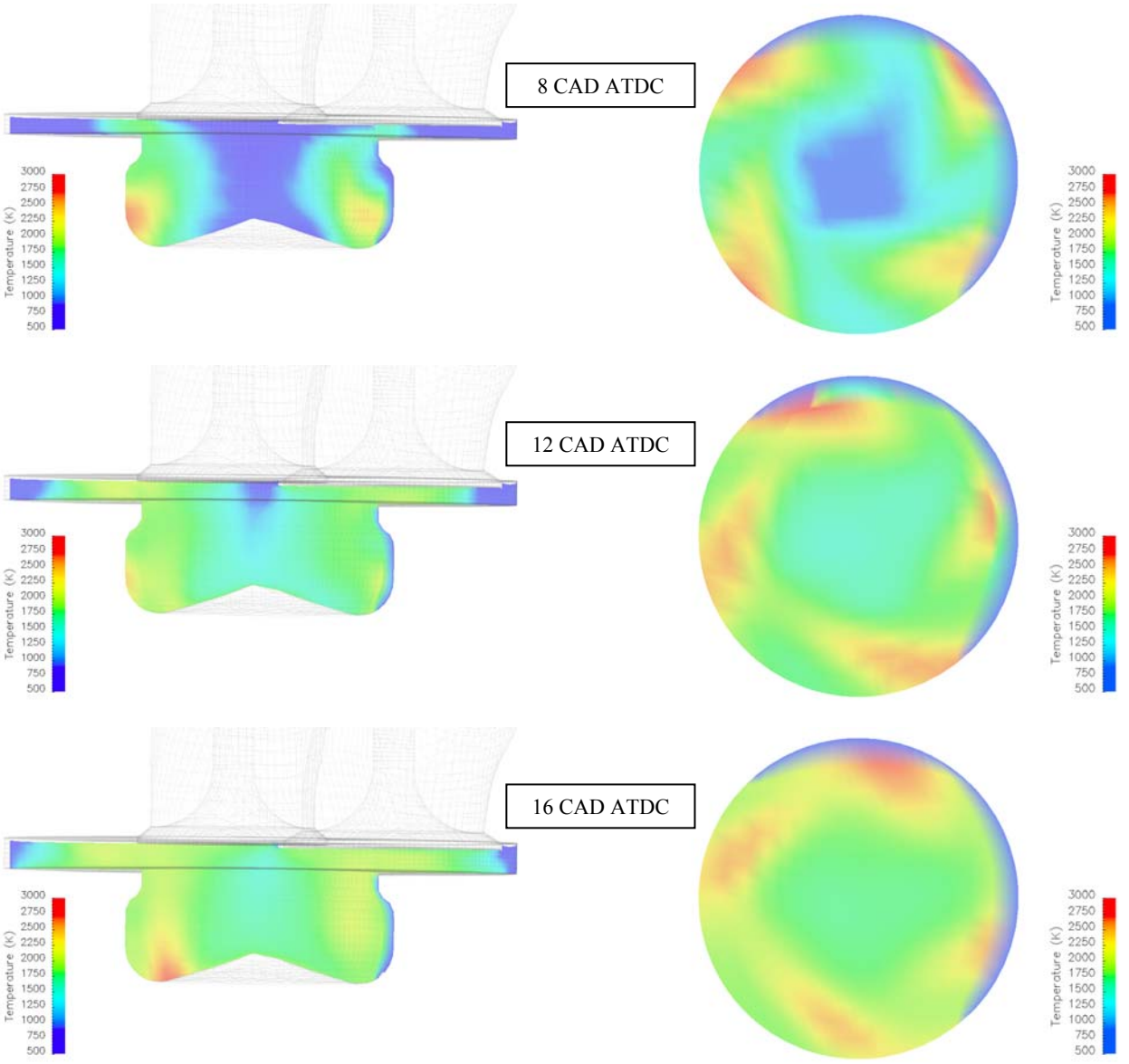

Figure 5. 12 Temperature map on a frontal section and on a cross-section of the piston bowl (MF6, CTC model)

As a result, MF6 case is well represented by CTC model, even though a slight difference with respect the experimental pressure trace can be detected during main combustion. Using a CFM approach, the flame propagation mechanism through the homogeneous mixture can be well described, even better than CTC model. Nevertheless, the contribution of diesel fuel to the total heat release cannot be neglected (Figure 5.13).

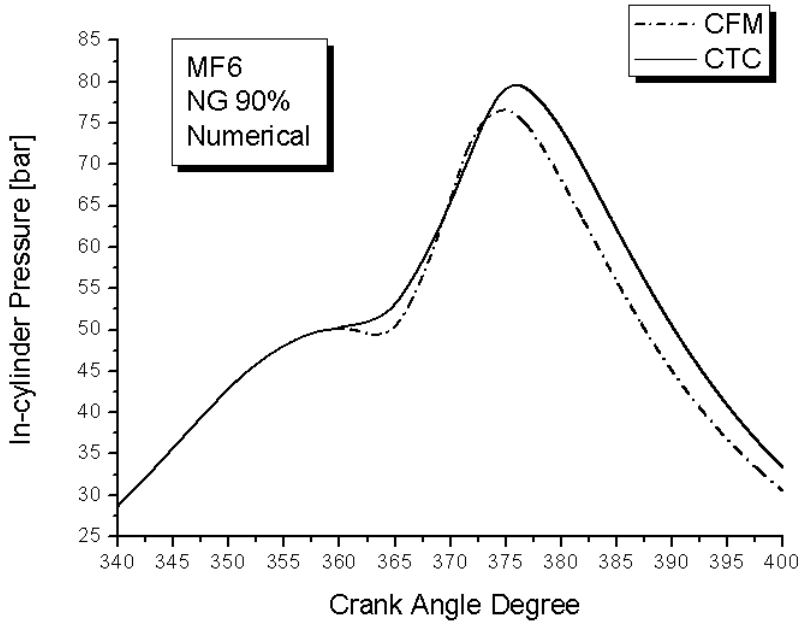

Figure 5. 13 Comparison between CFM and CTC model (MF6)

The flame propagation mechanism highly depends on the air/NG equivalence ratio. An interesting future development could be to define a hybrid model and switch between CTC and CFM on the basis of the local diesel/NG proportion and the local air/NG equivalence ratio. Moreover the CFM model (which is a typical "flamelet" model) could lose its validity for very lean air/NG mixtures. Thus a more general combustion model (G-equation or EDC) could be considered to represent flame propagation.

Once introduced the CTC model and represented diesel combustion in addition to natural gas, every operating condition can be simulated. Figures 5.14-5.16 show the comparison between experimental data for DF, MF1 and MF3 case. A good agreement can be observed, especially for low (0% NG, DF) and high (70% NG, MF3) degrees of NG utilization. On this point, it is worth noting that the CTC model constant C_2 (the turbulent time constant) has been varied from full-diesel to quasi-SI (90% NG) mode. This is due to the difference in the burning rate between diesel fuel and NG which ha to be considered. When an intermediate operating condition is simulated and there is no a prevailing fuel (MF1, 55%NG and 45% diesel), such a model cannot describe the correct burning rate step by step (Figure 5.15), even though the whole combustion is well

represented on the average. A possible solution consist in utilizing two different model constant (calculated at 100% diesel and 100% NG utilization) and to calculate C_2 as a local function of diesel/NG ratio.

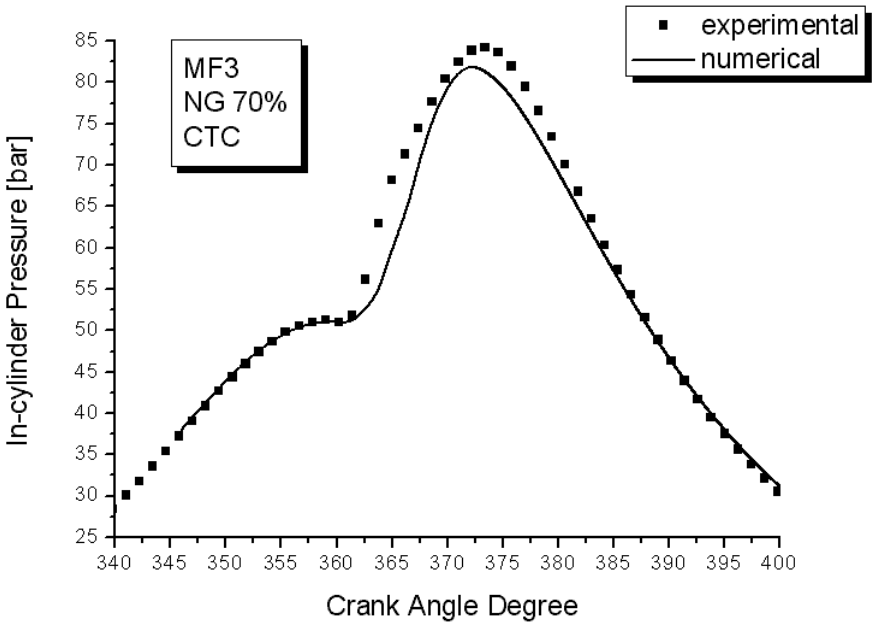

Figure 5. 14 Comparison between experimental and numerical pressure data (MF3, CTC model)

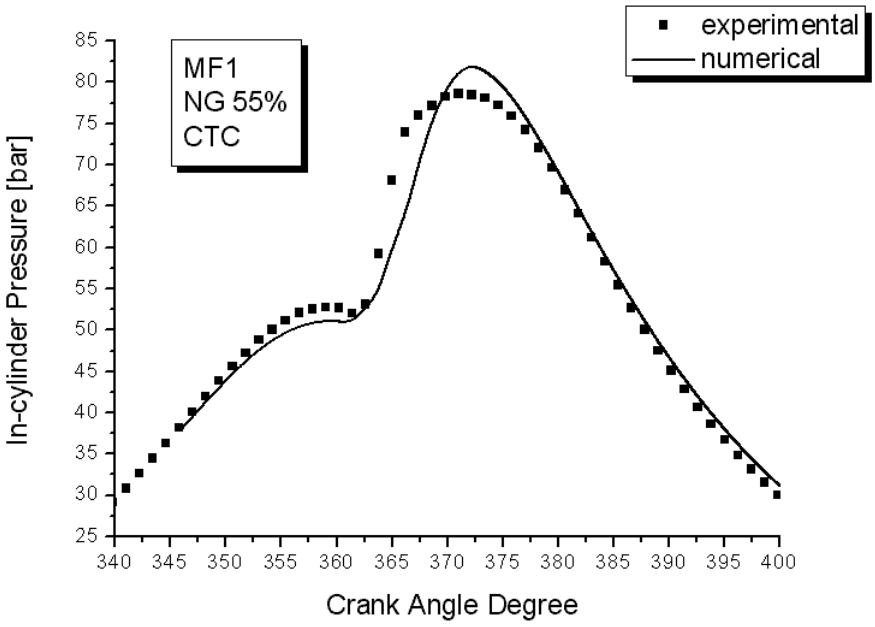

Figure 5. 15 Comparison between experimental and numerical pressure data (MF1, CTC model)

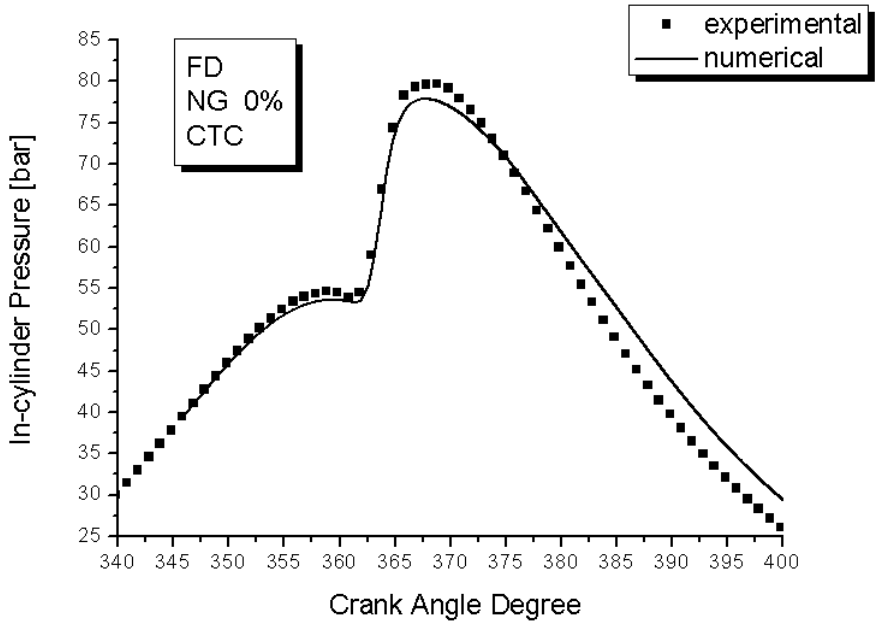

Figure 5. 16 Comparison between experimental and numerical pressure data (FD, CTC model)

Once the KIVA code and the CTC model have been validated for every diesel/NG ratio, a comparison can be carried out between full-diesel and dual-fuel mode.

Figure 5.17 shows the experimental pressure traces concerning the operating conditions above described, while Figure 5.18 reports the in-cylinder mean temperature for the same cases.

The rapid increase of temperature can be observed for the full-diesel case, while the introduction of low NG (55% NG) quantity initially checks the rise of pressure and temperature. This is mainly due to the lower temperature and pressures at the end of compression stroke, due to the different chemical composition of the homogeneous charge, which leads to a reduced value of the ratio of the specific heats $\gamma = c_p/c_v$ while increasing the NG percentage. Accordingly, the ignition of the pilot is slowed down, as well as the early stage of combustion. In fact, the CTC model assumes that early combustion occurring in a laminar regime, where the reaction rate is expressed by Arrhenius laws, being the temperature the most influencing parameter. When higher amounts of NG are introduced into the cylinder, its role in chemical reaction increases, due to the increased air /NG equivalence ratio ϕ (or reduced air index λ).

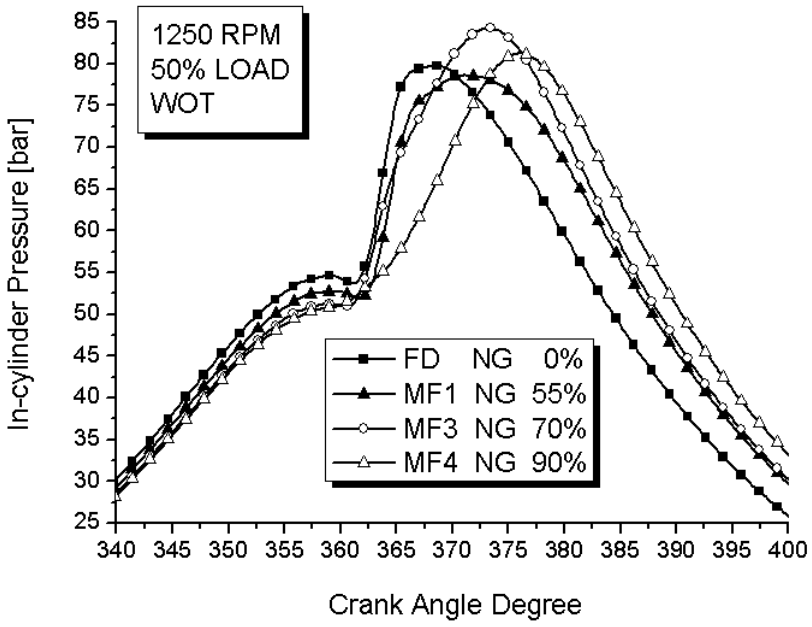

Figure 5. 17 Experimental in-cylinder pressure

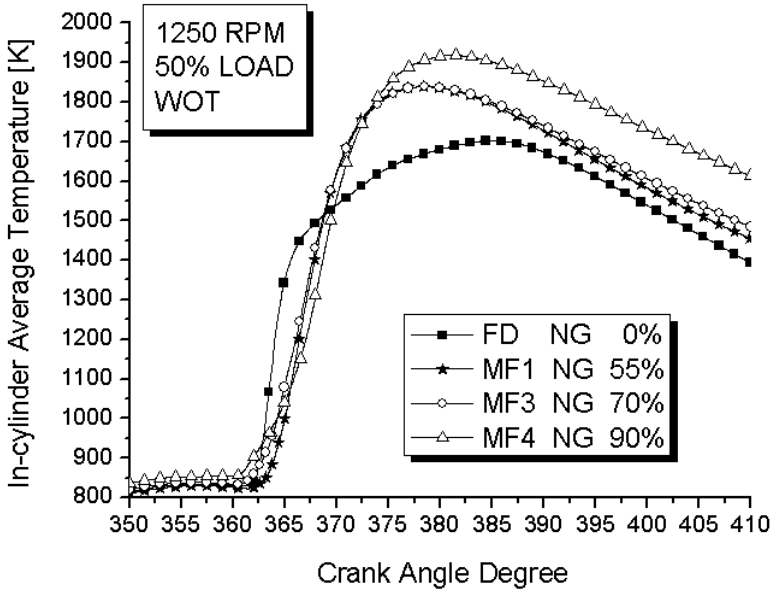

Figure 5. 18 Numerical in-cylinder average temperature

The situation results more evident by observing Figure 5.19, reproducing the temperature field at 2 CAD ATDC, just after the pilot ignition which has been observed to occur around the TDC.

First flame kernels have fully developed for the full-diesel case (FD), whereas the introduction of low amount of NG (MF1, 55% NG) has not a favorable effect. Nevertheless the further introduction of NG leads to an enhancement of the initial stage of combustion. This aspect could be due to the reduced air/NG AFR, from 3.14 (MF1) to 1.84 (MF6), which promotes NG combustion. Moreover, a greater quantity of NG is entrained in the zones which are involved in diesel flames.

Figures 5.19-5.24 show the temperature maps on a frontal section and on a cross-section of the piston bowl at 2, 8, 12, 16, 30 and 40 CAD ATDC, thus providing for a complete representation of the whole combustion process.

A different behavior can be immediately detected while comparing diesel and dual-fuel operations. On full-diesel mode, distinct flames can be detected during the fist stages of combustion while a wider high temperature zone can be observed on dual-fuel, due to the combustion of the surrounding natural gas. Flames on FD mode are strictly localized at the piston walls, where diesel fuel is injected, while involve the overall chamber on dual-fuel mode. Again, it is worth noting that, according to CTC approach, the proper propagation of flame under dual-fuel operations is not visible. The flame is rather spread and a proper flame front cannot be put into evidence.

When a higher amount of NG is utilized, and pilot injection is consequently shortened, the local temperature peaks can be significantly reduced, thus leading to a beneficial effect on NO_X emissions. Nevertheless the average temperature results to be higher on dual-fuel mode, in particular for high percentage of NG utilization (Figure 5.18). In fact, on full-diesel mode, a sizeable portion of the chamber is not affected by flames, while the whole cylinder is involved in combustion on dual-fuel mode.

The local peaks of temperature have been demonstrated to be the main cause of high NO_X concentration in the exhaust. However, the local availability of oxygen has also to be taken into account. Accordingly, the temperature fields cannot provide a correct prediction of NO_X emission without a proper NO_X formation model. This could be the next step in developing the present analysis.

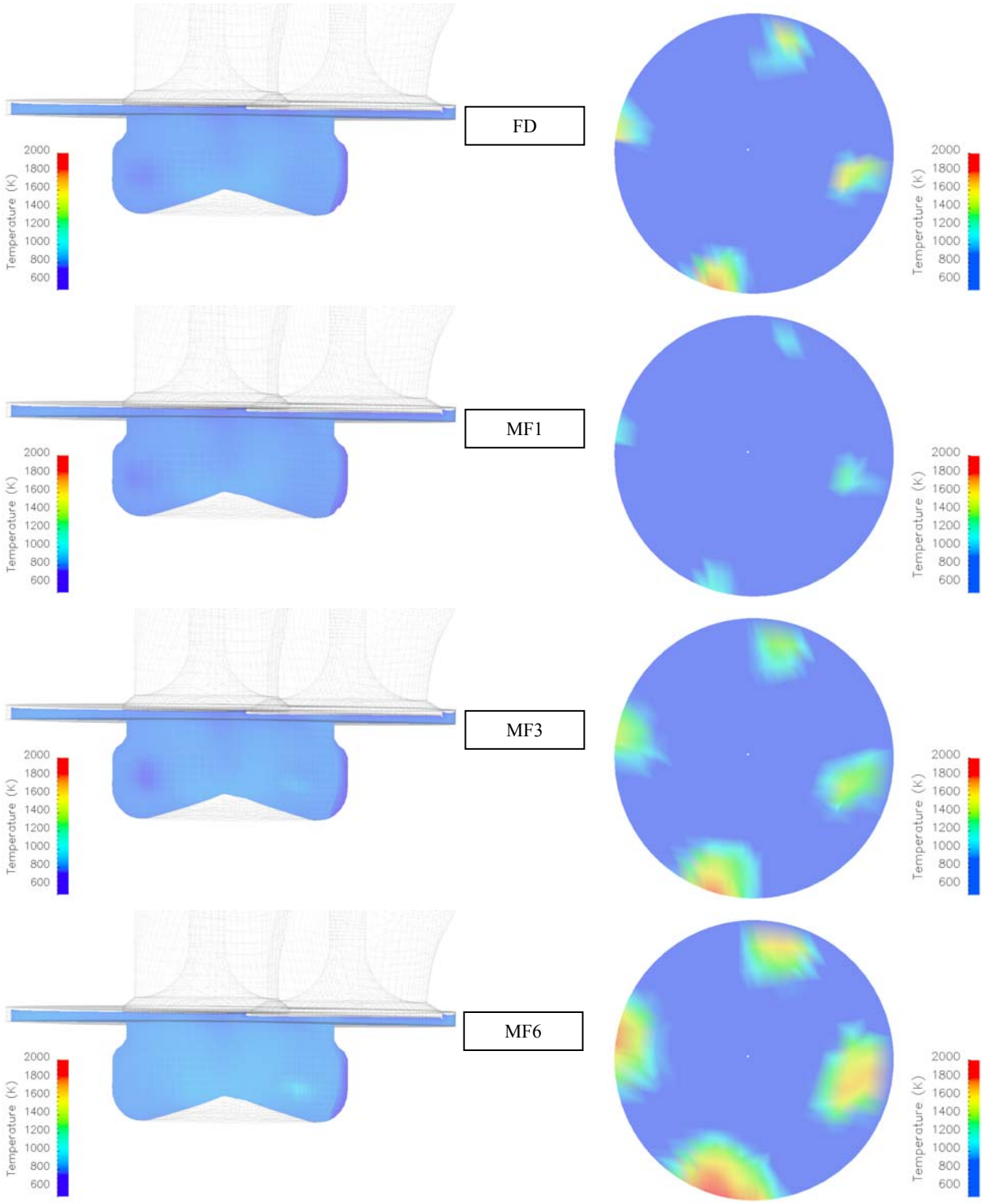

Figure 5. 19 Temperature map on a frontal section and on a cross-section of the piston bowl at 2 CAD ATDC (CTC model)

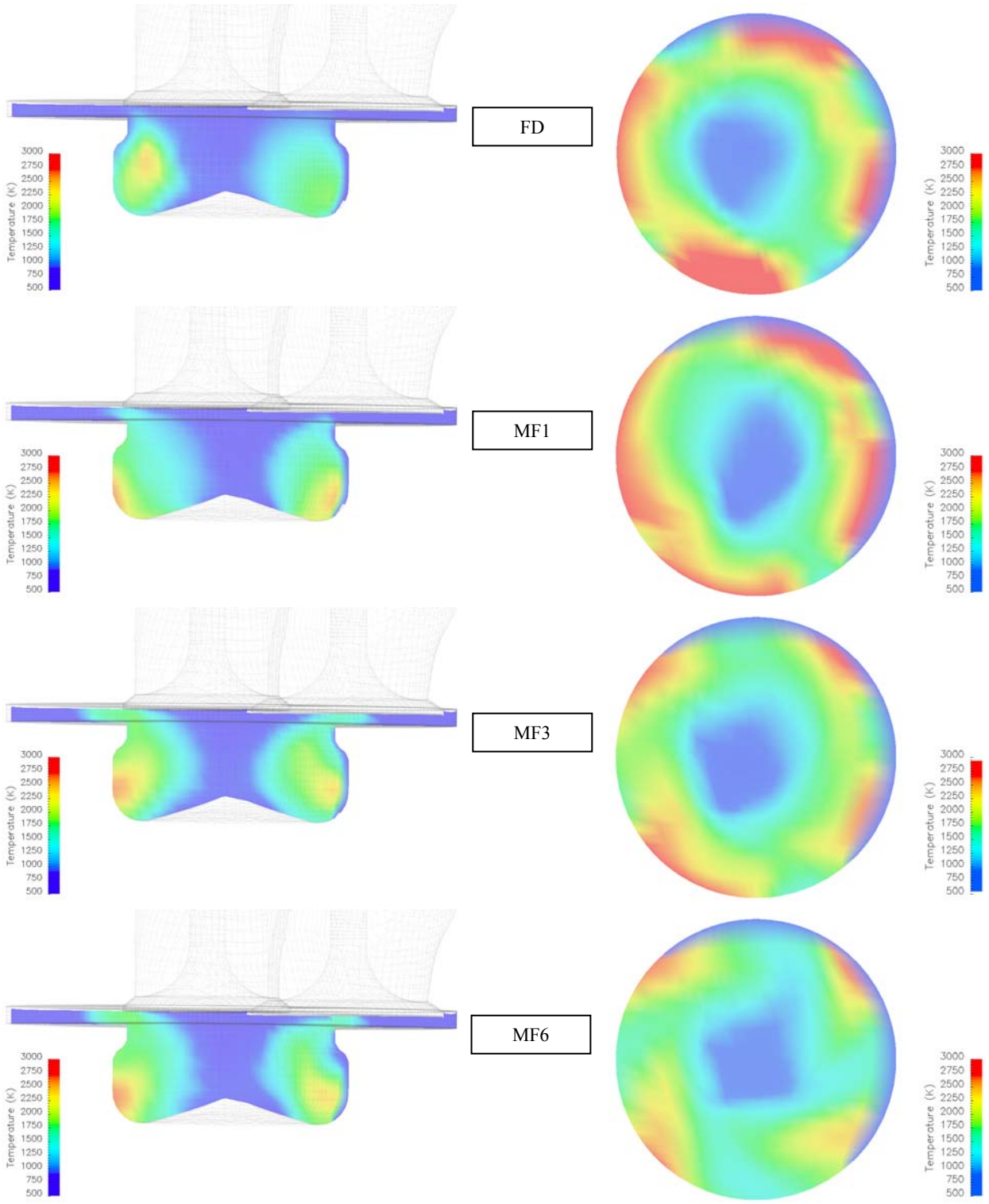

Figure 5. 20 Temperature map on a frontal section and on a cross-section of the piston bowl at 8 CAD ATDC (CTC model)

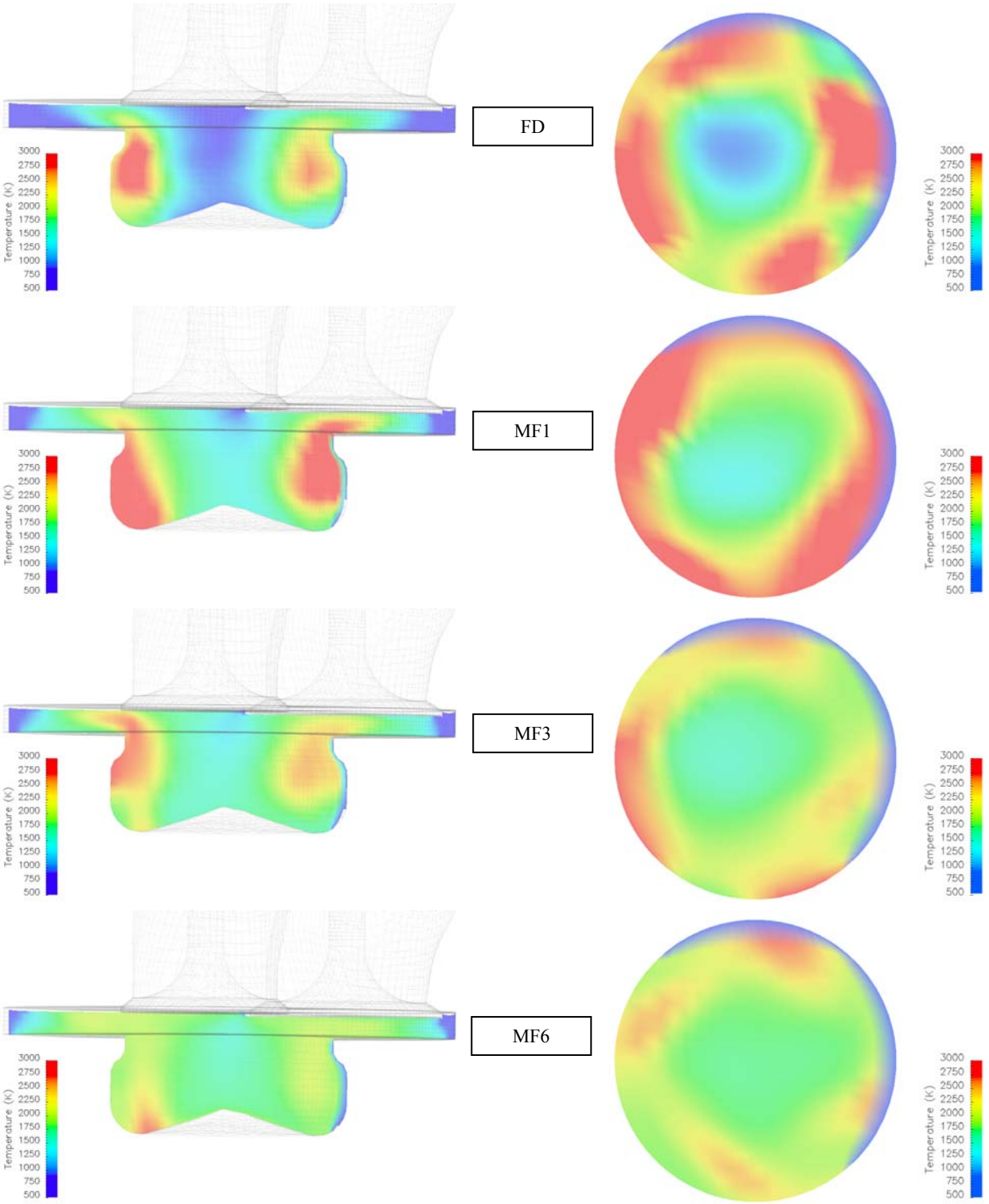

Figure 5. 21 Temperature map on a frontal section and on a cross-section of the piston bowl at 16 CAD ATDC (CTC model)

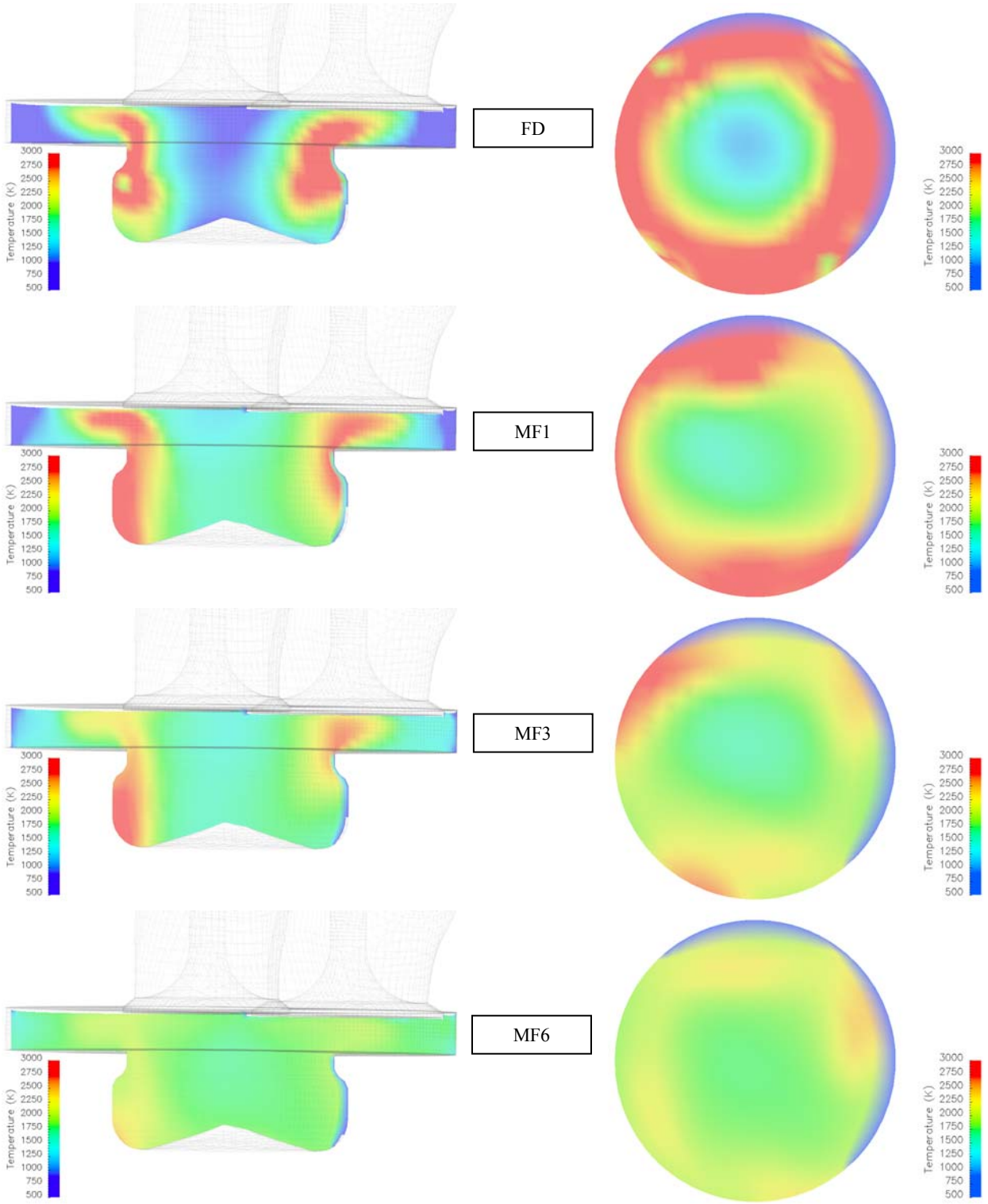

Figure 5. 22 Temperature map on a frontal section and on a cross-section of the piston bowl at 24 CAD ATDC (CTC model)

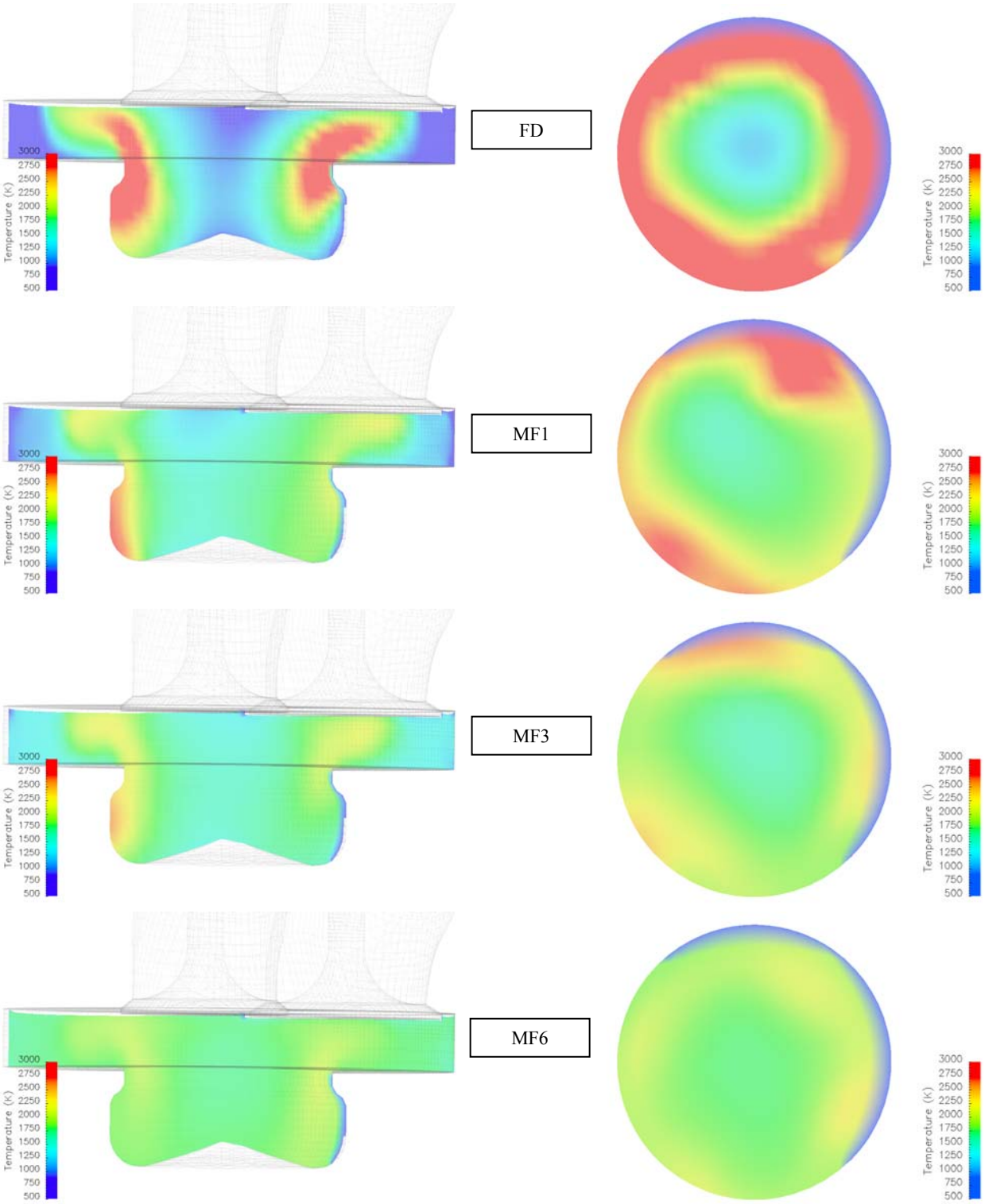

Figure 5. 23 Temperature map on a frontal section and on a cross-section of the piston bowl at 30 CAD ATDC (CTC model)

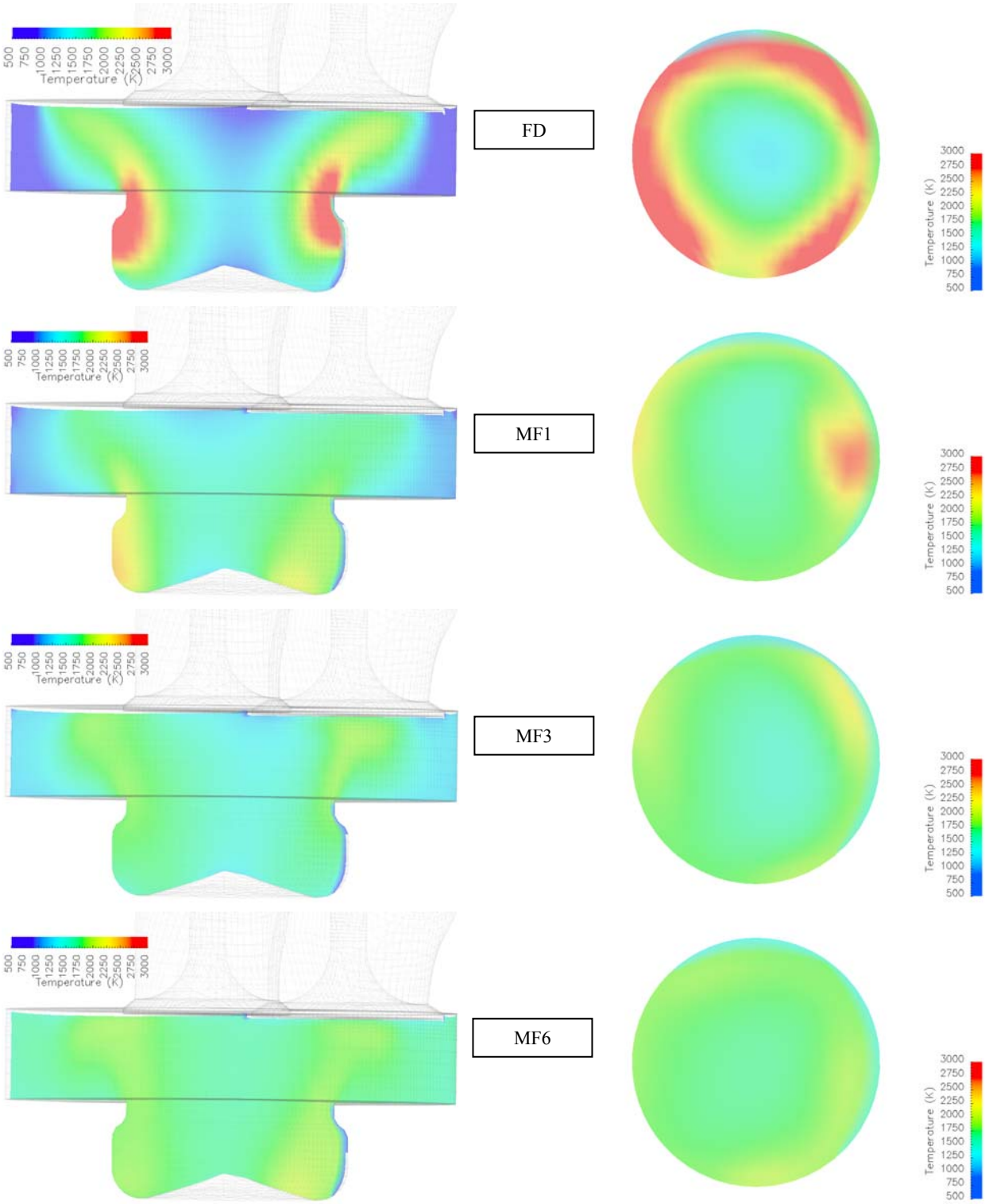

Figure 5. 24 Temperature map on a frontal section and on a cross-section of the piston bowl at 40 CAD ATDC (CTC model)

Chapter 6

FURTHER LEAN BURN NG APPLICATIONS: NG/H_2 BLENDS

6.1 Introduction

Generally speaking, the environmental problem is still far from being definitely solved. CO_2 represents a fairly recent concern since Kyoto targets are hard to be achieved for almost each participating country. The introduction of H_2 into the automotive field appears as the only long-term solution to consistently reduce CO_2 emissions on a global basis. Fuel cells certainly are the ideal technology to entirely exploit H_2 potential, but they are still undergoing research and development design stage to fix important issues such as material costs, durability and reliability.

H_2 however may still be thought as a short-term solution if utilized into assessed technologies, such as natural-gas (NG) internal combustion engines. The use of NG blended with H_2 may be a good solution since those blends are characterized by higher laminar flame speeds than pure NG [67,68], which in turn allows to get a more efficient combustion process (and then higher global efficiencies) and a reduction of CO_2 emissions for the lower fuel carbon content. Advantages are even more relevant under partial load conditions if lean-burn control strategies are adopted since H_2 addition extends the lean-limit of natural-gas [69,70] and reduces the penalties in terms of HC emissions [71,72].

The use of blends characterized by low H_2 content (up to 20-30% in volume) does not require essential modifications of a given native NG engine: higher NO_X emissions

[73] are the drawback for the higher temperatures occurring during combustion. Two strategies may be adopted to overcome that problem:

- Delaying spark advance if engine is fuelled by stoichiometric mixtures
- Lean burn operation

6.2 Numerical Approach

The whole experimental and numerical activities have been carried-out in the context of a project involving ASM Spa (the energy multi-utility of Brescia), ENEA research council, Universities of Rome “Tor Vergata” and “La Sapienza”, Catholic University of Brescia.

The engine performance have been numerically evaluated by means of a multi-dimensional (3-D) approach. Accordingly, a modified version of the KIVA-3V code has been utilized and the CFM (Coherent Flame Model) combustion model has been considered to represent combustion. Details are provided in § 3.2 and § 3.2.5.

6.3 Laminar Flame Speed Calculation Details

Laminar flame speed of H_2/NG blends has been evaluated as a function of H_2 percentage, equivalence ratio, unburned temperature and pressure. To that aim, the 1-D model of the premixed flame has been setup as a pre-processor of the full 3-D model, to build-up laminar flame speed libraries. Equations of the laminar flame speed model are reported below:

$$\rho u = \text{cost} \tag{6.1}$$

$$\rho c_p u \frac{dT}{dx} - \frac{d}{dx}\left(\lambda \frac{dT}{dx}\right) + \sum_{k=1}^{N} \dot{\omega}_k h_k W_k = 0 \tag{6.2}$$

$$\rho u \frac{dY_k}{dx} + \frac{d}{dx}\left(\rho Y_k V_k\right) - \dot{\omega}_k W_k = 0 \tag{6.3}$$

Where k varies from 1 to N_S, N_S being the total number of species. $\dot{\omega}_k = \sum_{i=1}^{N_R} \nu_{ki} q_i$ represents species k chemical reaction rate summed over the total number of reactions N_R and depends on the kinetic velocity of each chemical reaction q_i:

$$q_i = k_{fi} \prod_{j=1}^{N_S} \left[X_j\right]^{\nu'_{ik}} - k_{ri} \prod_{j=1}^{N_S} \left[X_j\right]^{\nu''_{ik}} \tag{6.4}$$

X_j being molar fractions of species j, k_{fi} and k_{ri} forward and backward reaction constants modeled via Arrhenius approach:

$$k_{fi} = A_i T^{B_i} \exp\left(-\frac{E_i}{RT}\right) \tag{6.5}$$

$$k_{ri} = \frac{k_{fi}}{K_{ci}} \tag{6.6}$$

A_i, B_i, E_i are kinetic parameters and K_{ci} the equilibrium constant of reaction i.

The accuracy of laminar flame speed computation strictly depend on the utilized chemical mechanism: GRI 3.0 has been used in this context which consists of 325 reactions over which 53 species are involved [74].

A specific open-source chemistry solver (CANTERA) has been used to discretize and solve equations (6.1-6.3): it is characterized by high accuracy and computational efficiency [75].

6.4 General Results

Numerical model has been first applied to the analysis of pure NG operation with respect to different operating conditions, to evaluate the capabilities of the tool. Pressure traces have been therefore compared to experimentally acquired ones, as it is displayed in

Figure 6.1. Data refer to three regimes characterized by quite different operating conditions (rpm=1500, 2500, 3500; load=25, 50%; spark advance=27, 28, 33 CA).

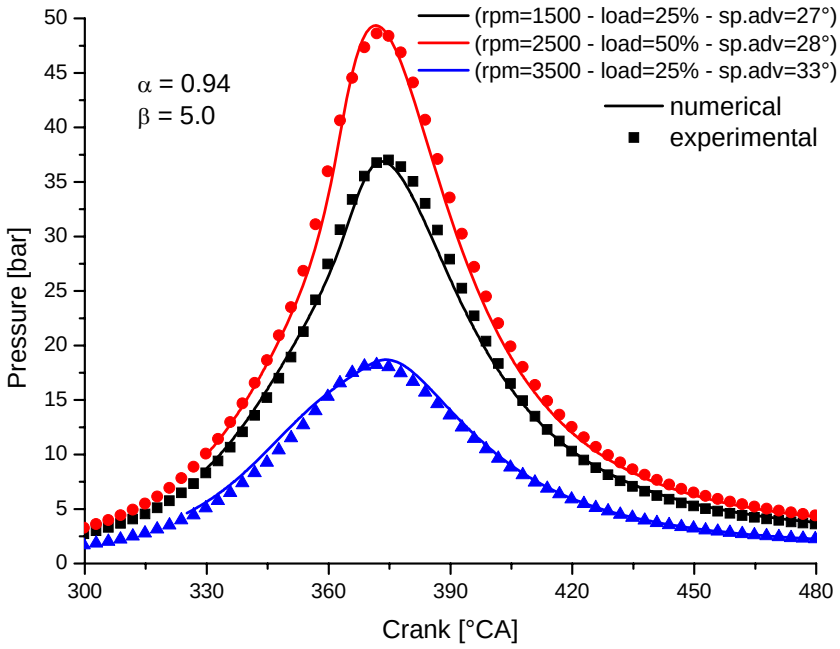

Figure 6. 1 Pure NG operation pressure traces

A satisfactory agreement may be observed between numerical and experimental pressure traces, so allowing considering the model as able to represent combustion process. It is further worth noting that the numerical model (CFM) main constants α and β have been put equal to respectively 0.94 and 5.0, and they have been kept unchanged by varying engine operating conditions.

The numerical tool has then been applied to the analysis of 15% vol. H_2/NG blends: this change in operating conditions first gives rise to a variation of laminar flame speed. Laminar flame speed is plotted in Figure 6.2 vs. CA for both pure NG and H_2/NG mixture (2500 rpm and 50% load operating conditions, stoichiometric mixtures). The evident increase of laminar flame speed in turn determines potentially higher heat release rate and then higher performance potential in terms of thermal efficiency.

After such modifications, the code was validated under the operation with NG/H_2 blends: the comparison between experimental and numerically predicted data is reported in Figure 6.3. It can be stated again that the numerical model performance are roughly

unchanged, underlying that α and β constants have not been changed with respect to pure NG cases.

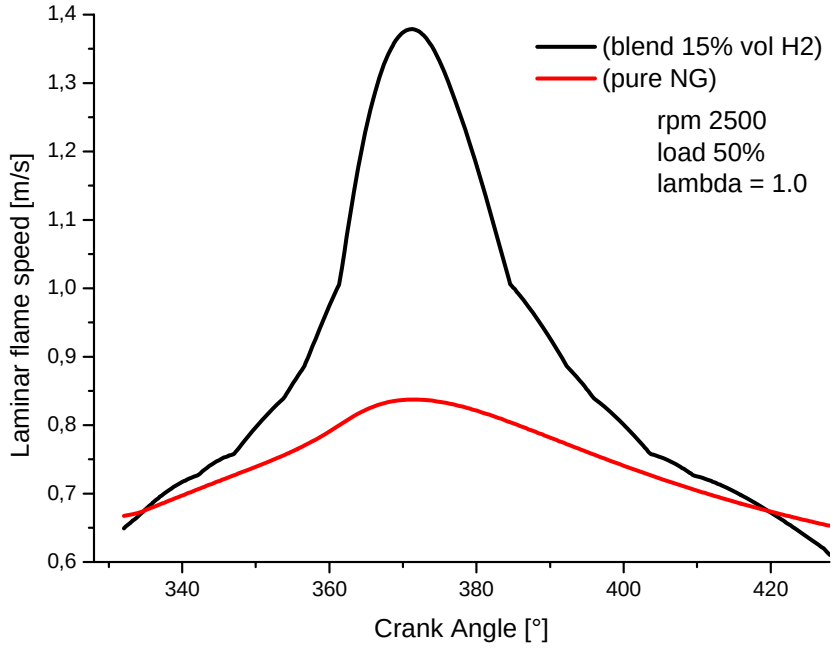

Figure 6. 2 Laminar flame speed vs. CA for pure NG and 15% vol. H_2 blend

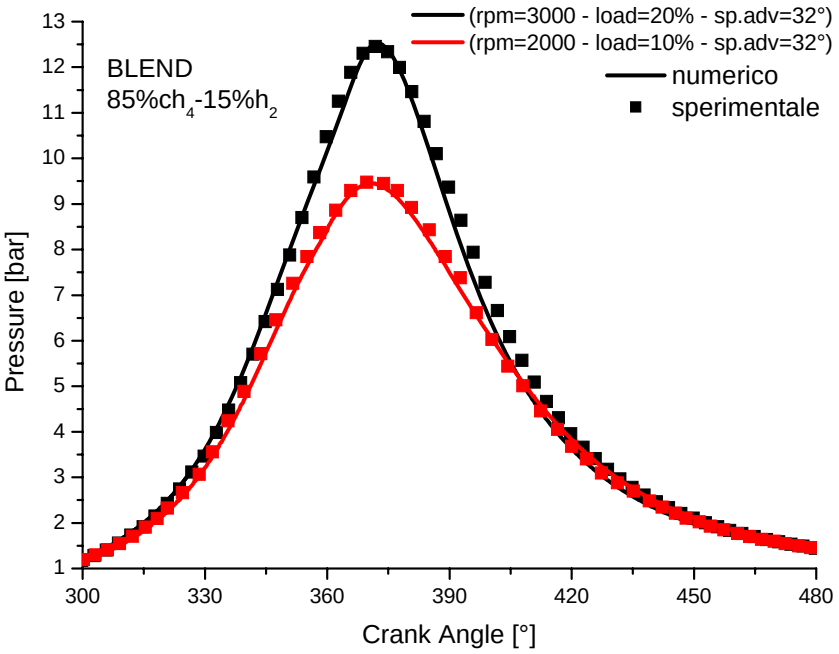

Figure 6. 3 NG/H_2 (15% H_2) blends operation pressure traces

Once assessed the model capabilities, the numerical tool has been applied to predict engine performance to the aim of optimizing the electrical spark advance (Table 6.1). Engine simulations have been performed to identify a related set of corrections to be applied to the engine control to approximately keep engine performance constant (in terms of average pressure) so reducing NO_X emissions to a value comparable to the native pure NG solution.

Operating Conditions	Spark Advance Correction
rpm=1500; load=25%	+2
rpm=1500; load=50%	+4
rpm=2500; load=25%	+2
rpm=2500; load=50%	+4
rpm=3500; load=25%	+3
rpm=3500; load=50%	+4

Table 6. 1 Engine operating conditions and related spark advance corrections

Moreover, the observed superior performance of blends under lean-burn conditions in terms of flammability limit suggests the use of that strategy to control engine output.

Higher efficiency, that is typical of lean-burn combustion processes, is also accompanied by a higher potential in terms of NO_X reduction, due to the occurrence of lower temperatures into the combustion chamber. The effect of Air Fuel Ratio (AFR) on engine performance (Figure 6.4) and on the average temperature (Figure 6.5) is highlighted.

Once implemented corrections to be applied by the engine control system, vehicle performance have been experimentally verified as far as the urban part of ECE cycle is concerned. Results, reported in Figure 6.6 for 15% H_2 blends for both stoichiometric and lean operating conditions [78], evidently underline the success in getting consistent improvements as far as fuel consumption and CO_2 emissions are concerned. Tailpipe emissions (Figure 6.7) represent the actual drawback of lean-burn operation: in those conditions HC are in fact remarkably increased. NO_X, which in lean-burn cases do not

take advantage of the equipped Three Way Catalyst, have been limited to about the same value of the native solution not to excessively affect engine performance.

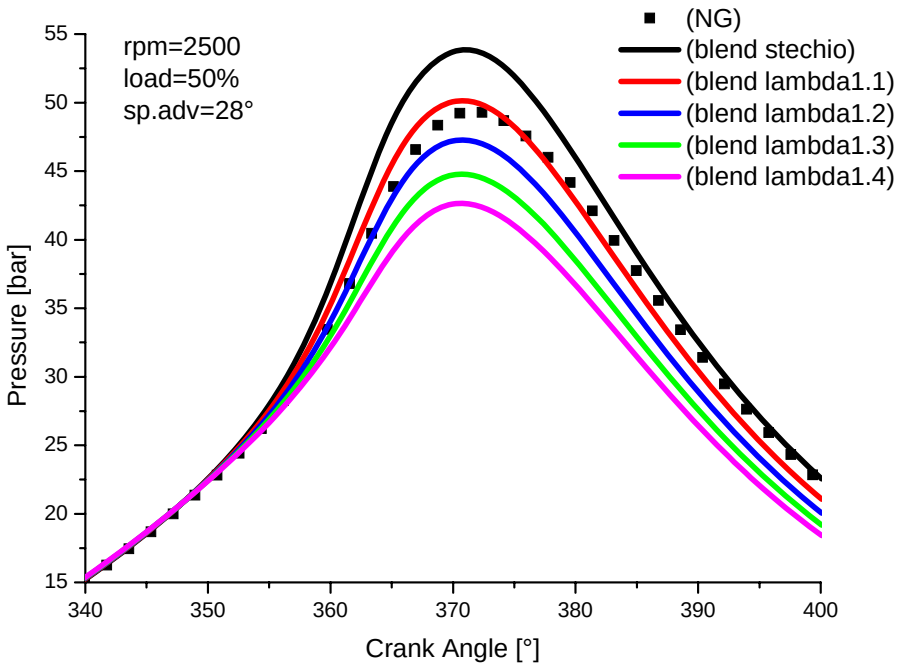

Figure 6. 4 The effect of AFR on engine performance

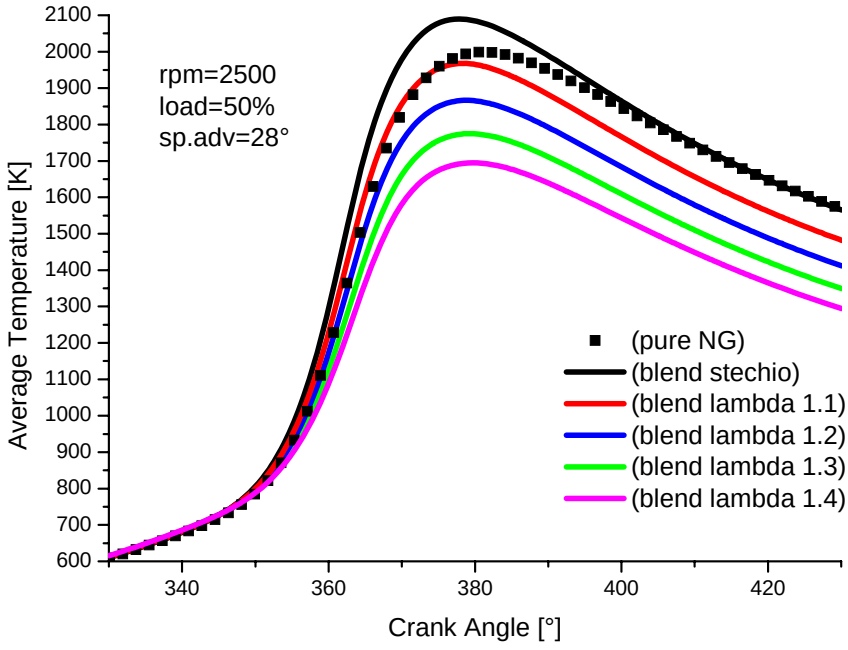

Figure 6. 5 The effect of AFR on chamber average temperature

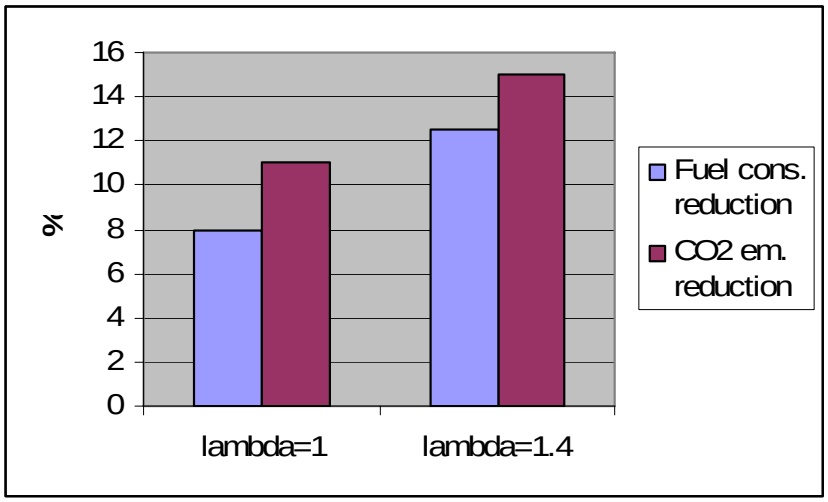

Figure 6. 6 NG/H_2 blends: fuel consumption and CO_2 reduction on the urban part of ECE cycle.

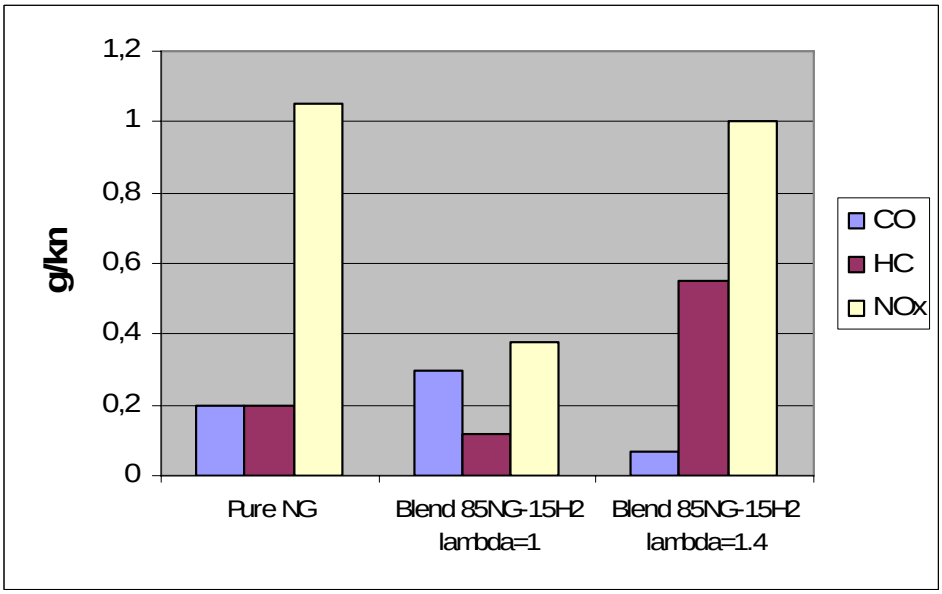

Figure 6. 7 NG/H_2 blends: pollutant emissions on the urban part of ECE cycle.

Chapter 7
CONCLUSIONS

7.1 Conclusions

Natural gas is commonly considered as the most inviting short-term fuel alternative for internal combustion engines applications. In addition to the significant benefits in terms of pollutant emissions, it is particularly suitable to be operated in high compression ratio (CR) engines, as well as under lean and ultra-lean conditions.

Accordingly, the dual-fuel natural gas/diesel engines can be considered as an inviting solution to extend the lean flammability limit of natural gas and simultaneously solve the trade off NO_X-PM affecting diesel engines. That is why dual-fuel engines are particularly interesting as retrofit concept of existing and running on-road diesel engines.

In fact, the dual-fuel conversion can be easily carried out. The original compression ratio of the diesel engine can still be operated with lean air/NG mixtures. After the conversion, the dual-fuel engines can ensure diesel-like performance, even for ultra lean gaseous mixtures ($\lambda > 1.84$), while reducing PM and NO_X emissions. Unfortunately, dual-fuel engines suffer from high HC and CO emissions, mainly due to the lean combustion of the homogeneous air/NG charge, especially under partial load conditions. With the introduction of a certain number of devices (intake throttling, three-way catalyst, EGR), and operating on full diesel at the lightest loads, it is possible to obtain interesting results on the ECE R49 13-mode test, compared with the diesel baseline case.

Numerical simulation can be a useful tool to help the experimental procedure to find the right direction. In the present study, a numerical procedure to correctly describe the behavior of the dual-fuel engines has been presented. A mixed 1-D / 3-D numerical

procedure has been utilized. The 1-D code FW2001, entirely developed at UTV, has been used for the initial understanding of the complex phenomena evolving during dual-fuel combustion. Experimental data have been thus managed by means of a diagnostic strategy to provide important information on the combustion progress (HRR calculations). Secondly, the 1-D code has been utilized to provide the pressure boundary conditions as input information for the subsequent multi-dimensional (3-D) analysis.

Concerning with 3-D tools, a version of KIVA-3V code, modified at UTV during the recent years has been utilized. A fair number of sub-models (WAVE, Shell, CFM, CTC) have been introduced and implemented within the “open source” code, in order to improve its reliability.

Numerical results have well predicted the engine performance. The WAVE and Shell model has well represented the evolution of the spray and the ignition delay. When a high degree of substitution of diesel fuel with NG is performed, the engine results quite similar to a SI engine, with the only difference of being characterized by a large number of spark plugs (ignition points, that is to say everywhere diesel fuel auto-ignites). That is why such an operating condition (90% NG) has been at first simulated by means of the CFM combustion model, while assuming the diesel fuel as the ignition source only. Nevertheless the contribution of the diesel pilot to the total heat release cannot be neglected, as an exception for very low percentage of diesel utilization (< 5%). To this aim a complete and modified CTC model has been introduced and has allowed well representing overall diesel and natural gas combustion, for every diesel/NG ratio. Nevertheless, for high degrees of NG utilization (> 95%), the CFM model can still represent a valid alternative, since it more properly describes the flame propagation mechanism.

The CFM model has also been utilized to simulate the stoichiometric and lean combustion of NG/H_2 blends. In this latter case the numerical approach results rather simplified, since NG and H_2 are characterized by the same combustion mechanism (by flame propagation). The main benefit of introducing a certain amount of H_2 in NG/air mixtures consists in the significant increase in the laminar flame speed which allows for reduced combustion duration. Accordingly, such a technological solution can

significantly improve the lean burn behavior of NG/air mixtures and further extend the lean flammability limit for NG. Here again, the numerical approach has provided for an accurate description of the actual combustion process. Moreover it has been utilized in a predictive way to optimize the main engine parameters (spark timing advance and air/NG AFR) for the final experimental tests.

7.2 Recommendations for Future Work

Future developments of the numerical activity on dual-fuel engines have to be mainly focused on a more detailed analysis of the spray evolution and on the evaluation of the single contribution of diesel fuel and natural gas to the total heat released during the dual-fuel combustion. Starting from the consideration that the CFM model has provided in the past significant results on the numerical simulation of SI-NG engines, it is worth noting that combustion in diesel engines in general needs major computational efforts to be well represented. This is mainly due to the remarkable difficulty to correctly simulate the evolution of the spray. In this study, fundamental processes as droplet splash, rebound and film at the cylinder walls has not been deeply investigated (the original models within the KIVA code have been considered), as well as the contribution of drop distortion to the drag coefficient. Moreover, cavitation and turbulent effects on jet atomization have been neglected as well, even though they are particularly relevant for high pressure diesel sprays, while the examined engine being characterized by a low injection pressure (240 bar).

As concerns with dual-fuel combustion, two paths are here suggested. First, the analysis of the single contribution of diesel and natural gas to the whole combustion has to be carried out and a local value of the CTC model constant has to be provided on the basis of the local composition of both fuels. Secondly, the actual lean flammability limit under dual-fuel mode has to be further investigated. To this aim, a hybrid CTC/CFM model can be developed and the switch condition can be related to the local AFR.

Moreover, the CFM could lose its validity if too lean conditions would occur. Therefore, in the far-off future a more general combustion model (EDC or G-equation)

could be considered to correctly represent combustion of every fuel at every equivalence ratio. Finally, the present analysis has to be extended to predict the pollutants formation, with particular regard to NO_X and PM emissions.

From an experimental point of view, the analysis has to be focused on the influence of the injection timing advance on performance and emissions. In fact, numerical simulation have pointed that ignition occurs around the TDC, thus it results widely delayed with respect SI operations. Advancing injection timing further (to 20, 30 CAD BTDC or even more) while increasing air/NG AFR (thus obtaining leaner mixtures) could provide for a simultaneous reduction of HC and NO_X, which usually follow an opposite trend.

References

[1] Gambino M., Migliaccio M. “Carburanti alternativi per l’autotrazione”, Liguori 2000.

[2] Umiersky M., Huchtebrock B. “CNG Concepts for Passenger Cars and Light-Duty Vehicle Challenging Diesel Powertrains”, SAE_NA Technical Paper 2003-01-45, 2003.

[3] Evans R. L., Blaszczyk J., Matys P. “An Experimental and Numerical Study of Combustion Chamber Design for Lean-Burn Natural Gas Engines”, SAE Technical Paper 961672, 1996.

[4] Evans R. L., De Castro F., Reynolds C., Cameron K., Gerty M. “A Partially Stratified-Charge Approach for Reduced Emissions from Gas Engines”, SAE Technical Paper 2001-01-037, 2001.

[5] Andreassi L., Cordiner S., Mulone V., Evans R. L., Reynolds C. “A Mixed Numerical-Experimental Analysis for the Development of a Partially Stratified Compressed Natural Gas engine”, SAE_NA Technical Paper 2003-01-45, 2003.

[6] Karim G. A., Liu Z., Jones W. “Exhaust Emissions from Dual-Fuel Engines at Light Load”, SAE Technical Paper 932822, 1993.

[7] Papagiannakis R.G., Hountalas D.T. “Experimental investigation concerning the effect of natural gas percentage on performance and emissions of a DI dual fuel diesel engine”, Int. J. Appl. Therm. Eng. 23 (353-365), 2003.

[8] Weaver C. S., Turner S. H. “Dual Fuel Natural Gas/Diesel Engines: Technology, Performance, and Emissions”, SAE Technical Paper 940548, 1994.

[9] Karim G. A., “Combustion in Gas Fueled Compression: Ignition Engines of the Dual Fuel Type”, J. Eng. Gas Turb. Power, 125 (827-836), 2003.

[10] Papagiannakis R.G., Hountalas D.T. “Combustion and Exhaust Emission characteristics of a dual fuel compression ignition engine operated with pilot diesel fuel and natural gas”, En. Conv. & Man. 45 (2971-2987), 2004.

[11] Krishnan S. R., Biruduganti M., MO Y., Bell S. R., Midkiff K. C. “Performance and Heat Release Analysis of a Pilot-Ignited Natural Gas Engine”, Int. J. Eng. Research 3 (171-184), 2002.

[12] Abd Alla G.H., Soliman H.A., Badr O.A., Abd Rabbo M.F “Effect of Pilot Quantity on the Performance of a Dual Fuel Engine”, En. Conv. & Man. 41 (559-572), 2000

[13] Abd Alla G.H., Soliman H.A., Badr O.A., Abd Rabbo M.F “Effect of Injection Timing on the Performance of a Dual Fuel Engine”, En. Conv. & Man. 43 (269-277), 2002

[14] Srinivasan, K.K., Krishnan, S.R., Singh, S., Midkiff, K.C., Bell, S.R., Gong, W., Fiveland, S., Willi, M., “The Advanced Low Pilot Ignition Natural Gas Engine – A Low NOx Alternative to the Diesel Engine”, Proc. of Int. Joint Power Gen. Conf. (IJPGC) 40098, 2003.

[15] Daisho Y., Yaeo T., Koseki T., Saito T., Kihara R., Quiros E., “Combustion and Exhaust Emissions in a Direct-Injection Diesel Engine Dual-Fueled With Natural Gas”, SAE Technical Paper 950465, 1995.

[16] Daisho Y., Takahashi Y. I., Nakayama S., Kihara R., Saito T. “Controlling Combustion and Exhaust Emissions in a Direct-Injection Diesel Engine Dual-Fueled with Natural Gas”, SAE Technical Paper 952436, 1995.

[17] Pope S. B. “Turbulent Flows”, Cambridge University Press, 2000.

[18] Borghi R. “On the structure and morphology of turbulent premixed flames”, Rec. Adv. Aerospace Sci., pp. 117-138, 1985.

[19] Peters N. “Laminar flamelet concepts in turbulent combustion”, Twenty-first Symposium (International) on combustion, pp.1231-1250, Pittsburgh, 1986.

[20] Spalding D.B. “Mixing and chemical reaction in steady confined turbulent flames”, Thirdteenth Symposium (International) on combustion, pp.649-657, Pittsburgh, 1971.

[21] Magnussen B.F., Hjertager B.H. Sixteenth Symposium (International) on combustion, pp.719-729, Pittsburgh, 1977.

[22] Abraham J., Bracco F. V., Reitz R. D. “Comparisons of computed and measured premixed charge engine combustion”, Combustion and flame, vol.60, pp.309-322, 1985.

[23] Bray K. N. C., Libby P. A., Moss J. B. Combustion and flame, vol.61, pp.87-102, 1985.

[24] Cant R. S., AbuOrf G. M. “A turbulent reaction rate model for premixed turbulent combustion in Spark-Ignition engines”, Combustion and flame, vol.122, pp.233-252, 2000.

[25] Liu Z.,. Karim G. A. “A Predictive Model for the Combustion Process in Dual Fuel Engines”, SAE Technical Paper 952435, 1995.

[26] Abd Alla G. H., Soliman H. A., Badr O. A., Abd Rabbo M. F. “Combustion quasi-two zone predictive model for dual fuel engines”, En. Conv. & Man. 42 (1477-1498), 2000.

[27] Hountalas D. T., Papagiannakis R. G. “Development of a Simulation Model for Direct Injection Dual Fuel Diesel-Natural Gas Engines”, SAE Technical Paper 2000-01-0286, 2000.

[28] Zhang Y., Kong S. C., Reitz R. D. “Modeling and Simulation of Dual Fuel (Diesel/Natural Gas) Engine with Multidimensional CFD”, SAE Technical Paper 2003-01-0755, 2003.

[29] Singh S., Kong S. C., Reitz R. D., Krishnan S. R., Midkiff K. C. “Modelling and Experiments of Dual Fuel Engine Combustion and Emissions”, SAE Technical Paper 2004-01-0092, 2004.

[30] Singh S., Liang L., Kong S. C., Reitz R. D. “Development of a Flame Propagation Model for Dual-Fuel Partially Premixed Compression Ignition Engines”, Int. J. Eng. Research., vol. 7 , 65-75, 2006.

[31] Heywood J. B. “Internal Combustion Engine Fundamentals”, McGraw–Hill, New York, 1988.

[32] Woschni, G. “Universally Applicable Equation for the Instantaneous Heat Transfer Coefficient in the Internal Combustion Engine”, SAE Technical Paper 670931, 1967.

[33] Ramos J. I. “Internal Combustion Engine Modelling”, Hemisphere Publishing Corporation, 1989.

[34] Miyamoto N., Chikahisa T., Murayama T., Sawyer R. “Description and Analysis of Diesel Engine Rate of Combustion and Performance Using Wiebe’s Functions”, SAE Technical Paper 850107, 1985.

[35] Cordiner S., Rocco V. “Modelling of Unburned Hydrocarbons Emissions in Gasoline Engines”, 3rd International Conference on Internal Combustion Engines: Experiments and Modelling, Capri (Italy) September 17 - 19, 1997.

[36] Biancolini M., Cordiner S., Rocco V. “A Hierarchical Approach to Describe Flow-Spray Interaction in the Transient of S.I Engines”, 4thInternational Conference on Internal Combustion Engines: Experiments and Modelling, Capri (Italy), 1999.

[37] Biancolini M., Cordiner S., Gambino M., Iannaccone S., Rocco V. “Valve timing optimization to reduce HC emissions for a heavy duty CNG fuelled Turbocharged Engine”, European Automotive Congress, Barcelona, 1999.

[38] Amsden A. A., Ramshaw J. D., O’Rourke P. J., Dukowicz J. K. “KIVA: A computer program for two- and three-dimensional fluid flows with chemical reactions and fuel sprays”, Los Alamos National Laboratory Report LA-10245-MS, 1985.

[39] Amsden A. A., O’Rourke P. J., Butler T D. “KIVA-II: A computer program for chemically reactive flows with sprays”, Los Alamos National Laboratory Report LA-115600-MS, 1989.

[40] Amsden A. A. “KIVA-3: A KIVA Program with block-structured mesh for complex geometries”, Los Alamos National Laboratory report LA-12503-MS, 1993.

[41] Amsden A. A. “KIVA-3V: A Block-Structured KIVA Program for Engines with Vertical or Canted Valves”, Los Alamos National Laboratory report LA-13313-MS, 1997.

[42] Andreassi L., De Maio A., Bella G., Bernaschi M. “Internal Combustion Engines computational tools: Use and Development”, 4thInternational Conference on Internal Combustion Engines: Experiments and Modeling, Capri (Italy), 1999.

[43] Launder B. E., Spalding D. B. “Lectures in Mathematical Models of Turbulence”, Academic Press, London, England, 1972.

[44] Reitz R. D., Bracco F. V., Phys. Fluids, 1982, 25, 1730-1742.

[45] Reitz R. D. Atomization Spray Techn., 1987, 3, 309-337.

[46] Reitz R. D., Diwakar R. SAE Technical Paper 870598, 1987.

[47] O'Rourke P. J., Amsden A. A. "The Tab Method for Numerical Calculation of Droplet Breakup", SAE Technical Paper 870289, 1987.

[48] Ibrahim E. A., Yang H. Q., Przekwas A.J. J. Propulsion, 1993, 9, 651-654.

[49] Halstead M., Kirsh, L., Quinn, C. "The Autoignition of Hydrocarbon Fuels at High Temperatures and Pressures - Fitting of a Mathematical Model", Combust. Flame, 30, 45-60, 1977.

[50] Kong S. C., Reitz R. D. ASME Trans., J. Eng. Gas Turb. Power, 1993, 115, 781-789.

[51] Kong S.C., Han Z., Reitz R.D. "The Development and Application of a Diesel Ignition and Combustion Model for Multidimensional Engine Simulation", SAE Technical Paper 950278, 1996.

[52] Sazhina E. M., Sazhin S. S., Heikal M. R., Marooney C. J. "The Shell Autoignition Model: Applications to Gasoline and Diesel Fuels", Fuel Paper Elsiever, vol.78, pp.389-401, 1999.

[53] Abraham J., Bracco F. V., Reitz R. D. Combust. Flame, 1985, 60, 309-322.

[54] Marble F., Broadwell J. Technical Report TRW-9-PU Project Squid, Purdue University West Lafayette, 1977.

[55] Candel S. M., Poinsot T. J. Combust. Sci. Techn., 1990, 70, 1-15.

[56] Meneveau C., Poinsot T. J. Combust. Flame, 1991, 81, 311-332.

[57] Williams F. A. "Combustion Theory", Benjamin/Cummings Publishing Inc., New York, 1986.

[58] Peters N. "Turbulent Combustion", Cambridge University Press, 2000.

[59] Mantel T., Borghi R. "A new model of premixed wrinkled flame propagation based on a scalar dissipation equation", Combustion and Flame, Vol./Issue 96:4, 1994.

[60] Ashurst W. T., SIAM Conference on Numerical Combustion St. Petersburg, 1991.

[61] Rutland C. J., Trouvè A. "Pre-mixed flame simulations for non-unity Lewis numbers", Studying Turbulence Using Numerical Simulation Databases III (NASA Ames/Stanford Center for Turbulence Research), p. 299, 1990.

[62] Aung K. T., Tseng L. K., Ismail M. A., Faeth G. M. “Response to Comment by S. C. Taylor and D. B. Smith on ‘Laminar Burning Velocities and Markstein Numbers of Hydrocarbon/Air Flames”, Combustion and Flame 102:526-530, 1995.

[63] Karpov V. P., Lipatnikov A. N., Wolanski P. “Finding the Markstein Number Using the Measurements of Expanding Spherical Laminar Flames”, Combustion and Flame 109:436-448, 1997.

[64] Abu-Orf G. M. PhD Thesis, University of Manchester Institute of Science and Technology, Manchester England, 1996.

[65] Cheng W. K., Diringer J. A. SAE Paper 910268, 1991.

[66] Zhao X., Matthews R. D., Elley J.L. SAE Paper 932713, 1993.

[67] Huang Z., Zhang Y., Zeng K., Liu B., Wang Q., Jiang D. “Measurements of Laminar Burning Velocities for Natural Gas-Hydrogen-Air Mixtures”, Comb. And Flame, vol. 146, pp. 302-311 (2006).

[68] Karim G.A., Wierzba I., Al-Alousi Y. “Methane-Hydrogen Mixtures as Fuels”, Int. Journal of Hydrogen Energy, vol. 21, pp. 625-631 (1996).

[69] Sierens R., Rosseel E. “Variable Composition Hydrogen/Natural Gas Mixtures for Increased Engine Efficiency and Decreased Emissions”, Journal of Eng. For Gas Turbines and Power, vol. 122, pp. 135-140 (2000).

[70] Tunestal P., Christensen M., Einewall P., Andersson T., Johansson B., Jonsson O. “Hydrogen Addition for Improved Lean Burn Capability of Slow and Fast Natural Gas Combustion Chambers”, SAE Technical Paper 2002-01-2686 (2002).

[71] Bauer C.G., Forest T.W. “Effect of Hydrogen on the Performance of Methane-Fueled Vehicles. Part I: Effect on S.I. Engine Performance”, Int. Journal of Hydrogen Energy, vol. 26, pp. 55-70 (2001).

[72] Li H., Karim G.A. “Exhaust Emissions from a SI Engine Operating on Gaseous Fuel Mixture Containing Hydrogen”, Int. Journal of Hydrogen Energy, vol. 30, pp. 1491-1499 (2005).

[73] Akansu S.O., Dulger Z., Kahraman N., Veziroglu T.N. “Internal Combustion Engines Fuelled by Natural Gas-Hydrogen Mixtures”, Int. Journal of Hydrogen Energy, vol. 29, pp. 1527-1539 (2004).

[74] Smith G.P., Golden D.M., Frenklach M., Moriarty N.W., Eiteneer B., Goldenberg M., Bowman T.C., Hanson R.K., Song S., Gardiner W.C. Jr., Lissianski V.V., Qin Z., http://www.me.berkeley.edu/gri_mech/.

[75] Goodwin D. G., "An Open-Source, Extensible Software Suite for CVD Process Simulation, Chemical Vapor Deposition", XVI and EUROCVD 14, ECS Proceedings Volume 2003-08, M. Allendorf, F. Maury, and F. Teyssandier, editors, The Electrochemical Society, pp. 155-162 (2003).

[76] Pede G., Rossi E., Chiesa M., Ortenzi F. "Test of Blends of Hydrogen and Natural Gas in a Light-Duty Vehicle", Kyoto 2007 JSAE/SAE International Fuels & Lubricants Meeting.

List of Tables

List of Figures

Nomenclature

ABBREVIATIONS

AFR	air fuel ratio
ALE	arbitrary lagrangian eulerian
ANG	adsorbed natural gas
ATDC	after top dead centre
BDC	bottom dead centre
BML	Bray-Moss-Libby Model
BSFC	brake specific fuel consumption
BSEC	brake specific energy consumption
BTDC	before top dead centre
CAD	crank angle degree
CFD	computational fluid-dynamics
CFM	Coherent Flame Model
CNG	compressed natural gas
CO	carbon monoxide
CO_2	carbon dioxide
CTC	Characteristic Time Combustion Model
DDB	Dynamic Drop Breakup Model
DF	dual-fuel operation
DNS	direct numerical simulation
EBU	Eddy Breakup Model
EDC	Eddy Dissipation Concept
EDM	Eddy Dissipation Model
EGR	exhaust gas recirculation
ECU	electric central unit
FD	full diesel operation

FVM	finite volume method
H_2O	water
HC	unburned hydrocarbons
HCLA	heated chemi-luminescence analyser
HFID	heated flame ionisation detector
ICE	internal combustion engines
IM-CNR	Istituto Motori of Italian National Research Council
IMEP	indicated mean effective pressure
LHS	left hand side
LNG	liquefied natural gas
MF	mixed fuel (= dual fuel) operation
NG	natural gas
NGV	natural gas vehicles
NO	nitrogen monoxide
NO_X	nitrogen oxides
NOR	research octane number
O2	oxygen
PAH	polycyclic aromatic hydrocarbons
PM	particulate matter
PSC	partially stratified concept
RHS	right hand side
RON	Research Octane Number
RPM	revolutions per minute
SI	spark ignition
TAB	Taylor Analogy Breakup Model
TC	turbocharger
TDC	top dead centre
UTV	University of Rome Tor Vergata
WOT	wide open throttle

Acknowledgements

First of all, I wish to thank my supervisor, Prof. Stefano Cordiner, for having guided, supported, encouraged and stood me during the last three (or rather four) years of my studies at UTV. I really hope that you are proud of me Prof! Special thanks for my friends and colleagues Luca Andreassi (Professor by now) and Vincenzo Mulone, who are of merit to have incited me to carry on my studies and start my PhD after the degree. A word of thanks to Prof. Vittorio Rocco, the director of the Department of Mechanical Engineering, for his valuable advices. I did my best to act for the UTV at every conference, meeting and something like that. I hope that I was able to do it.

No words are adequate for my students Daniele D'Orazio and Marco Pece (in chronological order). I have worked with them on the present activity and I am sure that I would have not obtained such results without their joint effort. Moreover, I have stayed friend with them, and in my opinion this is the most important result that I could have obtained. Thank you guys!

I also wish to thank all the people that I met during my PhD, in particular Michele Gambino and Sabato Iannaccone, co-authors for several papers on dual-fuel engines and respectable people, the technicians Enzo Bonanno and Pino Barese, the mythical Dr. Luigi Allocca, exceptional companion of Egyptian conferences, and all the researchers of IM-CNR, the extraordinary and charming Prof. Fabio Bozza, and my friends and PhD colleagues at UTV. I cannot mention you all here (you are so many), but I will never forget you!

A special mention for my close friends, especially because I have neglected them lately, and for Anna, who recently came into my life and turned me back on.

But after all (the last but not the least!), my greatest gratitude is for Vincenzo, Beatrice, Michela and Alessandro, that is to say my family, because if I am like this, it is exclusively thanks to them. I love you!